

Copyright
by
Neil McCarthy
2015

**The Dissertation Committee for Neil McCarthy Certifies that this is the
approved version of the following dissertation:**

**Gene-ethanol interactions underlie craniofacial variability in a
zebrafish model of FASD.**

Committee:

Johann K. Eberhart, Supervisor

Jeffrey M. Gross

R. Adron Harris

Steven A. Vokes

John B. Wallingford

**Gene-ethanol interactions underlie craniofacial variability in a
zebrafish model of FASD.**

by

Neil McCarthy, B.S.

Dissertation

Presented to the Faculty of the Graduate School of
The University of Texas at Austin
in Partial Fulfillment
of the Requirements
for the Degree of

Doctor of Philosophy

**The University of Texas at Austin
August, 2015**

Acknowledgements

I would like to acknowledge my mentor, Johann K. Eberhart, for his patience, wisdom, and time. Through his guidance, I have gained a strong foundation in the principles of the scientific method, and have acquired a skill set that will allow me to pursue a research career in many facets of biological science. I have also gained indispensable insight from a mentorship with Johann by being able to observe his transition from being an assistant to an associate professor, and the work that requires such success. It has been an incredible, enjoyable, and gratifying time working under Johann.

I would like to thank my committee members for their support, critique, and enthusiasm that allowed me to develop a strong dissertation. I also need to thank them for their letters of recommendation, which allowed me to interview for numerous post-doctoral positions.

I would like to thank Mary Swartz, who should have a co-mentorship with Johann in my dissertation. Many of the skills that I acquired in the lab are through direct training with her, and she has been an incredible asset in both scientific discussion and critique. I'd like to thank past members, including Kelly Sheehan-Rooney, Young-Jun Jeong, and Ben Wells, and current members, including Patrick McGurk, Alfire Sidic, Ben Lovely, and Anna Percy for their support, scientific insight and help. I would also like to thank all of my friends throughout the years who have supported and encouraged me in my endeavors as a scientist. I could not have survived graduate school without them.

Lastly, I would like to thank my parents and family who have supported and encouraged my scientific endeavours from the start.

Gene-ethanol interactions underlie craniofacial variability in a zebrafish model of FASD.

Neil McCarthy, PhD

The University of Texas at Austin, 2015

Supervisor: Johann K. Eberhart

Variation is common in human birth defects and this variability is influenced by genes and the environment. How genes and the environment interact in causing birth defect variability is a fundamental question in biology. I sought to investigate these interactions using a zebrafish model of fetal alcohol spectrum disorder. Fetal alcohol spectrum disorder (FASD) is an umbrella term that describes all ethanol-induced fetal defects. It is highly variable and also highly prevalent, with an estimated 1% of the population being affected. FASD can cause variable defects, including those affecting the craniofacial skeleton, a neural crest- and mesoderm-derived structure. Although both timing and dosage can influence FASD variability, genetics is an underlying factor. Little is known of the genes that cause susceptibility to FASD, and so I sought to uncover these genes and the mechanism of their interaction with ethanol.

Using a novel zebrafish genetic screen to uncover gene-ethanol interactions, we found a synergistic interaction between *platelet-derived growth factor receptor alpha* (*pdgfra*) and ethanol. *Pdgfra* is a receptor tyrosine kinase involved in cell migration, proliferation, and survival. Untreated *pdgfra* mutants display cleft palate. In a percentage of ethanol in which wildtype zebrafish are

unaffected, *pdgfra* mutants display exacerbated loss of the entire palatal skeleton. Furthermore, *pdgfra* heterozygotes display variable craniofacial defects, uncovering latent haploinsufficiency. Genetic analysis of a group of children with and without FASD suggests that this interaction is highly conserved. In zebrafish, further analysis of the mechanism of this *pdgfra*-ethanol interaction revealed a protective role of *pdgfra* to ethanol-induced neural crest cell death. Analysis of the *Pdgfra* downstream pathway PI3K/AKT/mTOR revealed an inhibitory effect of ethanol at the level of mTOR. Together, these data suggest that genes functioning in growth factor signaling could predispose to ethanol-induced defects.

Analysis of another growth factor signaling gene, *fgf8a*, supported this hypothesis. Ethanol interacts with *fgf8a* to cause posterior mesoderm-derived craniofacial defects. This phenotype can be recapitulated by blocking both *fgf8a* and *fgf3*, suggesting ethanol broadly attenuates growth factor signaling. Analysis of the *fgf8a;fgf3* phenotype suggests that Fgf signaling is required for proper specification, via *hyaluronan synthetase 2*, of the mesoderm-derived posterior craniofacial skeleton. To test whether ethanol may also broadly attenuate Pdgf signaling, we analyzed *pdgfra;pdgfrb* mutant phenotypes and saw a recapitulation of the *pdgfra*-ethanol interaction. The synergistic *pdgfra;pdgfrb* phenotype may be due to a similar increase in neural crest cell death observed in the *pdgfra*-ethanol interaction. Together, these data reveal genes involved in growth factor signaling may act to protect against ethanol-induced craniofacial defects.

Table of Contents

Acknowledgements.....	iv
List of Tables.....	xi
List of Figures.....	xii
Chapter 1: General Introduction and Significance	1
1.I. Fetal Alcohol Spectrum Disorder	2
1.II. Gene-ethanol interactions.....	2
1.II.a. Metabolic pathways	3
1.II.b. Sonic hedgehog (Shh) pathway.....	6
1.II.c. Growth factors.....	9
1.II.d. Zebrafish as a FASD model system	11
1.III. Craniofacial Development.....	13
1.III.a. Evolution of Vertebrates	13
1.III.b. Development of the vertebrate craniofacial skeleton	14
1.III.c. The neural crest	14
1.III.d. The cephalic mesoderm	16
1.III.e. Zebrafish craniofacial development and anatomy	18
1.IV. Growth factor signaling in craniofacial development	19
1.IV.a. Platelet-derived growth factor signaling	20
1.IV.b. Fibroblast growth factor signaling.....	21
1.V. Outline of dissertation	22
1.VI. Figures.....	24
Chapter 2: <i>Pdgfra</i> protects against ethanol-induced craniofacial defects in a zebrafish model of FASD	30
2.I. Abstract.....	30
2.II. Introduction	32
2.III. Results	36
2.III.a. <i>pdgfra</i> and ethanol synergistically interact.....	36

2.III.b. Neural crest cell apoptosis increases in ethanol-exposed <i>pdgfra</i> mutants	43
2.III.c. Combined loss of <i>Pdgf</i> signaling and ethanol exposure impinges on mTOR signaling	46
2.IV. Discussion	49
2.IV.a. <i>Pdgfra</i> regulates both neural-crest cell migration and protection from ethanol-induced apoptosis	49
2.IV.b. Ethanol may broadly disrupt growth-factor signaling pathways	52
2.IV.c Zebrafish as a model of gene-environment interactions	52
2.V. Materials and Methods	55
2.V.a. <i>Danio rerio</i> (zebrafish) care and use	55
2.V.b. Morpholino and RNA injection	55
2.V.c. Immunohistochemistry	56
2.V.d. Immunoblotting	56
2.V.e. Cartilage and Bone staining and area measurements ...	58
2.V.f. Confocal microscopy and figure processing	58
2.V.g. Statistical Analysis	58
2.V.h. Measurement of ethanol concentration using headspace gas chromatography	58
2.V.i. Human sample	60
2.V.j. Ethics Statement	62
2.V.k. Human GWAS	63
2.VI. Acknowledgements	64
2.VII. Figures	65
2.VIII Tables	96
Chapter 3: An <i>Fgf-Shh</i> signaling hierarchy regulates early specification of the zebrafish skull	99
3.I. Abstract	99
3.II. Introduction	100
3.III. Results	103
3.III.a. The postchordal neurocranium requires <i>fgf8a</i> and <i>fgf31</i>	103

3.III.b. The mesoderm and neural ectoderm are Fgf sources required for postchordal neurocranium formation	106
3.III.c. The postchordal neurocranium is primarily mesoderm-derived	107
3.III.d. Proper specification of the head paraxial mesoderm requires Fgf signaling	110
3.III.e. The notochord is dispensible in the formation of the postchordal neurocranium	115
3.IV. Discussion	116
3.IV.a. The dual origin of the zebrafish neurocranium	117
3.IV.b. Fibroblast growth factor signaling in the zebrafish neurocranium	118
3.IV.c. A signaling hierarchy orchestrates the specification and differentiation of the postchordal neurocranium.....	120
3.V. Materials and Methods	122
3.V.a. Fish husbandry and care.....	122
3.V.b. Morpholino and RNA injection	123
3.V.c. Cartilage and bone staining	124
3.V.d. Confocal Microscopy and figure processing.....	125
3.V.e. In Situ Hybridization	125
3.V.f. Cell Transplants.....	125
3.VI. Acknowledgements	126
3.VII. Figures.....	128
Chapter 4: <i>pdgfra</i> and <i>pdgfrb</i> synergistically interact in craniofacial development	156
4.I. Abstract.....	156
4.II. Introduction	157
4.III. Results	159
4.III.a. Dual knockdown of <i>pdgfra</i> and <i>pdgfrb</i> leads to exacerbated craniofacial defects	159
4.III.b. Pdgf activity is required between 6 and 30 hours post fertilization for proper craniofacial development	161

4.III.c. <i>pdgfra</i> and <i>pdgfrb</i> have overlapping expression in the head beginning at 20 hours post fertilization	162
4.III.d. Loss of both <i>pdgfra</i> and <i>pdgfrb</i> results in increased neural crest cell death.....	163
4.IV. Discussion and future directions.....	164
4.V. Materials and methods	167
4.V.a. Zebrafish care and use.....	167
4.V.b. Mice	167
4.V.c. Immunohistochemistry and <i>In situ</i> hybridization	167
4.V.d. Zebrafish cartilage staining	168
4.V.e. Confocal microscopy and figure processing.....	168
4.VI. Figures.....	169
4.VII. Tables	178
Chapter 5: Summary and future directions	179
5.I. Future Directions.....	182
5.I.a. Mechanistic understanding of the <i>fgf8a</i> -ethanol interaction	182
5.I.b. Other defects associated with gene-ethanol interactions.....	184
5.I.c. Screening for ethanol sensitivity in other growth factor signaling genes.....	185
5.I.d. Developing treatments and therapies to mitigate ethanol teratogenesis	186
Bibliography	189
Vita	241

List of Tables

Table 2.1: ANOVA statistics describing significant differences of skeletal elements across genotype and treatments	96
Table 2.2: Human SNP-ethanol interactions produce craniofacial measurement changes.....	97
Table 4.1: <i>pdgfra</i> ; <i>pdgfrb</i> double mutants show statistically significant differences in craniofacial measurements.....	178

List of Figures

Figure 1.1: Ethanol metabolism leads to cell-damaging reactive oxygen species (ROS), increased DNA damage, and cell death; a problem exacerbated by <i>Fancd2</i> deficiency.....	24
Figure 1.2: Ethanol has been shown to interact with several members of the Shh signaling pathways (denoted in red)	26
Figure 1.3: Zebrafish screen to uncover gene-ethanol interactions	27
Figure 1.4: The zebrafish cranial neural crest and craniofacial skeleton .	29
Figure 2.1: Ethanol exacerbates <i>pdgfra</i> mutant neurocranial defects and reveals haploinsufficiency	65
Figure 2.2: Ethanol induces pharyngeal hypoplasia in <i>pdgfra</i> mutants....	67
Figure 2.3: <i>pdgfra</i> mRNA partially rescues the ethanol-induced defects ..	69
Figure 2.4: <i>mirn140</i> morpholino protects <i>pdgfra</i> mutants against ethanol-induced defects	70
Figure 2.5: Ethanol-treatment causes a decrease in overall neurocranial length and width in <i>pdgfra</i> mutants	71
Figure 2.6: Ethanol treatment does not disrupt the pectoral fin in <i>pdgfra</i> mutants	73
Figure 2.7: <i>coll1a</i> expression is unaffected in cartilage elements not lost in ethanol-treated <i>pdgfra</i> mutants	74
Figure 2.8: Ethanol-treated <i>pdgfra</i> mutants exhibit an increase in neural crest cell death.....	75
Figure 2.9: Ethanol treatment does not cause developmental delay or global increases in cell death in <i>pdgfra</i> mutants.....	77

Figure 2.10: Neural crest-specific proliferation is not reduced in ethanol-treated <i>pdgfra</i> mutants	79
Figure 2.11: At 24 hpf ethanol-induced cell death occurs in pharyngeal arch areas destined to contribute to the jaw and jaw support elements.....	80
Figure 2.12: <i>pten</i> morpholino injection does not alter neurocranial development in untreated and ethanol-treated wild-type and <i>pdgfra</i> heterozygotes	82
Figure 2.13: <i>pten</i> morpholino injections do not alter jaw and jaw support development in untreated and ethanol-treated wild-type and <i>pdgfra</i> heterozygotes	84
Figure 2.14: Injection of <i>pten</i> morpholino rescues the craniofacial defects in ethanol-treated <i>pdgfra</i> mutants	85
Figure 2.15: L-leucine does not alter the craniofacial skeleton of untreated and ethanol-treated wild-type and <i>pdgfra</i> heterozygotes	86
Figure 2.16: L-leucine treatment from 24 to 48 hpf does not rescue the ethanol-induced defects in 10-24 hpf treated mutants	87
Figure 2.17: Both wortmannin and rapamycin phenocopy the effects of ethanol on <i>pdgfra</i> mutants	88
Figure 2.18: Both wortmannin- and rapamycin-treated <i>pdgfra</i> mutants show a decrease in overall neurocranial length and width	90
Figure 2.19: Treating <i>pdgfra</i> mutants with wortmannin or rapamycin induces pharyngeal skeleton hypoplasia.....	92
Figure 2.20: Ethanol affects phosphorylation of AKT and pEIF4B in ethanol-treated <i>pdgfra</i> mutants	94

Figure 2.21: Rapamycin-treatment leads to an increase in phosphorylated AKT in both <i>pdgfra</i> mutants and siblings as compared to DMSO- treated controls	95
Figure 3.1: <i>fgf8a</i> mutants interact with ethanol to cause postchordal neurocranial defects.....	128
Figure 3.2: The postchordal neurocranium requires Fgf signaling.....	129
Figure 3.3: Loss of Fgf signaling causes postchordal neurocranial defects.....	130
Figure 3.4: Fgfr3 and Fgf8 interact in postchordal neurocranial development	131
Figure 3.5: The mesoderm and neural ectoderm are Fgf sources required for postchordal neurocranial formation.....	132
Figure 3.6: The postchordal neurocranium is primarily intact in <i>dlx3b;foxi1</i> knockdown embryos	134
Figure 3.7: The zebrafish postchordal neurocranium is derived from both mesoderm and neural crest tissues	135
Figure 3.8: Mandibular- and hyoid-specific neural crest contributions to the postchordal neurocranium.....	137
Figure 3.9: <i>cre</i> expression in the <i>drl:CreERT2</i> line confirms mesoderm- specific labeling at 6 hours post fertilization (hpf)	138
Figure 3.10: Fate-mapping of head mesoderm shows the anterior/posterior organization of postchordal cells is set by 24 hours post fertilization (hpf).....	139
Figure 3.11: Individual kaede photoconversion fate mapping data points.....	141

Figure 3.12: Cartilage and pre-cartilage markers <i>col2a1a</i> and <i>sox9a</i> are absent at 24 hours post fertilization (hpf) in <i>fgf3;fgf8a</i> knockdown embryos	142
Figure 3.13: Kaede photoconverted endomesoderm postchordal-progenitor cells migrate appropriately in <i>fgf3;fgf8a</i> knockdown embryos	143
Figure 3.14: Loss of <i>has2</i> in Fgf knockdown embryos contributes to the postchordal neurocranial loss phenotype.....	144
Figure 3.15: Expression of <i>has2</i> at 6 hours post fertilization does not require <i>fgf3;fgf8</i> function	147
Figure 3.16: Inhibition of hyaluronic acid in <i>fgf8a</i> mutants causes postchordal neurocranial defects	148
Figure 3.17: Postchordal neurocranial development requires Fgf signaling during gastrulation.....	150
Figure 3.18: Postchordal neurocranial development does not require <i>brachyury</i> function or a notochord.....	152
Figure 3.19: Chondrocyte differentiation but not early cephalic mesoderm specification requires Hh signaling.....	154
Figure 3.20: Hh signaling is required after Fgf signaling for postchordal neurocranial development.....	155
Figure 4.1: <i>pdgfra</i> and <i>pdgfrb</i> synergistically interact in craniofacial development.....	169
Figure 4.2: Synergistic skeletal abnormalities observed in <i>pdgfra^{fl/fl};pdgfrb^{fl/fl};wnt1:Cre</i> mice.....	171

Figure 4.3: Pdgf signaling is required between 6 and 30 hours post fertilization for proper craniofacial development.....	173
Figure 4.4: PDGF Inhibitor V treatment does not affect melanocyte formation	174
Figure 4.5: The neural crest expresses <i>pdgfrb</i> in zebrafish at 24 and 36 hours post fertilization	175
Figure 4.6: Neural crest cells express both <i>pdgfra</i> and <i>pdgfrb</i> beginning at 20 hours post fertilization	176
Figure 4.7: <i>pdgfra;pdgfrb</i> mutants show increased neural crest cell death at 24 hours post fertilization	177

Chapter 1: General Introduction and Significance

How genetics and the environment influence morphological variation is a fundamental biological question. The primary bulk of this variation is generated during development, where gene-environment interactions can sculpt the multicellular organism. In instances of impaired genetics and suboptimal environments, synergistic effects can result in a wide variety of birth defects. Nowhere is this clearer than in examples of teratogenesis.

Teratogens are any environmental agent that can cause birth defects. One of the most well known teratogens is ethanol and fetal exposure to ethanol can cause fetal alcohol spectrum disorders (FASD, described in detail below). FASD is highly variable, with craniofacial tissues often damaged. While the timing and volume of ethanol exposure influence FASD variability, there is clear genetic susceptibility to FASD. What these predisposing FASD loci are is still an open question.

To address this question, we utilized a zebrafish model of FASD, focusing on the craniofacial skeleton, to uncover and characterize gene-ethanol interactions. The broader significance of this research was to understand how genes and environment cause phenotypic variation in general, to broaden FASD diagnosis, and to provide mechanistic understanding of these gene-ethanol interactions that may help in future treatments of this incredibly prevalent birth defect.

1.I. Fetal Alcohol Spectrum Disorder

Ethanol was first described as a human teratogen in 1968 (Lemoine et al., 1968), and diagnosed as Fetal Alcohol Syndrome in 1973 (Jones et al., 1973; Jones and Smith, 1973). Since then, a yet broader representation of the effects of ethanol on the developing fetus have been categorized and termed fetal alcohol spectrum disorders (FASD). FASD is reported to occur as frequently as 1:100 (Sampson et al., 1997) live births in the US, with some world communities showing a prevalence of 20% (May et al., 2013), making alcohol consumption one of the most common causes of human birth defects.

Alcohol's teratogenic endpoints are very diverse. The most severe end of the spectrum of FASD show pre- and post-natal growth retardation, intellectual disability coupled with abnormal morphogenesis of the brain, and craniofacial defects, diagnosed as FAS (Calhou and Warren, 2007; Hoyme et al., 2005; Jones, 2011). The most mild end of the FASD spectrum involves neurological cognitive disorders that are sometimes manifest as late as adolescence (Calhoun and Warren, 2007). Other FASD defects include heart, ear, ocular, and limb-associated malformations (Jones, 2011). The variability seen within FASD can be attributed to a number of factors, including the amount and timing of alcohol ingested by the mother during pregnancy, malnutrition, epigenetic changes, and underlying genetic susceptibility (Perkins et al., 2013). Recent research is beginning to shed new light on the latter.

1.II. Gene-ethanol interactions (from McCarthy and Eberhart, 2014)

Since as early as the 1970s, when the criteria for FAS diagnosis were established, underlying genetic factors have been considered to be important.

The most convincing evidence in humans for genetic susceptibility to FAS lies in the results of twin studies (Chasnoff, 1985). Monozygotic twins have been shown to be 100% concordant for FAS, while dizygotic twins, also sharing a common uterine environment, only displayed 63% concordance (Streissguth and Dehaene, 1993). The precise genetic players underlying susceptibility to FASD have remained elusive. Human FASD studies have primarily focused on candidate genes, including allelic variants of the alcohol dehydrogenase gene ADH1 (Etheredge et al., 2005; Mitchell et al., 2001; Romitti et al., 1999). Other genes that may predispose to human FASD remain elusive. Thus, research has come to rely on animal models to direct our understanding of genetics underlying FASD. Pathways uncovered in animal models that are especially sensitive to ethanol teratogenesis are reviewed below.

1.II.a. Metabolic Pathways

Alcohol is metabolized first into acetaldehyde via alcohol dehydrogenase (ADH), catalase, and cyp2E1 (Deehan et al., 2013; Figure 1.1). Acetaldehyde is further catabolized into acetate, an important biosynthetic molecule, via acetaldehyde dehydrogenase. This pathway produces harmful byproducts, including acetaldehyde itself and reactive oxygen species. Because of this, how well a mother and the fetus can catabolize ethanol and its constituent metabolites may be an important factor in FASD.

The first gene ever implicated in FASD was ADH. In humans, different alleles of ADH1 encode for enzymes that catabolize ethanol at different rates. A

number of studies have linked these allele-specific ADH genes to FASD prevalence. In humans, it has been shown that the *ADH1B2* and *ADH1B3* alleles encode for enzymes with faster catabolism (Das et al., 2004; Green and Stoler, 2007; Jacobson et al., 2006; May et al., 2007; McCarver et al., 1997; Viljoen et al., 2001). These alleles are underrepresented in FASD children and their mothers, suggesting that genes regulating ethanol catabolism may regulate FASD susceptibility.

Animal studies provide clear evidence that this catabolic pathway is important in ethanol teratogenesis. Superoxide dismutase is an essential enzyme for clearing reactive oxygen species. In mice, maternal transgenic overexpression of *Superoxide dismutase* protects litters from ethanol-induced decreases in fetal body weight and viability (Wentzel and Eriksson, 2006). Furthermore, dams harboring a targeted mutation in *Superoxide dismutase* were found to have increased risk of fetal resorptions and decreased body weight of embryos exposed to ethanol. However, zygotic *Superoxide dismutase* genotype had no apparent effect on resorption rates or viability, suggesting that the mother's ability to clear alcohol metabolites is important in susceptibility to ethanol-induced defects. Indeed, earlier mouse studies linked ethanol-metabolizing activity and maternal genotype to increased incidences of ethanol-induced fetal malformations and death (Chernoff, 1980; Gilliam and Irtenkauf, 1990). However, these studies did acknowledge that maternal genotype was not the only influencing factor in susceptibility to ethanol teratogenesis.

Zygotic genotype can also generate susceptibility to ethanol teratogenesis alone or in combination with the maternal genotype. Acetaldehyde accumulation has been linked to DNA damage and increased oxidative stress, hallmarks of ethanol teratogenesis (Dong et al., 2009; Ramachandran et al., 2001; Ramachandran et al., 2003). To counteract these damaging byproducts, cells further catabolize acetaldehyde via *Aldh* and mobilize DNA repair enzymes such as Fanconi anaemia genes (*Fancd*) (Mirchandani and D'Andrea, 2006). Recently, the function of both *Aldh2* and *Fancd2* has been shown to be essential for protection against ethanol teratogenesis (Langevin et al., 2011; see Fig. 1.1). In this study, mouse pups exposed prenatally to alcohol have no increase in mortality if they are born to wild-type mothers, regardless of zygotic genotype. Similarly, female mice heterozygous for *Aldh2* were able to have viable *Aldh2*^{-/-}; *Fancd2*^{-/-} pups. However, in the presence of ethanol these pups had a decrease in viability and an increase in the prevalence of exencephaly and eye abnormalities. Furthermore, a small percentage of ethanol-treated *Aldh2*^{+/-}; *Fancd2*^{-/-} pups also showed an increase in eye abnormalities and exencephaly. Collectively, these studies strongly suggest that in mammalian systems, teratogenesis caused by deficits in the ethanol catabolic pathway is the result of a complex interaction of maternal and zygotic genotypes.

Together, these studies strongly suggest that proper alcohol catabolizing activity during pregnancy, in both the mother and the fetus, is an important factor in FASD susceptibility. Increased alcohol intake leads to an increase in

acetaldehyde and reactive oxygen species formation, which together, can lead to deleterious effects including DNA damage and cell death. Concurrent with a lack of proper catabolizing activity, susceptibility increases in mice lacking proper DNA-damage repair enzymes, such as Fancd2. In effect, these types of deficits most likely lead to cell death, however, it is unclear if this would be a tissue-specific effect or not. Lastly, these studies promote the idea that FASD variability is most likely manifest as complex genetic interactions within the mother and/or the fetus.

1.II.b. Sonic Hedgehog (Shh) pathway

One of the most well-studied developmental signaling molecules is Sonic Hedgehog (Shh). Shh is a secreted glycoprotein first synthesized as a 45kDa precursor protein, which undergoes autocatalytic cleavage to produce a carboxy terminal fragment (Shh-C) and a 19kDa active fragment (Shh-N) (Stone et al., 1996; see Figure 1.2). Shh-N is then further modified via addition of cholesterol and palmitate to form the functionally active Shh ligand (Mann and Beachy, 2000; Porter et al., 1996). Upon sterol modification, Shh is transported to the cell membrane via lipid rafts and released from the secreting cell (Mao et al., 2009). Shh signaling occurs when the ligand attaches to patched, releasing inhibition of smoothened, leading to activation of Gli transcription factors to regulate gene expression (Ruiz I Altaba et al., 2002).

Mutation of Shh pathway genes causes developmental deficits in numerous tissues. These defects include neural crest-specific cell death, misspecification of the dorsal-ventral axis of the neural tube and loss of midline craniofacial structures as occurs in the holoprosencephaly (HPE) spectrum (Chiang et al., 1996; Cordero et al., 2004; Eberhart et al., 2006; Jeong et al., 2004; Pan et al., 2013; Roessler and Muenke, 2010; Wada et al., 2005). These same phenotypes can be present in children with FAS (Johnson and Rasmussen, 2010; Jones, 2011), suggesting that ethanol disrupts Shh signaling.

There is an abundance of molecular evidence that ethanol alters the Shh pathway in both cell culture and animal models (see Fig. 1.2). Ethanol has been found to decrease the expression of Shh in chicken (Ahlgren et al., 2002; Brennan and Giles, 2013), mouse (Aoto et al. 2008), and zebrafish (Li et al., 2007). Furthermore, co-application of exogenous Shh with ethanol has been shown to alleviate ethanol-induced defects (Ahlgren et al., 2002; Aoto et al., 2008; Li et al., 2007; Loucks and Ahlgren, 2009; Zhang et al., 2011; Zhang et al., 2012). In addition to altering levels of transcription, ethanol has also been shown to disrupt proper membrane fluidity and composition (Polley and Vemparala, 2012), which might account for some of ethanol's effects on the Shh pathway. *In vitro* studies have found that ethanol perturbs proper association of active Shh ligand with lipid rafts destined to the membrane (Mao et al., 2009). Ethanol exposure leads to a decrease in the amount of membrane-associated cholesterol (Li et al., 2007), which is vital for proper Shh signaling. Similar to the effects of

exogenous Shh ligand, supplemental cholesterol reduces the teratogenicity of ethanol (Li et al., 2007; Ehrlich et al., 2012). Additionally, microarray data suggests that differences in expression of polysaccharide genes, also important in membrane-based cell communication and function, partly contributes to strain sensitivity to ethanol-induced defects in mice (Downing et al., 2012). These data support the hypothesis that ethanol directly affects Shh-mediated and membrane-based signaling.

While Shh has long been implicated in ethanol teratogenesis, only recently has a genetic interaction between ethanol and the Shh pathway been discovered (see Fig. 1.2). Ethanol interacts with the gene encoding the Shh co-receptor *Cdon* to cause HPE (Hong and Krauss, 2012). *Cdon* mutant mice have a low penetrance of minor holoprosencephaly phenotypes, and the strain background used in this study has been shown to be resistant to ethanol teratogenesis. However, ethanol-exposed *Cdon* mutant mouse embryos have defects in early midline patterning, Shh signaling, and increased susceptibility to HPE and craniofacial defects. For example, ethanol increased lobar HPE by 50% in treated *Cdon* mutants. Increased prevalence of cranial defects including those affecting the palate and premaxillary bones occurred as well. While ethanol exacerbated the phenotypes present in *Cdon* mutants, no defects in ethanol-treated heterozygotes were reported, suggesting a weak interaction.

Ethanol may interact more strongly with other members of the Shh signaling pathway. Ethanol exposure reveals haploinsufficiency in mice carrying

mutant alleles of *Shh* or *Gli2* (Keitzman et al., unpublished). These ethanol-treated heterozygous mice have variable craniofacial and HPE-like defects. Additional evidence in zebrafish supports Shh's role in predisposing to ethanol teratogenesis. Ethanol acts synergistically with suboptimal morpholino knockdown of *agrin*, an extracellular membrane protein required for Shh-mediated signaling, or of *shh* which results in variable eye defects, including reduced size, in zebrafish (Zhang et al., 2011; Zhang et al., 2012). Collectively, both *in vitro* and *in vivo* data suggest that ethanol may broadly perturb Shh signaling at multiple levels, and that genetic predisposition may exacerbate these molecular disruptions.

1.II.c. Growth Factors

Growth factor signaling pathways are major mediators of tissue growth, proliferation, and survival; all of which are processes disrupted by ethanol. Growth factor signaling involves ligand activation, receptor dimerization, and activation. Receptor activation signals through cytoplasmic effectors that function in activating downstream intracellular pathways important for numerous cellular roles (de la Monte and Wands, 2010; Hsuan and Tan, 1997; Tallquist and Kauzlauskas, 2004). One of the most well studied effectors with relevance for ethanol teratogenesis is Phosphoinositide-3 kinase (PI3K).

PI3K functions partly through the AKT and mTOR pathways (McGough et al., 2009; Siegenthaler and Miller, 2005). PI3K phosphorylates inositol

phospholipids to generate second messenger phosphatidylinositol-3,4,5-triphosphates (PIP3). PIP3 levels are regulated via phosphatase and tensin homolog (PTEN), which converts PIP3 back into inactive PIP2. When PTEN is inactive, PIP3 activates AKT, which causes a cascade effect on a number of downstream constituents involved in cellular growth and survival including forkhead transcription factors, BCL-2, MDM2, and mTORC1 (Downward, 2004; Manning and Cantley, 2007). mTORC1 functions in cellular growth and survival via activation of elongation factors (EIF) and p70 S6 Kinase (Dobashi et al., 2011). Disruption of this pathway at the level of PI3K, AKT, or mTOR leads to decreased cellular survival, proliferation, and growth (Cai et al., 2013; Kim et al. 2013).

Numerous *in vitro* studies show that ethanol exposure leads to decreased signaling through the PI3K/AKT/mTOR pathway. Microarray data showed a disparity in activation of genes in the PI3K pathway, including Akt and Pten, in mouse strains with differing sensitivity to ethanol-induced defects (Green et al., 2007). PI3K activation is reduced in human neuronal cells exposed to ethanol (de la Monte et al., 2000), while in rat neuronal cell cultures ethanol causes a reduction in activated AKT (de la Monte and Wands, 2002). Ethanol decreases mTOR and S6 kinase phosphorylation in mouse myocytes (Hong-Brown et al., 2006), similarly, *in vivo* studies in rat hearts show decreased mTOR phosphorylation in the presence of ethanol (Vary et al., 2008). It has also been shown that the activity of PTEN, which inhibits PI3K signaling, increases in cell

cultures exposed to ethanol (Xu et al., 2003). Furthermore, increasing growth factor signaling or PI3K activity has been shown to alleviate some ethanol-induced defects (McGough et al., 2009; Siegenthaler and Miller, 2005; de la Monte et al., 2000; Jegou et al., 2013). Together, these data suggest that ethanol perturbs proper growth factor mediated PI3K/AKT/mTOR signaling, suggesting that variants in the PI3K pathway could underlie FASD.

Many growth factor pathways use PI3K/mTOR signaling, so it might be predicted that gene-ethanol interactions will exist for these growth factors. In support of this model, transgenic expression of *insulin-receptor*, which signals via PI3K, protects against ethanol-induced motor deficits in *Drosophila* (McClure et al., 2011). It is possible that ethanol perturbs growth factor signaling at many levels. Ethanol has been shown to inhibit phosphorylation of Insulin-receptor in cell cultures (de la Monte et al., 1999) and rat liver (Sasaki et al., 1994). Numerous studies have shown that ethanol perturbs proper expression of a number of growth factors and their receptors. These include insulin-receptor, brain-derived growth factor, TGFB, and VEGF (de la Monte et al., 2000; Jegou et al., 2013; Feng et al., 2005). Collectively, these results show that growth factor signaling may be a major target of ethanol, underlying FASD susceptibility.

1.II.d. Zebrafish as a FASD model system

While these examples of gene-ethanol interactions strongly support a genetic susceptibility to FASD, they are likely just scratching the surface of gene-ethanol

interactions that exist. Furthermore, few of the above mentioned studies characterized the gene-ethanol interactions mechanistically, prompting further analysis and detail. To uncover other gene-ethanol interactions and to be able to describe the mechanism of these interactions, it prompts the use of the highly versatile model system *Danio rerio*, also known as the zebrafish.

Zebrafish have been used to study the effects of ethanol since as early as 1910 (Stockard, 1910). These early studies described relatively high ethanol concentrations causing cyclopia, a defect observed only in very severe cases of FAS (Cohen and Sulik, 1992; Johnston and Bronsky, 1995). Since then, zebrafish research has added to these initial findings showing similarities in more subtle FAS and FASD characteristics including neuronal (Blader and Strahle, 1998; Joya et al., 2014), ocular (Dlugos and Rabin, 2007), heart (Dlugos and Rabin, 2010), and craniofacial (Ali et al., 2011) deficits. While one study showed strain-specific defects to ethanol (Dlugos and Rabin, 2003), none of these studies sought to identify specific gene–ethanol interactions.

Zebrafish is highly amenable to uncovering gene-ethanol interactions due to the ease of both forward and reverse genetics. Zebrafish allow for fast screening of genes for phenotypic traits because of their high fecundity and rapid maturation. Furthermore, because they fertilize their eggs externally, zebrafish allow for control over both the timing and dosage of ethanol (Fig. 1.3). Transgenics also allow for precise cell-tracking and tissue labeling to be

employed in investigating the mechanisms by which ethanol and genes interact to affect normal craniofacial development.

1.III. Craniofacial Development

The craniofacial skeleton is a vertebrate novelty. The evolutionary premise of the craniofacial skeleton is thought to be two-fold: 1) to house and protect the brain and head sensory organs; and, 2) to allow for a predatory lifestyle (Northcutt and Gans, 1983). The development of this structure is incredibly conserved across vertebrate species (Knight and Schilling, 2006), and, as such, analysis of craniofacial development in zebrafish informs our understanding of human development (Knight and Schilling, 2006).

1.III.a. Evolution of Vertebrates

Vertebrates are a subphyla of chordata. The chordates all share distinct attributes that separate them from other phyla: 1) the appearance of the mesoderm-derived notochord, which is a structurally important organ that provides rigidity; 2) a dorsal neural tube, which will contribute to the expansion of the neural network including the brain; 3) somites, a mesoderm-derived tissue that forms along the anterior-posterior axis that functions to form muscles for movement; 4) a postanal tail; and, 5) pharyngeal slits (Satoh et al., 2012). Several characteristics separate vertebrates from invertebrate chordates including the generation of a vertebral column, and the formation of a craniofacial skeleton (Green et al., 2015; Knight and Schilling, 2006; Yu, 2010).

1.III.b. Development of the vertebrate craniofacial skeleton

Although vertebrates include an incredible array of different organisms from fish, amphibians, birds and mammals, the development of the craniofacial skeleton is incredibly conserved across these species (Knight and Schilling, 2006).

Craniofacial form strictly adheres to fundamental similarities among species due to a shared phylotypic stage (Schmidt and Starck, 2010; Galis and Metz, 2001). In vertebrates this stage is called the pharyngeal stage and it occurs following gastrulation, the time at which all three germ layers become specified (Wolpert, 1992). It is characterized by the formation of the head, including the appearance of pharyngeal arches, eyes, and a swelling of the brain (Graham and Richardson, 2012; Graham, 2001; Frisdal and Trainor, 2014). One of the most significant similarities between vertebrates at this stage is the appearance of the neural crest.

1.III.c. The neural crest

The neural crest is a multipotent tissue that is novel to vertebrates and is often dubbed the “fourth germ-layer” (Baker and Bronner-Fraser, 1997b; Hall, 2000; Green et al., 2015; Knight and Schilling, 2006; Sauka-Spengler et al., 2008; Yu, 2010). As a multipotent cell type, the neural crest generates the peripheral nervous system, cardiomyocytes, melanocytes, and most of the craniofacial skeleton, among other tissues (Kunisada et al., 2014; Mayor and Theveneau, 2013; Sauka-Spengler and Bronner-Fraser, 2010). Neural crest cells are specified at the boundary between the neural and non-neural ectoderm (Baker and Bronner-Fraser, 1997a; Basch et al., 2006). They then undergo an epithelial-

to-mesenchymal transition, migrate, and collect into regions where they will terminally differentiate (Baker and Bronner-Fraser, 1997b; Hall, 2000; Knight and Schilling, 2006; Sauka-Spengler et al., 2008). In the anterior, cranial neural crest cells migrate in distinct streams to populate the reiterated pharyngeal arches. Within the pharyngeal arches neural crest cells are bounded by endodermal and ectodermal epithelia and surround a mesoderm core (Knight and Schilling, 2006).

Within the pharyngeal arch the neural crest rely on surrounding tissues, including all three germ layers, for proper patterning and morphogenesis (Couly et al., 2002; David et al., 2002; Kimmel et al., 2001; Knight and Schilling, 2006; Noden, 1983; Schilling et al., 2001; Seufert and Hall, 1990; Trainor and Krumlauf, 2000). Patterning of the neural crest along the anterior-posterior and dorsal-ventral axes is critical for craniofacial development and is regulated by numerous genes including Hox (Rijili et al., 1993; Trainor, 2003) and Dlx (Depew et al., 2002; Takechi et al., 2012; Talbot et al., 2010) genes, respectively. Similarly, numerous signaling molecules including BMP (Alexander et al., 2011), Shh (Eberhart et al., 2006; Wada et al., 2005), and Wnt (Alexander et al., 2014; Le Pabic et al., 2014) shape individual skeletal elements. Occurring simultaneously during morphogenesis is the terminal differentiation of these neural crest cells into cartilage or bone (Kobayashi and Kronenberg, 2014). The embryological craniofacial structures that will eventually form are called the viscerocranium and the neurocranium.

The general organization of the embryonic craniofacial skeleton includes the viscerocranium, which gives rise to all of the jaw, pharyngeal, and inner ear skeleton, and the neurocranium, which will give rise to the palate, skull base, and skull vault. The palate and skull base are connected and demarcated into pre- and postchordal structures, respectively. The postchordal neurocranium forms along the notochord, and the prechordal forms anterior of the notochord. In mouse, chick, *xenopus*, and axolotl, the neural crest will contribute to all of the viscerocranial elements as well as the prechordal neurocranium (Chai et al., 2000; Couly et al., 1993; Gross et al., 2008; Koentges and Lumsden, 1996; McBratney-Owen et al., 2008; Sefton et al., 2015). In chick and mouse, some regions of the postchordal neurocranium are also neural crest derived, forming connective sites with more anterior neural crest-derived structures (Koentges and Lumsden, 1996; McBratney-Owen et al., 2008). Studies in zebrafish confirm these findings (Crump et al., 2004; Eberhart et al., 2006; Wada et al., 2011), and a more in-depth analysis of the neural crest contributions to the zebrafish craniofacial skeleton will be reviewed later in more detail in this, and following, chapters. Regions of the craniofacial skeleton that are not generated by neural crest are mesoderm derived.

1.III.d. The cephalic mesoderm

While the neural crest give rise to most of the craniofacial skeleton, there is also contribution by the cephalic mesoderm (Couly et al., 1993; McBratney-Owen et al., 2008). In mouse and chick, the cephalic mesoderm forms most of the

postchordal neurocranium around the tip of the notochord, as well as the posterior skull vault, forming sutures with the neural crest-derived anterior skull vault (Couly et al., 1993; McBratney-Owen et al., 2008). These processes occur after much of the organogenesis of the brain and other tissues have ceased (Balczerski et al., 2012). Although we know what craniofacial structures the cephalic mesoderm gives rise to, we know little of the morphogenetic pathways that direct this formation.

All mesoderm derives from a population of endomesoderm at the beginning of gastrulation (Cooke, 1989). The prechondrogenic cephalic mesoderm is among this group of cells and all mesoderm undergoes cellular movements as gastrulation proceeds (David, 2015; Denoyelle et al., 2001; Dumortier and Rohde and Heisenberg, 2007). At the end of gastrulation, the prechondrogenic cephalic mesoderm forms abutting the notochord, where they begin chondrogenic differentiation via interactions with surrounding tissues, and in mouse, this occurs in a posterior to anterior fashion (McBratney-Owen et al., 2008). Like the neural crest, the cephalic mesoderm undergoes terminal chondrogenic differentiation. One of the few signaling pathways we know regulate the proper chondrogenic differentiation of the cephalic mesoderm is Shh (Balczerski et al., 2012). Early in development, *Shh* is initially expressed by the notochord, which later activates *Shh* in the ventral neural tube (Dessaud et al., 2008). Balczerski and colleagues showed that Shh from the notochord was the signaling source required for the activation of the prechondrogenic and chondrogenic genes *sox9a* and *col2a1a* in the cephalic mesoderm, respectively. In chapter 3, I will revisit the development of postchordal neurocranial, adding the Fgf signaling pathway as an important contributor to this process.

1.III.e. Zebrafish craniofacial development and anatomy

Zebrafish undergo similar events shared by all vertebrates that culminate into the formation of the head. In zebrafish, gastrulation begins at 6 hours post fertilization (hpf) and ends at 10 hpf. At this time point, precursors of the cephalic mesoderm have migrated to the notochord (Hammerschmidt et al., 2004), and the neural crest is being specified at the dorsal neural tube (Baker and Bronner-Fraser, 1997a; Knight and Schilling, 2006). At 12 hpf, the cranial neural crest begin migrating and will populate the pharyngeal arches beginning at approximately 24 hpf (Eberhart et al., 2008). Here, they will undergo numerous genetic and morphogenetic programs to give rise to the embryonic structures of the craniofacial skeleton.

In zebrafish, the craniofacial skeleton is readily observed as early as 4 days post fertilization (Fig. 1.4; Schilling and Kimmel, 1997). The neurocranium can be split into prechordal and postchordal structures (Fig. 1.4). The prechordal structures include the ethmoid plate and the trabeculae, collectively called the palate (Fig. 1.4; Schilling and Kimmel, 1997; Swartz et al., 2011). The postchordal neurocranium is composed of the parachordals, the anterior basicapsular commissures, the posterior basicapsular commissures, the lateral commissures, the auditory capsule, and the occipital arches (Fig. 1.4; Schilling and Kimmel, 1997; van de beer, 1934).

The viscerocranium is composed of numerous cartilage elements including Meckel's cartilage, palatoquadrate, hyosymplectic, interhyal, ceratohyal, and ceratobranchial (Schilling and Kimmel, 1997). The first pharyngeal arch will give rise to the Meckels cartilage and the palatoquadrate, as

well as the ethmoid plate and trabeculae (Fig. 1.4; Crump et al., 2004), while the second arch will give rise to the hyosymplectic, interhyal and ceratohyal (Fig. 1.4), and the more posterior arches (3-7) giving rise to the ceratobranchial cartilages (not shown). The postchordal neurocranium is primarily derived from cephalic mesoderm in all species examined, with data in zebrafish shown in chapter 3.

1.IV. Growth factor signaling in craniofacial development

Numerous genetic pathways regulate proper craniofacial development including both the Platelet-derived growth factor (Pdgf) and Fibroblast growth factor (Fgf) signaling families. Growth factor signaling pathways share common attributes including receptor activation and signal transduction (Fambrough et al., 1999; Pawson and Scott, 1997). The general makeup of a growth factor signaling pathway involves receptors and their ligands. The receptors are transmembrane, hosting an extracellular domain required for ligand binding, and an intracellular cytoplasmic domain that functions in signal transduction (Pawson and Scott, 1997). Most growth factor receptors dimerize to function, which is activated by dimerization of ligands. After ligand binding, receptors auto-phosphorylate each other on their intracellular tyrosine kinase domains. This promotes the activation of multiple downstream pathways involved in a diversity of cellular functions including cellular migration, proliferation, morphogenesis, patterning, and survival (Lemmon and Schlessinger, 2010; Pawson and Scott, 1997; Tallquist and Kazlauskas, 2004). While numerous growth factor signaling pathways are

involved in proper craniofacial development, here, I will focus specifically on the Pdgf and Fgf signaling pathways.

1.IV.a. Platelet-derived growth factor signaling

The platelet-derived growth factor signaling family is composed of two receptors, alpha and beta, with four ligands in mouse and humans and six in zebrafish (Eberhart et al., 2008; Hoch and Soriano, 2003; Tallquist and Kazlauskas, 2004). The receptors can both homo- and heterodimerize and have ligand-preference for activation (Tallquist and Kazlauskas, 2004). Pdgfr's contain two intracellular tyrosine kinase domains that can activate numerous intracellular pathways, namely PI3K, PLCg, Ras, and Src (Klinghoffer et al., 2002; Tallquist and Kazlauskas, 2004). Although both *Pdgfra* and *Pdgfrb* have similar intracellular activation domains, they function differently in development.

Numerous genetic mutants have been generated to uncover the varying functions of the Pdgf receptors. Null mutants of both *Pdgfra* and *Pdgfrb* are embryonic lethal (Soriano, 1994; Soriano, 1997) and display differing phenotypes. *Pdgfra* knockout mice have severe developmental deficits, including those affecting heart, vertebrae, and craniofacial tissues (Soriano, 1997). Loss of the PI3K-activating tyrosine site of *Pdgfra* leads to phenotypes most similar to the null (Klinghoffer et al., 2002), suggesting that PI3K is the effector most vital for *Pdgfra* function in development. *Pdgfrb* knockout mice have defects in vasculogenesis, as well as defects in kidney and heart formation (Soriano, 1994). Of the two Pdgf receptors, *Pdgfrb* seems dispensable for proper craniofacial development. However, *Pdgfra*;*Pdgfrb* PI3K double mutants have defects closely mirroring the *Pdgfra* null knockout (Klinghoffer et al., 2002). The mechanism of

this interaction is still unclear and is the focus of chapter 4. How *Pdgfra* functions in the cranial neural crest, however, has been much more extensively studied.

In both mouse and zebrafish, *Pdgfra* is expressed in the migrating cranial neural crest (Eberhart et al., 2008; Liu et al., 2002; Schatteman et al., 1992), and reduced *Pdgfra* function results in cleft palate (Eberhart et al., 2008; Klinghoffer et al., 2002; Tallquist and Soriano, 2003). Furthermore, in humans, *PDGFRA* has been linked to congenital cleft palate (Rattanasopha et al., 2012). These data suggest a strong conservation of gene function across species. Mechanistically, palatal clefting is due to a neural crest migration defect in both mice and zebrafish (Eberhart et al. 2008, Vesudevan and Soriano, 2014), where the most anterior neural crest cells fail to properly populate the first pharyngeal arch (Eberhart et al., 2008). *Pdgf* ligands act as chemoattractants to the *pdgfra*-expressing neural crest, and this allows for proper neural crest migration (Eberhart et al., 2008). In these genetic analyses, the functions of *Pdgfra* are observed when the environmental conditions are optimal. When placed in stressed conditions, such as ethanol, *Pdgfra* plays a second role in the neural crest beside migration, namely survival. This is the focus of chapter 2.

1.IV.b. Fibroblast growth factor signaling

Fibroblast growth factors (Fgf's) are part of a large family of intercellular signaling molecules that consists of 4 receptors in all vertebrates with 22 ligands in mouse and human and 27 ligands in zebrafish (Itoh, 2007). They are crucial throughout development (Carter et al., 2014; Ornitz and Itoh, 2001; Thisse and Thisse, 2005), including neural and mesoderm induction and specification (Sivak et al., 2005), cartilage homeostasis (Ellman et al., 2013), as well as numerous aspects

of craniofacial development. For example, Fgf3 and Fgf8 are required for proper migration, survival, and patterning of the neural crest (Creuzet et al., 2004; Crump et al., 2004). Multiple Fgf receptors are implicated in cranial suture formation (Nie et al., 2006; Rice et al., 2000) and, furthermore, Fgfs are implicated in a number of congenital craniofacial disorders with reported skull base defects including Aperts, Crouzon, and DiGeorge Syndromes (Tokumaru et al., 1996; Aggarwal et al., 2006). While Fgfs function in early mesoderm induction, specification, and migration (Ornitz and Itoh, 2001; Sivak et al., 2005; Thisse and Thisse, 2005), no known role has been determined in the later-forming cephalic mesoderm. This is the focus of chapter 3.

1.V. Outline of dissertation

The main goal of my dissertation research was to identify and characterize gene-ethanol interactions. In short, I found that genes involved in growth factor signaling are especially vulnerable to ethanol teratogenesis. I focused on elucidating the ethanol interaction with *platelet-derived growth factor receptor alpha (pdgfra)*, and, through this work, uncovered a second ethanol-interacting gene *fibroblast growth factor 8a (fgf8a)*. Due to the nature of the *fgf8a*-ethanol interaction, I then focused my efforts in elucidating the function of Fgfs in craniofacial development.

In an initial ethanol-sensitivity screen using known craniofacial mutants, we found a synergistic interaction between ethanol and *pdgfra*. Using a number of different assays, I found an increase in cranial neural crest cell death in ethanol-treated *pdgfra* mutants, and that *pdgfra* protects against this cell death via activation of the PI3K/AKT/mTOR pathway. I developed a two-hit model of

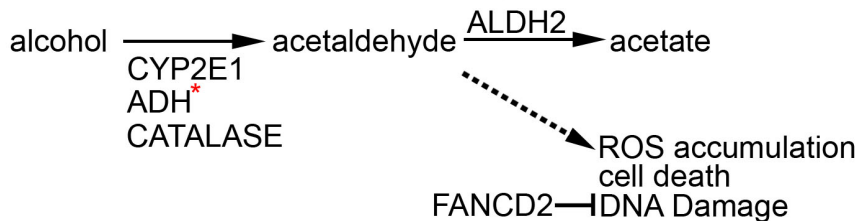
ethanol teratogenesis, where subteratogenic levels of ethanol and suboptimal levels of growth factor signaling synergize to cause FASD.

Building on the hypothesis that reduced growth factor signaling predisposes to ethanol-induced defects, we tested a different growth factor signaling gene, *fgf8a*. It interacted with ethanol to cause a completely different craniofacial defect than that observed with *pdgfra* and ethanol. It caused the postchordal neurocranium to be lost. Due to the nature of this phenotype, I was interested in understanding the function of Fgfs in postchordal neurocranial development. Using a number of genetic, cell tracking, and *in situ* hybridization assays, I uncovered a hierarchy of genetic signaling pathways regulating the formation of the postchordal neurocranium. This involved Fgfs functioning in specification of the mesoderm precursors of this structure, and Shh functioning in later differentiation.

Lastly, I wanted to revisit the function of Pdgf signaling in craniofacial development. There are two Pdgf receptors, alpha and beta, and it was unclear whether ethanol interacted with *pdgfra* alone to cause the exacerbated craniofacial defects, or whether ethanol broadly attenuated all Pdgf signaling, including *pdgfrb*. Using double *pdgfra;pdgfrb* mutants, we tested whether dual loss of *pdgfra* and *pdgfrb* could phenocopy the ethanol-treated *pdgfra* mutant phenotype. Indeed, we found that *pdgfra* and *pdgfrb* synergistically function in craniofacial development. I am currently determining the mechanism of this genetic interaction.

1.VI. Figures

wildtype maternal/zygotic genotype



maternal: ALDH2^{+/-};FANCD2^{+/-}
zygotic: ALDH2^{-/-};FANCD2^{-/-} or ALDH2^{+/-};FANCD2^{-/-}

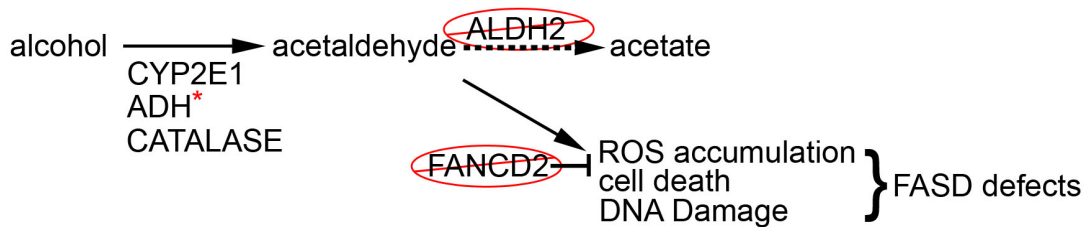


Figure 1.1: Ethanol metabolism leads to cell-damaging reactive oxygen species (ROS), increased DNA damage, and cell death; a problem exacerbated by *Fancd2* deficiency. (Top panel) In wildtype animals, alcohol is catabolized to acetaldehyde, a potentially harmful degradation product. Its accumulation is prevented by further enzymatic degradation to acetate (represented by the solid line), via alcohol dehydrogenase 2 (Aldh2). The proper function of Aldh2 also prevents accumulation of reactive oxygen species (ROS), cell death, and DNA damage (represented by the dashed line). Furthermore, *Fancd2* functions in repairing DNA damage that may accrue during alcohol exposure. (Bottom panel) In *Aldh2*;*Fancd2* double mutant fetuses carried by double heterozygous dams,

acetaldehyde is not degraded (represented by the dashed line), yielding an increase in ROS, cell death and DNA damage (represented by the solid line). Loss of Fancd2 may increase risk of DNA damage, and, with the effects of acetaldehyde accumulation, lead to FASD-like defects. Double-cross denotes members of the pathway implicated in ethanol-teratogenesis in human studies.

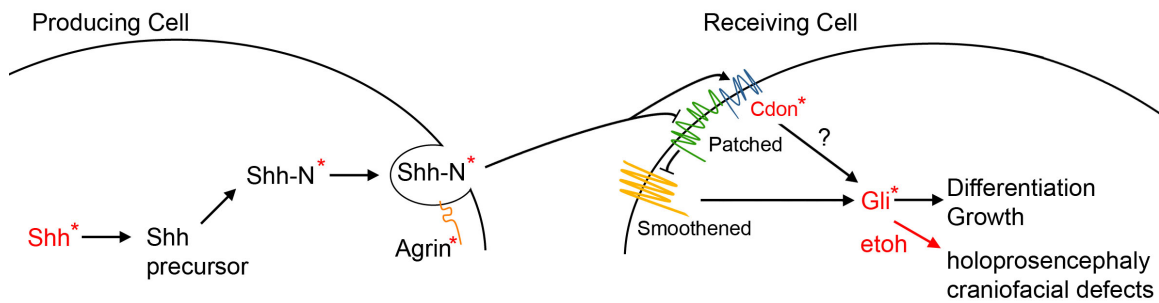


Figure 1.2: Ethanol has been shown to interact with several members of the Shh signaling pathway (denoted in red). In the producing cell, Shh mRNA is first translated into a precursor protein, which is then modified via glycosylation (Shh-N). Shh-N is then packaged into lipid raft domains, in which Agrin also gets packaged, and is then shipped extracellularly to the receiving cell. Shh-N binds to Patched, which releases Smoothed to activate Gli transcription factors. Cdon is a co-receptor of Patched. Ethanol causes holoprosencephaly and craniofacial defects in *Cdon* mutant mouse embryos and heterozygous *Gli2* and *Shh* mice (Keitzman et al., unpublished, red arrow). Injection of *shh* or *agrin* morpholinos results in ocular defects in zebrafish. Asterisks denote members of the pathway implicated in ethanol-teratogenesis.

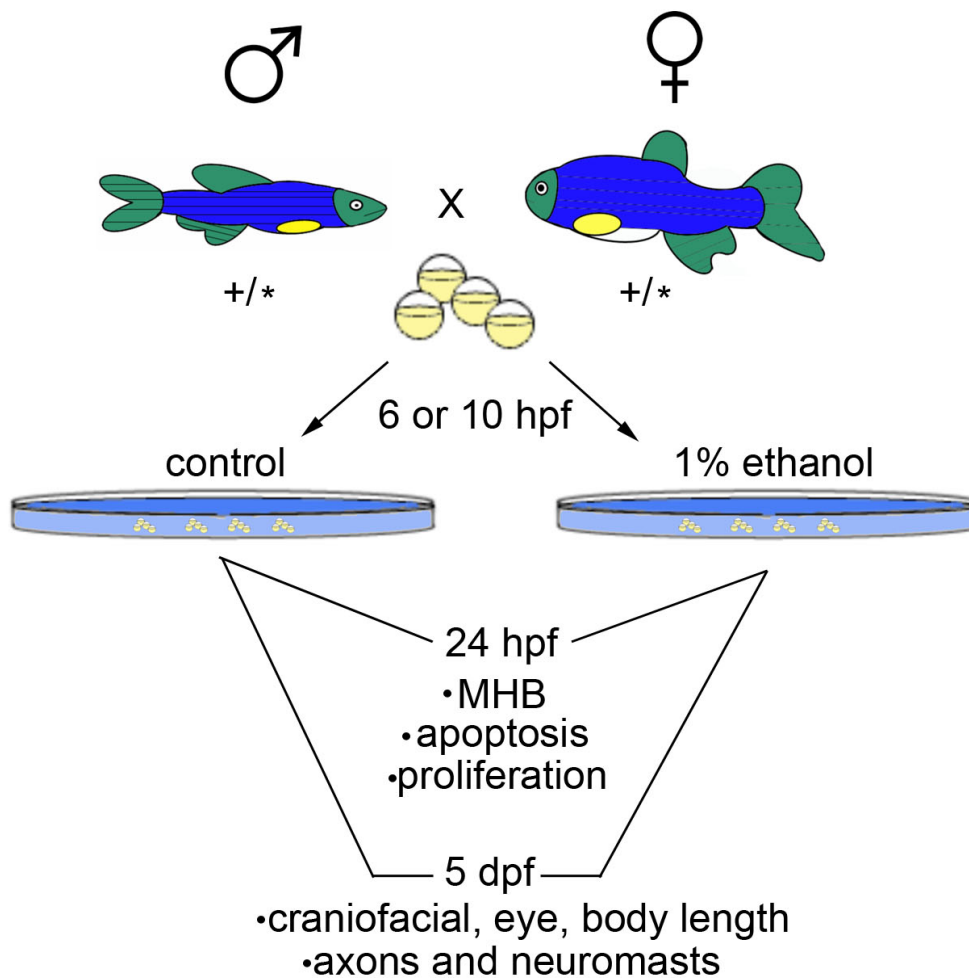


Figure 1.3: Zebrafish screen to uncover gene-ethanol interactions. To test for ethanol sensitive genes, zebrafish with known mutations (marked by asterisk) were interbred to give rise to clutches that will be composed of wildtype, heterozygous, and mutant offspring. These were split into two groups, one treated with 1% ethanol at various times, and tested for ethanol sensitivity of

various morphological attributes at 24 hours post fertilization and/or 5 days post fertilization.

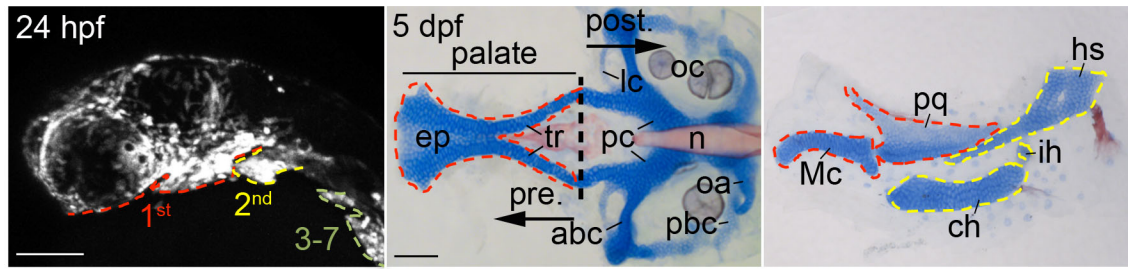


Figure 1.4: The zebrafish cranial neural crest and craniofacial skeleton. The panel on the far left shows a 24 hour post fertilization embryo labeling neural crest cells in white. These neural crest cells are formed into pharyngeal arches labeled 1-7. At 5 days post fertilization, zebrafish neural crest cells will give rise to corresponding neurocrania (middle panel) and viscerocrania (right panel) marked by coloration (red=first arch, yellow=second arch). The neurocranium is separated into prechordal (pre.) and postchordal (post.) regions, respectively. The prechordal neurocranium is called the palate. abc= anterior basicapsilur commissure, ch=ceratohyal, hs=hyosymplectic, ep=ethmoid plate, hs=hyosymplectic, ih=interhyal, lc=lateral commissure, Mc=Meckels cartilage, n=notochord, oa= occipital arch, pbc= posterior basicapsilur commissure, pc=parachordals, pq=paraquadrate, tr=trabeculae.

Chapter 2: *Pdgfra* protects against ethanol-induced craniofacial defects in a zebrafish model of FASD. (McCarthy et al., 2013)

2.1. Abstract

Human birth defects are highly variable and phenotypic variability can be influenced by both the environment and genetics. However, the synergistic interactions between these two variables are not well-understood. Fetal Alcohol Spectrum Disorders (FASD) is the umbrella term used to encompass the wide range of outcomes following prenatal alcohol exposure. While FASD are caused by prenatal ethanol exposure, FASD are thought to be genetically modulated, although the genes regulating sensitivity to ethanol teratogenesis are largely unknown. In a small shelf screen for ethanol susceptibility loci, we found that *platelet-derived growth factor receptor alpha (pdgfra)* interacted synergistically with ethanol during zebrafish craniofacial development. Analysis of the PDGF family in a human FASD genome-wide dataset links *PDGFRA* to craniofacial phenotypes in FASD, prompting a mechanistic understanding of this interaction. In zebrafish, untreated *pdgfra* mutants have cleft palate due to defective neural crest cell migration, while *pdgfra* heterozygotes develop normally. Ethanol-exposed *pdgfra* mutants have profound craniofacial defects that include the loss of the palatal skeleton and hypoplasia of the pharyngeal skeleton. Furthermore, ethanol treatment revealed latent haploinsufficiency, causing palatal defects in approximately 62% of *pdgfra* heterozygotes. Neural crest apoptosis partially

underlies these ethanol-induced defects in *pdgfra* mutants, demonstrating a protective role for Pdgfra. The PI3K/mTOR pathway mediates the protective functions of Pdgfra. Collectively, our results suggest a model where combined genetic and environmental inhibition of PI3K signaling leads to variability within FASD.

2.II. Introduction

Phenotypic variability is typical in human disorders. This variability can be caused by a combination of genetic and environmental factors. While we have gained insight into these separate genetic and environmental influences, the synergistic interactions between the two are largely unknown. We sought to understand these interactions by examining the effects of embryonic alcohol exposure on craniofacial development using a zebrafish model.

Fetal alcohol spectrum disorders (FASD) encompass the range of defects associated with prenatal exposure to ethanol. By some estimates, FASD affect somewhere from 1% of the North American population (Sampson et al., 1997) to 2-5% of the United States and Western Europe (May et al., 2005; May et al., 2007). Defects and deficits associated with FASD are variable and lie along a continuum with the most severe form represented by Fetal Alcohol Syndrome (FAS), which is clinically diagnosed by growth retardation, deficiencies in brain growth (reduced head circumference and/or structural brain anomaly), and distinct facial features (microcephaly, short palpebral fissures, thin upper lip, and/or smooth philtrum) (Jones and Smith, 1973). Other craniofacial defects can arise in FAS, including cleft palate (Swayze et al., 1997). The variability of the defects found in FAS and FASD are partly attributed to the timing and dosage of fetal exposure to ethanol (Ali et al., 2011; Sulik, 2005; Sulik et al., 1986).

However, genetic factors are also likely to influence FASD, yet these influences are poorly understood.

Several lines of evidence suggest a genetic component to FASD (Warren and Li, 2005). Different strains of mice, rats, chickens and zebrafish show differing sensitivity to ethanol exposure (Boehm et al., 1997; Debelak and Smith, 2000; Dlugos and Rabin, 2003; Thomas et al., 1998). Recently, work in mouse has shown that the Hh pathway gene, *Cdon*, interacts with ethanol (Hong and Krauss, 2012). The Hh pathway has also recently been shown to interact with ethanol during zebrafish neural development (Zhang et al., 2013). In humans, the most compelling evidence for a genetic component to FASD is twin studies showing greater concordance for FAS between monozygotic than for dizygotic twins (Streissguth and Dehaene, 1993). In a small South African cohort, resistance to FAS associates with carrying the alcohol dehydrogenase (ADH) B*2 allele, which catabolizes alcohol at a faster rate than other ADH isozymes (Viljoen et al., 2001). Together, these studies provide evidence for gene-environment interactions being involved in susceptibility to FASD.

The zebrafish provides an excellent model system in which to study gene-ethanol interactions. Zebrafish eggs are fertilized externally, simplifying the analysis of zygotic genes that interact with ethanol. Furthermore, this external development allows for the precise timing and dosage of ethanol exposure. Zebrafish embryos display FASD defects when exposed to ethanol and the effects of ethanol timing and dosage have been well studied in zebrafish as far

back as 1910 (Ali et al., 2011; Arenzana et al., 2006; Dlugos and Rabin, 2003; Lockwood et al., 2004; Loucks and Carvan, 2004; Stockard, 1910). Yet we know very little about how genetic factors influence ethanol-induced phenotypes, such as perturbations of proper craniofacial development.

In all vertebrate species, the majority of the craniofacial skeleton derives from the cranial neural crest (Couly et al., 1993; Evans and Noden, 2006; Gross and Hanken, 2008; Knight and Schilling, 2006; LeLievre, 1978; Noden, 1978; Yoshida et al., 2008). Neural crest cells are generated between neural and non-neural ectoderm. Neural crest cells undergo an epithelial-to-mesenchymal transition, which allows them to migrate into the periphery to form a wide variety of cell types (Theveneau and Mayor, 2012). In cranial regions these cells will migrate into serially reiterated structures called pharyngeal arches (Grevellec and Tucker, 2010). In the zebrafish, this occurs beginning at 10 hours post fertilization (hpf), and ends around 30 hpf (Eberhart et al., 2008). Morphogenetic processes within the pharyngeal arches will eventually shape the craniofacial skeleton by 5 days post fertilization (dpf). In the zebrafish, the first pharyngeal arch contributes to jaw structures including Meckel's cartilage and the palatoquadrate, as well as palatal elements, including the ethmoid plate and trabeculae (Cubbage and Mabee, 1996; Kesteven, 1922; Shah et al., 1990; Swartz et al., 2011). The second arch contributes to the jaw support skeleton including the hyosymplectic, ceratohyal and interhyal.

From genetic screens and cell lineage analyses, a great deal has been learned concerning the genetic pathways controlling the development of these craniofacial elements. Numerous signaling pathways regulate craniofacial development, including the Platelet-derived growth factor (Pdgf) signaling pathway. *Pdgfra* is a receptor tyrosine kinase, known to regulate a number of processes including cellular migration, proliferation, and survival (Tallquist and Kazlauskas, 2004; Wu et al., 2008). A key effector of *Pdgfra* signaling is PI3K, which can regulate numerous cell behaviors, including migration via activation of small GTPases and survival and growth via activation of mTOR (Downward, 2004; Klinghoffer et al., 2002; Zhou and Huang, 2010). In both mouse and zebrafish, most, if not all, cranial neural-crest cells express *Pdgfra* and *Pdgfra* function is required in the neural crest (Eberhart et al., 2008; Soriano, 1997; Tallquist and Soriano, 2003). While the precise function of *Pdgfra* is not known in mouse, in zebrafish *Pdgfra* is necessary for proper neural crest cell migration (Eberhart et al., 2008).

The work described here uncovers a second role for *pdgfra* in the neural crest: protection against ethanol-induced teratogenesis. Testing five craniofacial mutants, *cyp26b1*, *gata3*, *pdgfra*, *smad5*, and *smoothened*, for dominant enhancement of ethanol teratogenesis we found that only *pdgfra* heterozygotes and mutants showed enhanced craniofacial defects after ethanol exposure. In a small human dataset with variable prenatal alcohol exposure, we find support for a gene-ethanol interaction with single nucleotide polymorphisms (SNPs) in PDGF

family members associating with different craniofacial phenotypes. In zebrafish, the susceptibility to craniofacial defects is at least partly due to neural crest cell apoptosis following ethanol exposure. The *pdgfra*-ethanol interaction is due to the combined genetic and environmental attenuation at or downstream of the mechanistic target of rapamycin (mTOR), part of the Phosphoinositide 3 kinase (PI3K) pathway. Collectively, our data show that genetic screens using zebrafish will have important implications in FASD research, both in uncovering genetic susceptibility loci and in characterizing the mechanisms underlying gene-ethanol interactions.

2.III. Results

2.III.a. *pdgfra* and ethanol synergistically interact

We sought to identify gene-ethanol interactions that might underlie the craniofacial variability observed in FASD. We reasoned that some genetic loci that influence ethanol teratogenicity would cause craniofacial phenotypes when mutated. We initially screened five craniofacial mutants for ethanol sensitivity: *smo*^{b577}, *cyp26b1*^{b1024}, *gata3*^{b1075}, *smad5*^{b1100} and *pdgfra*^{b1059}. For this initial screen, embryos were placed in media containing 1% ethanol from 6 hours post fertilization (hpf) until 5 dpf, when craniofacial phenotypes were examined. At this concentration, the tissue levels of ethanol are approximately 41 mM (188.6 mg/dL or 0.18 BAC), as determined by headspace gas chromatography, and wild-type embryos are largely unaffected. This is a concentration of ethanol

achieved in binge drinkers (Lange and Voas, 2000). We found no clear differences in phenotypes between ethanol-treated and untreated *smo*, *cyp26b1*, *gata3* or *smad5* mutants nor any indication that ethanol caused haploinsufficiency in heterozygotes. In contrast, ethanol appeared to interact synergistically with the hypomorphic *pdgfra*^{b1059} allele, dramatically exacerbating mutant phenotypes and uncovering latent haploinsufficiency (Figs., 2.1 and 2.2, discussed in greater detail below). We partially rescued these ethanol-induced defects by elevating *Pdgfra* levels via *pdgfra* mRNA injection or morpholino knockdown of *miR140*, which negatively regulates *pdgfra*, (Fig. 2.3, Fig. 2.4, Eberhart et al., 2008), demonstrating specificity of the interaction. The variability that we observed in these rescues was consistent with the variation that we previously observed in rescuing untreated *pdgfra* mutants and our finding that the craniofacial skeleton is highly sensitive to the overall levels of *Pdgfra* (Eberhart et al., 2008). There are also likely to be between embryo differences in signal strength downstream of the receptor, such as altered *Pten* function, which would impact negative feedback into the signaling pathway (Carracedo and Pandolfi, 2008) to add to the inherent variability in these rescue experiments. Collectively, these results show that ethanol interacts with a subset of gene products involved in craniofacial development.

Untreated *pdgfra* mutants have a loss of the ethmoid plate which leads to a significant reduction in the length of the palate (Fig. 2.1C, asterisk, Fig. 2.5) and have slightly smaller pharyngeal skeletal elements (Fig. 2.2C,G-I, Table 2.1).

Untreated heterozygous siblings develop normally (Fig. 2.1B, Fig. 2.2B,G-I, Fig. 2.5, Table 2.1). Treatment with 1% ethanol from 10 hpf to 5 dpf had a minor effect on the neurocranium of wild-type embryos, with 11% of treated wild types having a reduced ethmoid-plate (Fig. 2.1D,G) and the overall length of the palate was not significantly reduced (Fig. 2.5). Treated wild-type embryos displayed a slightly smaller hyosymplectic (Fig. 2.2I, Table 2.1) cartilage, however, Meckel's cartilage and the palatoquadrate appeared unaffected (Fig. 2.2G,H and Table 2.1). Statistical analyses of the size of these elements showed that, indeed, only the hyosymplectic was reduced by ethanol.

Ethanol-treatment caused craniofacial defects in 62% of *pdgfra* heterozygotes (Fig 2.1E,G), a dramatic increase compared to 11% of wild-type embryos with an identical treatment. Because heterozygous embryos rarely have craniofacial defects, this substantial increase in the number of embryos with craniofacial defects is specific to the *pdgfra*/ethanol interaction. The defects observed included gaps in the ethmoid-plate (asterisk and arrow in Fig. 2.1E) and breaks in the trabeculae (arrowheads in Fig. 2.1E). Ethanol-treated heterozygotes also displayed significantly shorter palates when compared to untreated heterozygotes and ethanol-treated wildtypes (Fig. 2.5A).

Heterozygosity for *pdgfra* alone had no effect on the size of the palatal skeleton and ethanol caused a slight, nonsignificant, reduction to the palate in wild-type siblings (Fig. 2.5A). The palatal skeleton was significantly reduced in ethanol-treated *pdgfra* heterozygotes, compared to these two comparison groups.

Therefore, ethanol has a specific synergistic effect on palatal development in *pdgfra* heterozygotes. Furthermore, ethanol caused a statistically significant reduction in the size of the hyosymplectic cartilage in heterozygotes compared to ethanol-treated wildtypes and untreated heterozygotes (Fig. 2.2E,I and Table 2.1). Because the hyosymplectic is reduced in ethanol treated wild-type embryos and untreated heterozygotes, this effect appears additive. These results show that the *pdgfra* and ethanol interact synergistically in palatal development and that the hyosymplectic is further reduced in ethanol-treated *pdgfra* heterozygotes as compared to treated wild-type embryos.

In 100% of treated *pdgfra* mutants, as compared to approximately 10% of untreated mutants, the anterior neurocranium was completely lost (Fig. 2.1F). Not surprisingly, this loss led to a statistically significant decrease in the length of the palate, relative to treated wild-type embryos and untreated mutants (Fig. 2.5). The ethanol-treated mutant embryos also had a statistically significant reduction of the palatoquadrate, Meckel's cartilage, and the hyosymplectic compared to untreated mutant and ethanol-treated wild-type and heterozygotes (Fig. 2.2F,G-I, and Table 2.1). All of the reductions observed in the ethanol-treated mutants are far beyond that predicted by an additive effect of ethanol-treatment in wild-types and loss of *pdgfra* without ethanol. Ectodermal and cardiac edema was also present in 100% of treated *pdgfra* mutants (not shown). Collectively, these results provide strong support that *pdgfra* and ethanol synergistically interact during craniofacial development.

The severity and variability of ethanol-induced defects is partly dependent on concentration and developmental timing (Ali et al., 2011; Sulik, 2005). Therefore, we tested these variables across ethanol-treated *pdgfra* genotypes. We initially tested 24-hour time windows for sensitivity and then narrowed down the sensitive window. While treatments initiating after 24 hpf had no effect, we found that a 1% ethanol treatment from 10-24 hpf is the shortest time window sufficient to fully recapitulate the mutant phenotypes obtained by treatment from 10 hpf to 5 dpf (Fig. 2.1G, Fig. 2.2G-I, Fig. 2.5, Table 2.1). In heterozygotes this shorter exposure still lead to significant differences in the neurocranium, in fact the difference in length between the treated wild-type and heterozygous embryos was even more marked (Fig. 2.1G, Fig. 2.5). No significant alterations to the hyosymplectic were observed (Fig. 2.2G-I, Table 2.1). These results suggest that the palatal skeleton is most sensitive to brief ethanol exposure.

We tested lower ethanol concentrations to determine how sensitive *pdgfra* mutants and heterozygotes were to ethanol teratogenesis. Treatment with 0.5% ethanol, a tissue concentration of 19 mM (88 mg/dL), from 10 hpf to 5 dpf caused neurocranial defects in 3% and 13% of wild-type and heterozygotes, respectively (Fig. 2.1G). Under these conditions, 38% of *pdgfra* mutants completely lacked the palatal skeleton (Fig. 2.1G). This clear increase in the percentage of heterozygous and mutant embryos with palatal defects, is associated with reductions in the size of the crest-derived cartilages (Fig. 2.2G-I, Table 2.1), although these differences did not reach a level of significance. Shorter

treatments with 0.5% ethanol had no apparent effect (data not shown). Thus, attenuation of Pdgf signaling sensitizes embryos to ethanol-induced craniofacial defects, and this sensitivity occurs roughly when neural crest cells are migrating to and populating the pharyngeal arches, although migration does continue after 24 hpf in zebrafish palatal development (Dougherty et al., 2013).

We analyzed non-crest-derived cartilages to determine if ethanol had a general effect on cartilage development. First, we examined the posterior neurocranium because it is of presumed mesoderm origin. Surprisingly, we discovered a previously undescribed function of *Pdgfra* in posterior neurocranial development, with the size of the posterior neurocranium significantly reduced in untreated mutants, relative to wild-type embryos (Fig. 2.5). This requirement may relate to the requirement for *Pdgfra* function for migration and survival of early mesoderm precursors (Van Stry et al., 2005; Van Stry et al., 2004). As then would be expected, ethanol did interact with *pdgfra* in the development of these cartilages (Fig. 2.5) to generate an overall effect of microcephaly. Second, we analyzed cartilage of the pectoral fin and found no difference between ethanol-treated mutants, ethanol-treated wild-type embryos and untreated mutants (Fig. 2.6). This result suggests that there is no generalized chondrogenic defect in the ethanol-treated *pdgfra* mutants. Consistent with this, we found that *coll1a* was expressed appropriately in the posterior neurocranium of ethanol-treated mutants, although, as expected from the phenotype, no ethmoid plate or trabeculae condensations were present (Fig. 2.7). Collectively, these findings

show that proper development of the entire neurocranium requires *Pdgfra* function and that ethanol interacts synergistically with *pdgfra* having the most profound effects on the neural crest-derived skeleton, which we focus on here.

The regulation and function of Pdgf signaling is highly conserved across vertebrate species, prompting us to seek evidence from a published human sample (Jones et al., 2006) for interactions between PDGF family members and prenatal ethanol exposure. We asked whether there was evidence for ethanol usage/SNP interaction on human craniofacial features. We tested members of the human PDGF family, including *PDGFB*, *PDGFC*, *PDGFD*, *PDGFRA* and *PDGFRB*, using a well-characterized sample from the US (See Table 2.2 for a complete list of the SNPs analyzed) (Mattson et al., 2010; Moore et al., 2007). Due to the small size of *PDGFA* (12,700 bp), no SNPs were genotyped or analyzed in this gene. The best evidence for gene-ethanol interactions in humans was found in the two PDGF Receptor genes. The most significant evidence for a gene-ethanol interaction was observed with 2 SNPs in *PDGFRB*, when analyzing midfacial depth (rs2304061; $p=3.7 \times 10^{-6}$ and rs1075846; $p<3.5 \times 10^{-5}$). These SNPs are in modest linkage disequilibrium ($r^2=0.57$). These SNPs were also moderately associated with lower facial depth (both $p<9.9 \times 10^{-4}$). In addition, a single SNP in *PDGFRA* was associated with the measures of outer canthal width and midfacial depth ($p=1.3 \times 10^{-4}$ and $p=1.7 \times 10^{-4}$). Together, these results provide evidence that zebrafish gene-ethanol interactions may be conserved in humans.

2.III.b. Neural crest cell apoptosis increases in ethanol-exposed *pdgfra* mutants.

High doses of ethanol can cause neural crest cell apoptosis (Cartwright and Smith, 1995; Sulik, 2005), and Pdgf signaling has been implicated in mesoderm-cell survival (Van Stry et al., 2005). We postulated that the craniofacial defects in ethanol-treated mutants and heterozygotes could be due, at least in part, to an increase in cranial neural crest cell death. In support of this model, treating *pdgfra* mutants with ethanol and caspase-inhibitor III partially rescued the ethanol-induced craniofacial defects (Fig. 2.8G, compare to Fig. 2.1C,F). We do not expect a full rescue with this treatment, because clefting of the ethmoid plate is due to a migratory defect (Eberhart et al., 2008). Thus, this partial rescue supports the model in which elevated apoptosis underlies some of the effect of ethanol on *pdgfra* mutants.

We directly determined the levels of apoptosis using anti-active caspase immunohistochemistry in the neural crest cell labeling *fli1:EGFP* transgenic line. We quantified neural crest cell death in the first and second arch at 20 and 24 hpf, encompassing the developmental time window in which *pdgfra* mutants are most sensitive to ethanol (Fig. 2.8A-D and A'-D'). We did not observe any increase in cell death in ethanol-treated groups at 20 hpf compared to untreated controls (not shown). At 24 hpf, there were low levels of neural crest cell death in all untreated genotypes, ranging from 1-2 cells/side of the embryo (Fig. 2.8E). The frequency of cell death was slightly increased in ethanol-treated wild-type

embryos (3.4 cells/side) and further increased in ethanol-treated heterozygotes (4.79 cells/side, Fig. 2.8E), although this effect was not clearly synergistic. In ethanol-treated *pdgfra* mutants, we found a statistically significant and non-additive increase in apoptosis compared to all other groups (Fig. 2.8E, 10.3 cells/side, tukey test *p-value=<0.01). In all ethanol-treated genotypes, there were frequently non-*fli1:GFP*-positive cells undergoing apoptosis just dorsal to the first arch, in the relative position of the trigeminal ganglion. There were, however, no global elevations in apoptosis at 24 hpf between ethanol-treated mutants and sibling counterparts compared to their untreated mutants and siblings (Fig. 2.9), suggesting that the *pdgfra*-ethanol interaction leads to an increase in neural-crest specific cell death. Quantification of the ratio of cell death compared to total cells showed a linear increase in all ethanol-treated groups at 24 hpf (Fig. 2.8F). Ethanol-treatment did not reduce cell proliferation at 24 hpf in *pdgfra* mutants relative to untreated controls, however, we did observe a rise in cell proliferation in wild-type embryos (Fig. 2.10). This rise in proliferation may compensate for the slight increase of cell death at this time.

While *pdgfra* mutants are most sensitive to ethanol from 10-24 hpf, the effects of ethanol could potentially continue after the treatment. Therefore, we analyzed cell death after a 6-hour recovery period from ethanol. Strikingly, we observed a significant and synergistic increase in cell death at 30 hpf, after ethanol was removed at 24 hpf in *pdgfra* mutants (14.2 cells/side, tukey test *p-value=<0.01, Fig 2.8E). The trend for elevated cell death in *pdgfra*

heterozygotes, seen at 24 hpf, was abolished with just 6 hours recovery (Fig. 2.8E,F). This timing of 24-30 hpf correlates with when *Pdgfra* ligands begin to be expressed in the epithelia adjacent to the neural crest (Eberhart et al., 2008). These data suggest that *pdgfra* protects against ethanol-induced neural crest cell death during neural crest condensation in the arches, and may be a compensatory mechanism against ethanol-induced cell death following ethanol exposure.

Detailed fate maps of the pharyngeal arches in the zebrafish at 24 hpf allow us to directly compare the location of cell death to the skeletal structures disrupted across ethanol-treated *pdgfra* genotypes. At 24 hpf, neural-crest cells condensing on the roof of the oral ectoderm contribute to most of the anterior neurocranium (Crump et al., 2006; Eberhart et al., 2006). Also, cells located dorsally in the 1st and 2nd pharyngeal arches contribute to the palatoquadrate and hyosymplectic (Crump et al., 2004; Crump et al., 2006; Eberhart et al., 2006). These are the skeletal elements that were reduced to the greatest extent in ethanol-treated *pdgfra* mutants, and increased cell death in ethanol-treated mutants and heterozygotes occurred in these precursor regions (Fig. 2.11). The regions of enhanced cell death are also adjacent to the oral ectoderm and pharyngeal pouches, sources of ligands for *Pdgfra* (Eberhart et al., 2008). Collectively, these data show that the *pdgfra*-ethanol interaction causes an increase in neural crest cell death starting at 24 hpf, which contributes to the ethanol-induced craniofacial defects at 5 dpf.

2.III.c. Combined loss of Pdgf signaling and ethanol exposure impinges on mTOR signaling.

In combination with our previous analyses (Eberhart et al., 2008), our results show that Pdgf signaling functions in both neural crest migration and protection from ethanol-induced apoptosis. A main *pdgfra* effector regulating cell survival and migration *in vitro* and in *Xenopus* mesoderm cells is Phosphoinositide 3 kinase (PI3K) (Downward, 2004; Van Stry et al., 2005; Xiong et al., 2010).

Additionally, PI3K is the major effector of *Pdgfra* regulating craniofacial development in mouse (Klinghoffer et al., 2002). In different *in vitro* analyses, ethanol has been suggested to downregulate several components of the PI3K pathway, including PI3K itself, AKT and mTOR, both downstream of PI3K (Guo et al., 2009; Hong-Brown et al., 2010; Vary et al., 2008; Xu et al., 2003). We hypothesized that PI3K signaling mediates *Pdgfra* protection from ethanol-induced apoptosis. We increased PI3K signaling by injecting untreated and ethanol-treated hypomorphic *pdgfra* mutants with morpholinos against the negative regulator of PI3K, *pten* (Croushore et al., 2005). These injections left wild-type and heterozygous embryos largely unaffected as compared to controls (Figs. 2.12 and 2.13). Upregulating the PI3K pathway in either untreated or ethanol-treated mutants nearly fully rescued the palate defects when compared to untreated and ethanol-treated mutant controls (Fig. 2.14A-D). Injection of *pten* morpholinos also rescued the pharyngeal skeletal elements of ethanol-treated mutants to a nearly wild-type appearance (Fig. 2.14A' compare D').

We wanted to test whether activation of this pathway at the level of mTOR could also rescue the ethanol-induced mutant phenotypes. L-Leucine has been shown to increase mTOR activity, leading to a rise in cell growth and survival (Hong-Brown et al., 2012; Kimball and Jefferson, 2006). Supplementing ethanol with 50mM L-Leucine partially rescued the ethanol-treated phenotype (Fig. 2.14E-F,E'-F'), and had no apparent affect on either untreated heterozygote or wildtype siblings (Fig. 2.15). However, following a 10-24 hpf ethanol treatment with L-Leucine treatment alone from 24 to 48 hpf did not rescue ethanol-induced defects in mutants (Fig. 2.16, compare to Fig. 2.1). These data show that elevating either PI3K or mTOR signaling is sufficient to protect against ethanol-induced craniofacial defects in a *Pdgfra* attenuated embryo.

If the *pdgfra*/ethanol interaction is due to inhibition of the PI3K pathway downstream of *Pdgfra*, then pharmacological blockade of the PI3K pathway should recapitulate the ethanol defects in *pdgfra* mutants. Consistent with this model, treating *pdgfra* mutants with inhibitors of either PI3K (wortmannin) or mTOR (rapamycin) from 10 hpf to 24 hpf phenocopied the ethanol-induced defects of the palatal skeleton (Figs 2.17F,I,L and M, Fig. 2.18) and caused reductions in the pharyngeal skeleton compared to mutant controls and wild type- and heterozygous-treated counterparts (Fig. 2.19F,I,L-O). Furthermore, these treatments also uncovered latent haploinsufficiency, causing variable defects including those affecting the ethmoid plate and trabeculae (Fig. 2.17H,K,M). While there are subtle differences between the treatments that could be due to

dosage or mechanism of action, the overall pattern of pharyngeal reduction is highly similar across treatments (Fig. 2.19). These data suggest that attenuation of the PI3K-mTOR pathway may underlie the *pdgfra*/ethanol interaction.

To directly test the effects of ethanol on the PI3K pathway in *pdgfra* mutants, we detected phosphorylated forms of the PI3K target, AKT, and the mTOR target, eIF4B (Fig. 2.20). Heads from untreated and ethanol-treated *pdgfra* mutants and siblings were collected at 24 hpf. Downstream of mTOR, ethanol-treated mutants showed a decrease in levels of phospho-eIF4B compared to untreated embryos and ethanol-treated controls (Fig. 2.20C,D). Upstream of mTOR, we observed an increase in levels of phospho-AKT in both ethanol-treated mutants and controls compared to their untreated counterparts (Fig. 2.20A,B). These data are consistent with a growing body of evidence, primarily *in vitro* and in cancer models, that shows that inhibiting mTOR leads to an increase in AKT phosphorylation (Carracedo and Pandolfi, 2008; Hsu et al., 2011; Soares et al., 2013). To validate this feedback in the developing zebrafish, we assayed phospho-AKT levels in rapamycin-treated embryos. Indeed blocking mTOR led to an increase in levels of phosphorylated AKT in both mutants and wildtypes compared to DMSO-treated controls (Fig. 2.21), similar to the effects of ethanol. These data support a model in which ethanol, in combination with loss of Pdgf signaling, attenuates the activity of mTOR, leading to hypophosphorylation of targets such as eIF4B, but also an increase in phosphorylated AKT.

2.IV. Discussion

Collectively, our results provide insight into the genetic susceptibility to ethanol-induced defects. Using zebrafish, we show that attenuated Pdgf signaling and ethanol exposure synergistically interact to cause variable craniofacial defects. This interaction may be conserved in humans, through our analysis of the human dataset herein, although further analysis in humans is necessary to confirm this finding. We suggest a model in which attenuated growth factor signaling interacts with ethanol to reduce the activity of PI3K/mTOR signaling, at or downstream of mTOR thus causing developmental perturbations. At low levels of attenuation, whether from slight reduction in growth factor signaling or low doses of ethanol, the system can compensate. However, those embryos with reduced growth factor signaling, even reductions that would not cause defects alone, that receive a “second hit” via ethanol, can develop craniofacial defects.

2.IV.a. Pdgfra regulates both neural-crest cell migration and protection from ethanol-induced apoptosis.

Pdgf signaling is essential for midfacial development across vertebrate species (Eberhart et al., 2008; Soriano, 1997; Tallquist and Soriano, 2003). At least in zebrafish, Pdgfra regulates the appropriate migration of neural-crest cells that will generate the midfacial skeleton (Eberhart et al., 2008). It is only in the presence of ethanol that we reveal the requirement of Pdgfra signaling in neural-crest cell survival. The increased apoptosis in ethanol-treated *pdgfra* mutants could be

attributed to the fact that the *pdgra*^{b1059/b1059} mutant allele is a hypomorph (Eberhart et al., 2008). In this model, the amount of *Pdgfra* signaling left in the hypomorph is sufficient for cellular survival. However, in the presence of ethanol, these signals no longer promote survival. This model is consistent with the finding that there is elevated cell death in *Pdgfra* null mice (Soriano, 1997). However, in a neural crest conditional *Pdgfra* mutant, apoptosis did not appear elevated (Tallquist and Soriano, 2003), which may suggest an alternate model. The *pdgra*-ethanol interaction could be due to broad inhibition of mTOR signaling, across growth factor pathways. The zebrafish mutation project (http://www.sanger.ac.uk/Projects/D_rerio/zmp/) has identified a putative null *pdgra* allele. Analysis of this mutant allele will aid in distinguishing between these two possibilities.

Proper *Pdgfra* signaling relies heavily on PI3K activation. In mouse, knockout of the PI3K-domain of *Pdgfra* leads to craniofacial defects, which mimic the full knockout phenotype (Klinghoffer et al., 2002). In frog, the PI3K domain of *Pdgfra* is necessary and sufficient for proper mesoderm migration and survival (Nagel et al., 2004; Van Stry et al., 2005). In our studies, increasing PI3K-mediated signaling through *pten* morpholino knockdown leads to a near wild-type phenotype in both untreated and ethanol-treated *pdgra* mutants. This finding suggests that increasing PI3K function in ethanol-treated *pdgra* mutant embryos rescues both survival and migration, since the midline defects are due to a migratory defect.

While elevating PI3K signaling does rescue the defects in *pdgfra* mutants, understanding the precise mechanism will require additional studies. GTPases, which promote migration, and AKT, which supports survival and migration, rely on the PIP3 substrate of PI3K (Zhou and Huang, 2010). Thus, it is possible that the migratory and survival functions of *Pdgfra* are controlled by different signaling components immediately downstream of PI3K.

mTOR most likely regulates cell survival and growth in ethanol-treated embryos. L-leucine supplementation does not rescue the midline defects in our *pdgfra* mutants, which are caused by a migratory defect. In ethanol-treated mutants, we observe a decrease in the levels of activated eIF4B and an increase in levels of activated AKT, suggesting that ethanol impairs growth signaling at the level of mTOR or below. Further evidence that ethanol may be impairing mTOR activity specifically is the finding that phosphorylated levels of AKT are increased in ethanol treatment. A similar increase in activated AKT is observed in our model via rapamycin treatment of *pdgfra* mutants. Blocking mTOR function may release inhibitory feedback loops; for example, pancreatic cancer cells treated with rapamycin show elevated levels of phosphorylated AKT compared to untreated controls (Soares et al., 2013). It is interesting to speculate that the upregulation of AKT in ethanol-treated siblings may buffer against deleterious phenotypes by elevating cell proliferation. However, a more extensive analysis of the PI3K and mTOR pathways will be necessary to fully understand how *Pdgfra*-mediated migration and protection are controlled intracellularly.

2.IV.b. Ethanol may broadly disrupt growth-factor signaling pathways

The interaction observed between ethanol and *pdgfra* supports a model in which PI3K-dependent growth-factor genes interact with ethanol. Notable among these genes is *insulin receptor (Insr)*. *Insr* functions in proper brain development. Reducing the expression of *insr* in newly born rat pups causes defects similar to those found in rat models of FASD (de la Monte et al., 2011). Increasing insulin receptor expression in a drosophila model of FASD rescues neurobehavioral defects caused by ethanol-exposure (McClure et al., 2011). These data, along with our observations of *pdgfra*, strongly suggest that growth factor genes play a significant role in the susceptibility to ethanol teratogenesis. Because growth factor signaling is used throughout development, attenuated growth factor signaling, along with ethanol exposure, could explain a large portion of the variability found in FASD. This model is consistent with the human dataset in which the phenotypes associated with gene/ethanol interactions are different between *PDGFRA* and *PDGFRB*. As the human dataset grows, it will be of great interest to further examine the extent of interactions between ethanol and PI3K-dependent growth factors.

2.IV.c. Zebrafish as a model of gene-environment interactions

The zebrafish provides a powerful tool in uncovering both the genetics and the mechanisms involved in FASD susceptibility. Due to the vast array of genetic

resources available and the ease of administering ethanol to the externally fertilized embryos, it is feasible to screen hundreds of genes in a relatively short period of time. As we have done here, findings in zebrafish can be used to direct analyses in human datasets that may not yet be large enough for genome-wide power. We have found evidence for *pdgfra*-ethanol interactions in both zebrafish and human. Although the human dataset we analyzed is small, by focusing on a small number of genes the likelihood of detecting false associations was greatly decreased. After correcting for the testing of SNPs across five genes, and therefore five essentially independent tests, the associations we found in the genes encoding for the human PDGF receptors were significant, with all p-values < 0.01. This significant association even withstands a more strict correction of treating all 118 SNPs as independent tests ($0.05/118=4.2 \times 10^{-4}$). Thus the zebrafish model has guided focused studies in a human dataset with variable alcohol exposure and allowed us to detect a gene-ethanol interaction that contributes to the observed variation in craniofacial measures. Importantly, due to the conservation of gene function across vertebrate species, we can then understand the mechanism of these interactions using the zebrafish model system. Collectively, our findings provide a predictive mechanistic model for at least some gene-ethanol interactions that underlie the craniofacial defects in FASD.

Although we have focused on the craniofacial aspect of FASD, the zebrafish also provides an excellent model in which to study the neural aspects

of this disorder. The brain is the most commonly affected organ in FASD, with defects to the cerebellum and oligodendrocytes being common (Hoyme et al., 2005; Swayze et al., 1997). Further analysis of our *pdgfra*-ethanol interaction could reveal more subtle neural-specific defects. *Pdgfra* is important for oligodendrocyte maturation and migration in mouse (McKinnon et al., 2005), although the function of *pdgfra* in zebrafish oligodendrocyte development has not been tested. It would be of interest to determine if oligodendrocytes are disrupted in ethanol-treated *pdgfra* mutants.

Due to its genetic tractability the zebrafish has long been a valuable model system for understanding developmental processes. We currently understand an enormous amount regarding the genetics regulating development from work in numerous model systems. Due to the level of this understanding, we are now well poised to gain substantial knowledge about how the environment impinges on the genetic networks underlying development (so called Eco-Devo). Our work here and recent work examining gene-environment interactions underlying ototoxicity (Coffin et al., 2010) demonstrate that the same characteristics (e.g. genetic amenability, ease of imaging and external fertilization) that make zebrafish useful for understanding development make it useful for understanding Eco-Devo.

2.V. Materials and Methods

2.V.a. Danio rerio (zebrafish) care and use

All embryos were raised and cared for using established protocols (Westerfield, 1993) with IACUC approval from the University of Texas at Austin. *Tg(fli1:EGFP)y1* transgenic embryos express GFP in neural crest cells shortly after the onset of migration, and in the vasculature (Lawson and Weinstein, 2002). Here they are called *fli1:EGFP* throughout the text. Embryos were treated in EM with 1.0% and 0.5% ethanol, 1.5uM wortmannin (W1628, Sigma) ; 3uM rapamycin (S1120, Selleck); and 25uM caspase inhibitor 3 (Cat#264155, Calbiochem). L-leucine has been used at 100mM in zebrafish (Payne et al., 2012), we found that a 50mM solution was sufficient to provide rescue in our experiments. The *pdgfra*^{b1059} (Eberhart et al., 2008), *smad5*^{b1100} (Sheehan-Rooney et al., 2013) and *smo*^{b577} (Varga et al., 2001) alleles have been described. The *gata3*^{b1075} and *cyp26b1*^{b1024} alleles were recovered from a forward genetic screen at the University of Oregon and will be described in detail elsewhere.

2.V.b. Morpholino and RNA injection

Gene Tools (Philomath, OR, USA, <http://www.gene-tools.com>) supplied morpholino oligonucleotides *ptena* and *ptenb* (Croushore et al., 2005) as well as *mir140* MO (Eberhart et al., 2008). We injected one or two-cell stage zebrafish embryos with approximately 3 nl of morpholinos with working concentrations of: 3.5 mg/ml *ptena/ptenb*, and 1.2 mM *mir140*. *pdgfra* mRNA was made using the

mMessenger mMachine and Poly A cloning kits (Ambion, Austin, TX). Stock solutions (concentration approximately 300 ug/ml) were either injected (approximately 3 nl) directly or diluted at ratios of 1:10 and 1:20 into 1-cell stage embryos.

2.V.c. Immunohistochemistry

Embryos were fixed and prepared for immunohistochemistry following the procedure outlined in (Maves et al., 2002). Primary antibody solution (anti-active caspase III, G748A, Promega; phospho-Histone H3, 012M4830, Sigma) was added at a 1:300 dilution in blocking solution, and embryos were incubated overnight at 4C on a shaker. Embryos were then washed 3X 20 minutes in PBDTx at room temperature. Embryos were incubated with secondary antibody (Alexa Fluor 568 anti-rabbit IgG, A10042, Invitrogen) at a dilution of 1:300 in blocking solution for 5 hours, covered, at room temperature. Embryos were washed 1-2X in PBS, and neural-crest cell death was viewed and quantified using a Zeiss LSM 710 confocal. For quantification of the ratio of cell death, embryos were counter stained with ToPro (Invitrogen) and all nuclei within a single representative z plane were counted. The z plane was aligned through the lateral 1st and 2nd arches such that the oral ectoderm and 1st pouch, but not the mesodermal cores, were visible.

2.V.d. Immunoblotting

Tissue samples were harvested from the *pdgfra*^{b1059};*fli:EGFP* line. Mutants were visually sorted from wild-type/heterozygotes by their neural crest cell migration

defect (Eberhart et al., 2008). Embryos were euthanized, dechorionated and then deyolked using a fire-pulled glass pipette. Heads were separated from the tail at the posterior end of the otic vesicle. Heads were collected in a 1.5 ml microcentrifuge tube. Samples were placed in HKET buffer (25 mM HEPES HCl 7.4; 150 mM KCl; 1 mM EDTA; 1% Triton-X) with a protease inhibitor cocktail mix (complete Mini, 04 693 124 001, Roche), homogenized, centrifuged at 15,000 rpm for 15 min at 4C, and the resulting lysate removed and quantified using the Pierce BCA protein assay kit (#23227, Thermo Scientific). Lysates were analyzed by electrophoresis using the NUPAGE SDS-PAGE gel system (Invitrogen). After electrophoresis, proteins were transferred to a nitrocellulose membrane and blocked by immersion in PBST (phosphate-buffered saline containing 0.1% Tween-20 and 5% BSA) overnight at 4C. The membranes were then incubated overnight in 4C with the following antibodies: AKT (#4691, Cell Signaling), pAKT (#4060, Cell Signaling), eIF4B (#3592, Cell Signaling), pEIF4B (#3591, Cell Signaling), and b-actin (#4967, Cell Signaling). After 3 successive 10 min PBST washes, membranes were incubated at room temperature for 1 hour in secondary antibody (anti-rabbit for all antibodies; #7074, Cell Signaling). Membranes were washed 3X 10 min in PBST, and treated for 5 minutes in SuperSignal West Pico Chemiluminescent Substrate (#34077, Thermo Scientific) and exposed on UV film. Membranes were reprobed using stripping buffer containing 0.2 M Glycine, 0.05% Tween-20, pH 2.5 for 30 min. at 70C. Membranes were washed 2X with TBST, reblocked for 1 hour at room

temperature, and placed in primary antibody. ImageJ was used to quantify blots (Schneider et al., 2012).

2.V.e. Cartilage and Bone staining and area measurements

Five day postfertilization (dpf) zebrafish embryos were stained with Alcian Blue and Alizarin Red (Walker and Kimmel, 2007), then flat mounted (Kimmel et al., 1998). Images were taken with a Zeiss Axio Imager-A1 microscope, and palate and neurocranial lengths and widths and jaw and jaw-support elements were measured using AxiovisionLE software (AxioVs40 V4.7.1.0). All graphs were made in Microsoft Excel 2011.

2.V.f. Confocal microscopy and figure processing

Confocal z-stacks were collected on a Zeiss LSM 710 using Zen software. Images were processed in Adobe Photoshop CS.

2.V.g. Statistical Analysis

Origin 7.0 was used for oneway ANOVA and Tukey's range test for the cell death, cell death ratio, palate and neurocranial and pharyngeal arch measurement analysis, statistical significance was set at 0.05. Graphpad Prism 5.02 was used for the gas chromatography data.

2.V.h. Measurement of ethanol concentration using headspace gas chromatography

To determine ethanol tissue concentration relative to media exposure, headspace gas chromatography (GC) was utilized. Embryos were exposed to ethanol in media at 1% or .5%. Samples were taken at 1 hour and 14 hours post

ethanol exposure coordinating with 11 hours and 24 hpf, respectively. Additional embryos were removed from ethanol at 14 hours post ethanol exposure, washed three times with fresh media and allowed to equilibrate in fresh media for one hour where samples were again taken. Samples consisted of 10-pooled embryos that were quickly rinsed in fresh media and treated with 50 μ L of Pronase (2 mg / mL) for 10 minutes to aid in the removal of the chorion. 450 μ L of 5 M NaCl was then added to each sample and the samples were vortexed for 10 minutes to homogenate the embryos. For each sample, an aliquot of 10 μ L was transferred to a 2 mL GC vial and sealed with a PTFE silicon septum and plastic cap. For each time point, a media reference sample was also collected, diluted 10 fold in 5 M NaCl and a 10 μ L aliquot was transferred to a 2 mL GC vial and sealed. A Varian CP 3800 gas chromatograph with flame ionization detection and a Varian CP 8400 headspace autosampler, heated to 58°C, was used to analyze the concentrations of ethanol in the samples. The stationary phase was an HP Innowax capillary column (30 m \times 0.53 mm \times 1.0 μ m film thickness) and helium was the mobile phase. Resulting ethanol peaks were recorded using Varian Star Chromatography Workstation software, and calibration was achieved using external standards from .3125 to 40 mM ethanol in 5 M NaCl. Ethanol concentration in the embryos samples were compared to media controls by a paired t-test in Graphpad Prism 5.02 (Graphpad Software Inc., La Jolla, CA).

2.V.i. Human sample

The published data were collected as part of an ongoing international consortium, the Collaborative Initiative on Fetal Alcohol Spectrum Disorders (CIFASD). Participants were recruited from three sites (San Diego and Los Angeles, California and Atlanta, Georgia). This study was approved by the Institutional Review Board at each site. All participants and/or their parent(s)/legal guardian(s) provided written informed consent.

As part of the study visit, each participant was examined by a trained dysmorphologist who completed a standardized, uniform assessment (Jones et al., 2006). Patients with a recognizable craniofacial syndrome other than FAS were excluded. An objective classification system, based solely on structural features (palpebral fissure, philtrum, and vermillion border) and growth deficiency (head size and height and/or weight) consistent with the revised Institute of Medicine criteria (Hoyme et al., 2005), was used to classify subjects. Under this scheme, a participant could receive a preliminary diagnosis of FAS, no FAS, or deferred (Jones et al., 2006). Alcohol exposure data were collected at the interview, or from a review of available study data. The extent of reported prenatal alcohol exposure information was then classified into one of three categories: none, minimal (> 1 drink/week average and never more than two drinks on any one occasion during pregnancy), and greater than minimal (>4 drinks/occasion at least once/week or >3 drinks/week). Alcohol exposure was

confirmed via review of records or maternal report, if available (Mattson et al., 2010).

As part of the study visit, a three-dimensional facial image was collected using the 3dMD system (3dMD, Atlanta, Georgia). Landmarks were identified on the 3D model and used to obtain linear measurements. Replication of landmark placement was required, with less than 2 mm difference per linear measurement. If the tolerance criterion was not met, a third measurement was taken and the average of the two closest measurements was chosen for analysis. For bilateral measurements, only the left side was used in analyses. Although a set of sixteen standard anthropometric measurements (Moore et al., 2007) were obtained, for this study we only utilized a subset: inner canthal width, outer canthal width, lower facial height, lower facial depth and midfacial depth – which best modeled the craniofacial defects seen in the zebrafish model.

Genomewide single nucleotide polymorphism (SNP) genotyping was completed at the Johns Hopkins GRCF SNP Center using OmniExpress genome array, which includes over 700,000 SNPs. Standard review of both sample and SNP was performed (see supplemental text). Race and ethnicity were reported by the participant or the parent/guardian as part of the study visit and were then confirmed based on the SNP genotypes using a principal component analysis (see Supplemental Text for more details). To reduce phenotypic heterogeneity due to race, we limited the analyses to those subjects who based on their SNP genotypes were of European American descent (n=102).

The regulation and function of Pdgf signaling is highly conserved across vertebrate species; therefore, we identified the SNPs within each of the 5 genes in the PDGF pathway. Due to the small size of *PDGFA* (12,700 bp), no SNPs were genotyped or analyzed in this gene, therefore, we could only test the role of 5 of the 6 genes in the PDGF pathway. Univariate analysis was performed for each SNP using linear regression framework to test whether the SNP genotype x alcohol exposure interaction accounted for a significant proportion of the variation in the 5 key anthropometric measures. Within the model we also included the main effects of SNP genotype and alcohol exposure. All measures were corrected for age and gender. We utilized a Bonferroni correction for the number of genes (5 genes) being tested, which resulted in a significance threshold of 0.01 (0.05/5).

2.V.j. Ethics Statement

Data were collected as part of an ongoing international consortium, the Collaborative Initiative on Fetal Alcohol Spectrum Disorders (CIFASD). Participants were recruited from three sites (San Diego and Los Angeles, California and Atlanta, Georgia). This study was approved by the Institutional Review Board at each site. All participants and/or their parent(s)/legal guardian(s) provided written informed consent. All embryos were raised and cared for using established protocols with IACUC approval (Westerfield, 1993).

2V.k. Human GWAS

Genotyping was performed at the Center for Inherited Disease Research (CIDR). All DNA sources consisted of saliva samples. A total of 731,442 SNPs were genotyped on the OmniExpress array, of which 728,140 SNPs passed CIDR genotyping control and were released for analysis. Out of the 240 samples submitted for genotyping, three samples were dropped by CIDR due to poor quality genotyping. Two additional samples were dropped due to chromosomal abnormalities. All remaining individuals were genotyped on at least 98% of the SNPs. All samples were examined for cryptic relatedness and population stratification. There were 16 half-sibling pairs and 37 full sibling pairs in the sample. A principal component-based analysis was performed in eigenstrat (Price et al., 2006) on both the sample data and HapMap reference samples to assign subjects to racial groups. The final European American sample consisted of 102 individuals, of which 102 had both a 3D image and alcohol exposure information.

SNPs were included for analysis if the call rate was greater than 98% in the entire sample, and SNPs were removed if the minor allele frequency was less than 0.01 or if there was significant deviation from Hardy Weinberg equilibrium ($p < 10^{-6}$). The final dataset consisted of 688,359, of which 118 were analyzed in the PDGF pathway.

2.VI. Acknowledgments

We would like to thank Jeffrey Gross, for help on the western blot analysis, as well as Jennifer Morgan, for use of her labs analytical software. For the GC analysis, we would like to thank both Rueben Gonzalez and Regina Nobles. We would also like to thank Michael Charness and Ed Riley for their advice and input in the making of this manuscript. We would also like to thank Young-Jun Jeon for his advice regarding ethanol and mTOR. Thanks also to Charles B. Kimmel and the University of Oregon Fish researchers and staff for their contributions to the forward genetic screen, supported by P01 HD22486 to C.B.K.

2.VII. Figures

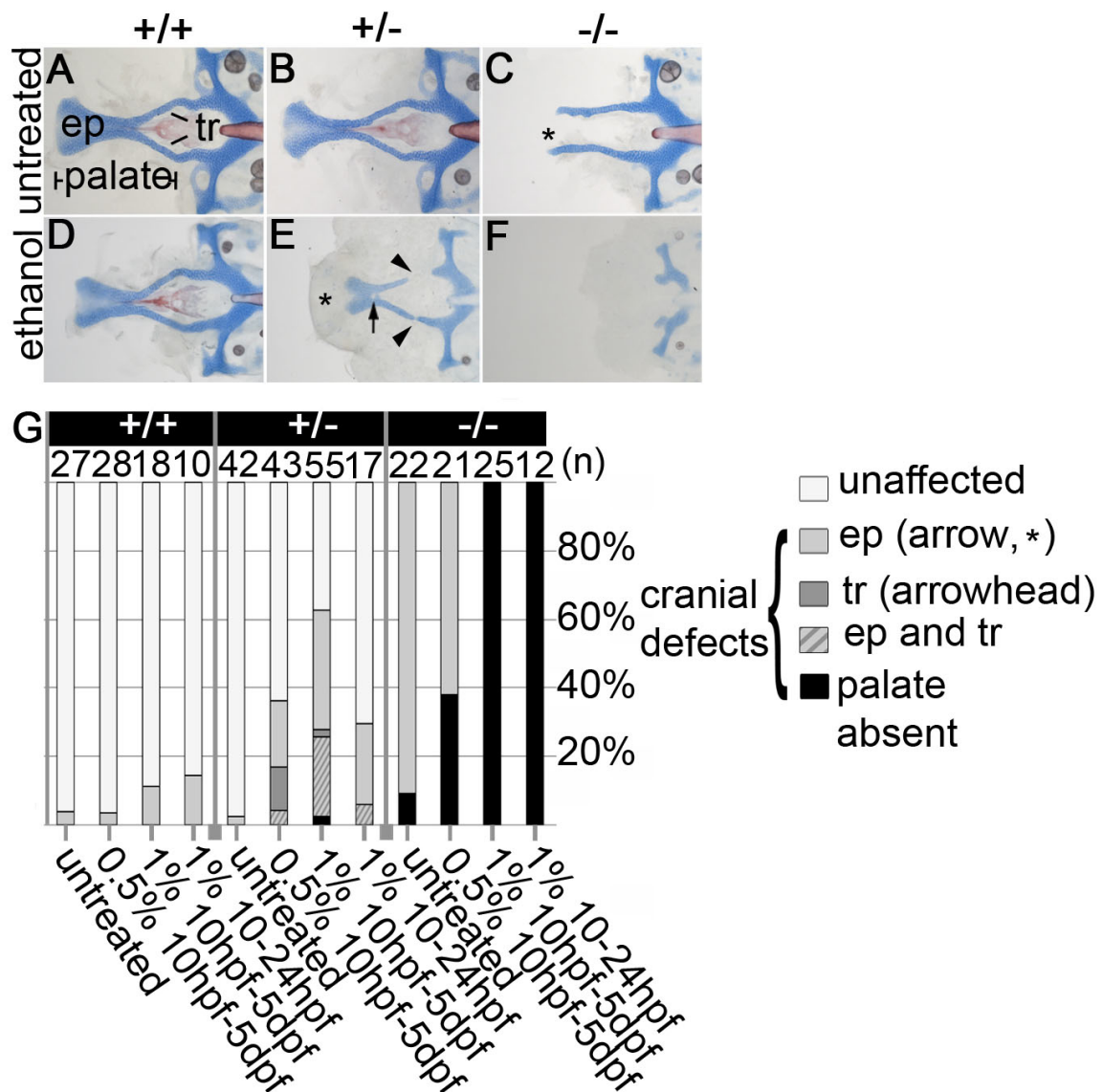


Figure 2.1: Ethanol exacerbates *pdgfra* mutant neurocranial defects and reveals haploinsufficiency. (A-F) show flat-mounted dorsal views of 5 dpf zebrafish neurocrania, stained for cartilage and bone using Alcian Blue and Alizarin Red, respectively. Anterior is to the left. (A) Control wild-type neurocranium. (B)

Control *pdgfra* heterozygotes develop normally. (C) Untreated *pdgfra* mutants have clefting of the ethmoid plate (asterisk), although the trabeculae are still present. (D-E) Neurocrania of embryos treated with 1.0% ethanol from 10 hours post fertilization (hpf) to 5 days post fertilization (dpf). (D) Wild-type embryos are predominantly normal following ethanol treatment. (E) Ethanol-treated *pdgfra* heterozygotes display variable palatal defects, including partial clefting of the ethmoid plate (asterisk), holes in the ethmoid plate (arrow) and breaks in the trabeculae (arrowhead). (F) Ethanol-exposed mutants have an invariant and complete loss of the palatal skeleton. (G) Quantification of palatal defects across genotypes and treatments: control (no ethanol), 0.5% ethanol from 10 hpf to 5 dpf, 1.0% ethanol from 10 hpf to 5 dpf, and 1.0% ethanol from 10-24 hpf. The zebrafish palate consists of the ethmoid plate, ep and trabeculae, tr.

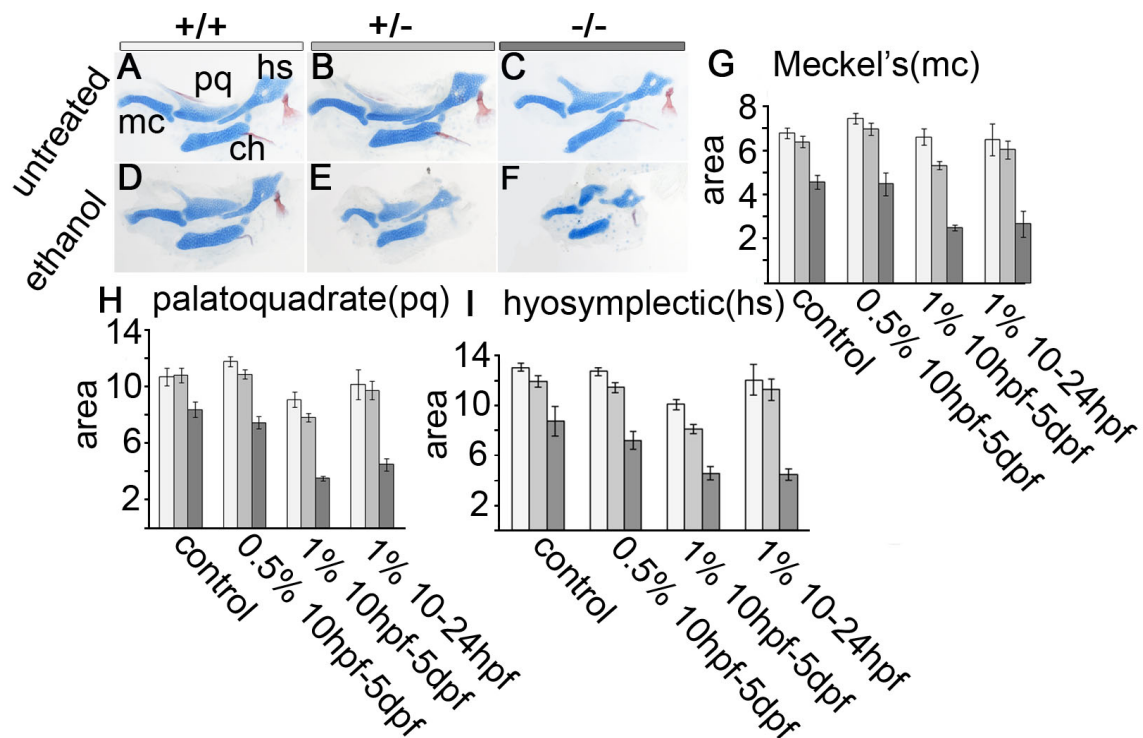


Figure 2.2: Ethanol induces pharyngeal hypoplasia in *pdgfra* mutants. (A-F) show flat mounted jaw and jaw support elements, anterior to the left, stained for cartilage and bone with Alcian Blue and Alizarin Red, respectively. Untreated control (A) wild-type, (B) *pdgfra* heterozygous and (C) *pdgfra* mutant embryos all have normally shaped cartilages. (D & E) Treatment with 1.0% ethanol from 10 hpf to 5 dpf does not effect the overall shape of cartilages in (D) wild-type or (E) *pdgfra* heterozygous embryos. (F) Ethanol treatment greatly disrupts the shape of the palatoquadrate and hyosymplectic cartilages in *pdgfra* mutants. (G-I) Graphs show the quantification of the average area of the (G) Meckel's (mc), (H) palatoquadrate (pq) and (I) hyosymplectic (hs) cartilages (standard error bars are depicted at 1.5 SEM, see Supplemental Table 1 for full ANOVA statistical

analysis). wild-type, light bar; *pdgfra* heterozygote, gray bar; *pdgfra* mutants, dark bar. Jaw cartilages are Meckel's cartilage (mc) and the palatoquadrate (pq). Jaw support cartilages are the hyosymplectic (hs) and the ceratohyal (ch).

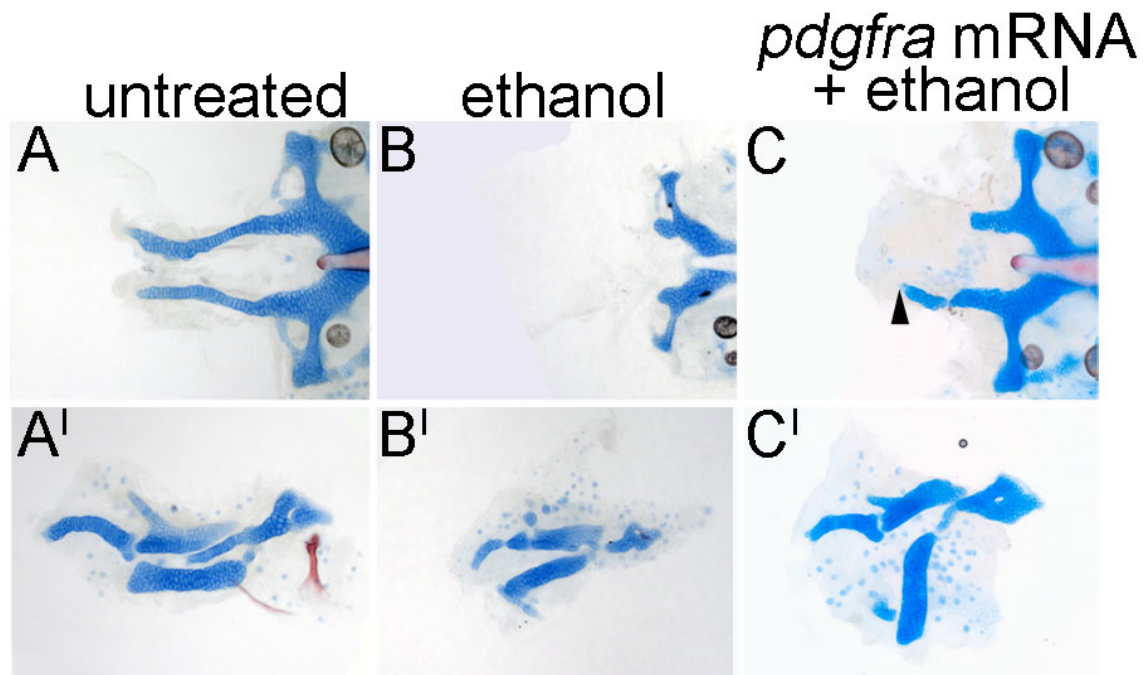


Figure 2.3: *pdgfra* mRNA partially rescues the ethanol-induced defects. (A-C) show *pdgfra* mutant (-/-) 5 dpf neurocrania, and (A'-C') are the corresponding jaw and jaw support elements collectively stained for cartilage and bone using Alcian Blue and Alizarin Red, respectively. Anterior is to the left. (A,A') Untreated control *pdgfra* mutant; (B, B') 1.0% ethanol-treated *pdgfra* mutant from 10-24 hpf, (C, C') *pdgfra* mRNA injection partially rescues the trabeculae (D, arrowhead), jaw and jaw support defects in 1.0% ethanol-treated *pdgfra* mutants (note particularly the shape of the cartilage elements in D').

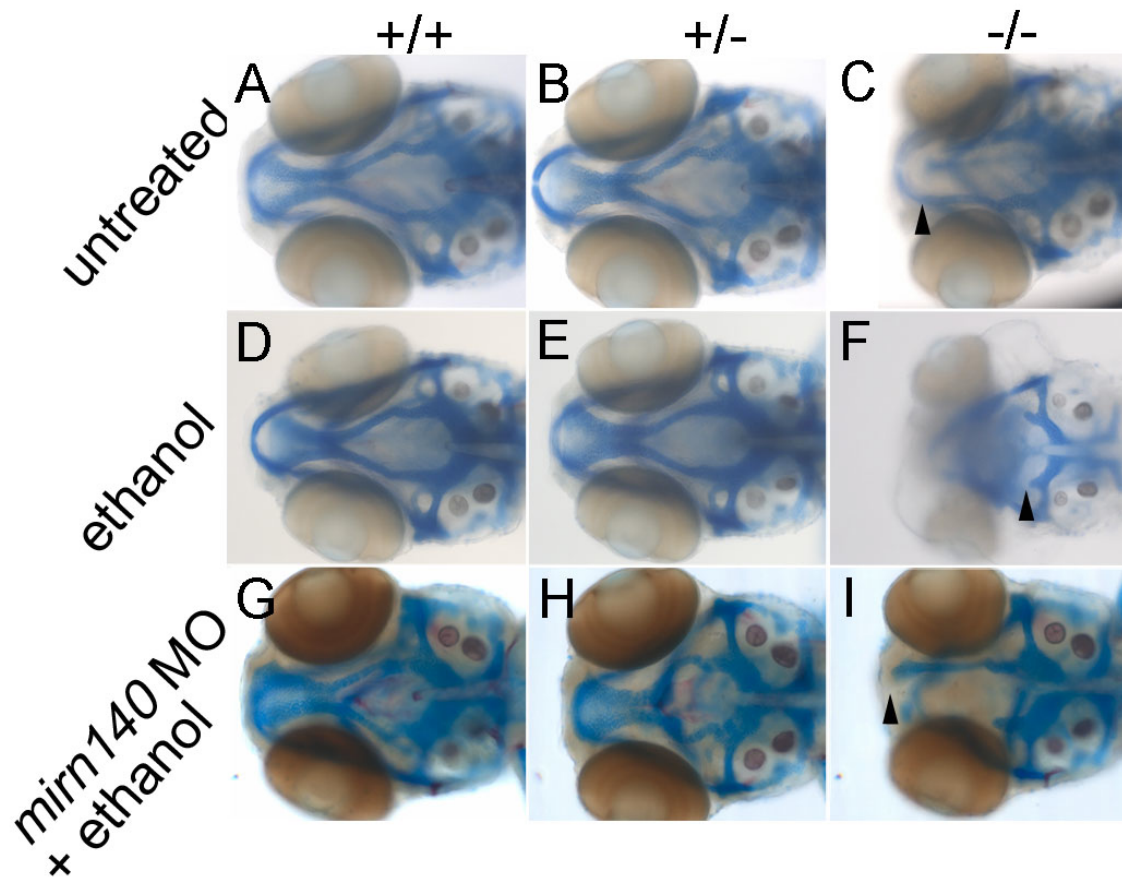


Figure 2.4: *mirn140* morpholino protects *pdgfra* mutants against ethanol-induced defects. (A-I) show dorsal views of 5 dpf zebrafish neurocrania stained for cartilage and bone using Alcian Blue and Alizarin Red, respectively. Anterior is to the left. (A-C) Untreated control embryos of each genotype. (D-F) Embryos from each genotype treated with 1.0% ethanol from 10-24 hpf. (G-I) Embryos injected with *mirn140* morpholino (MO) and treated with 1.0% ethanol from 10-24 hpf. Arrowhead points to the distal tip of the trabeculae in the mutants in each treatment. Figure provided by Mary E. Swartz.

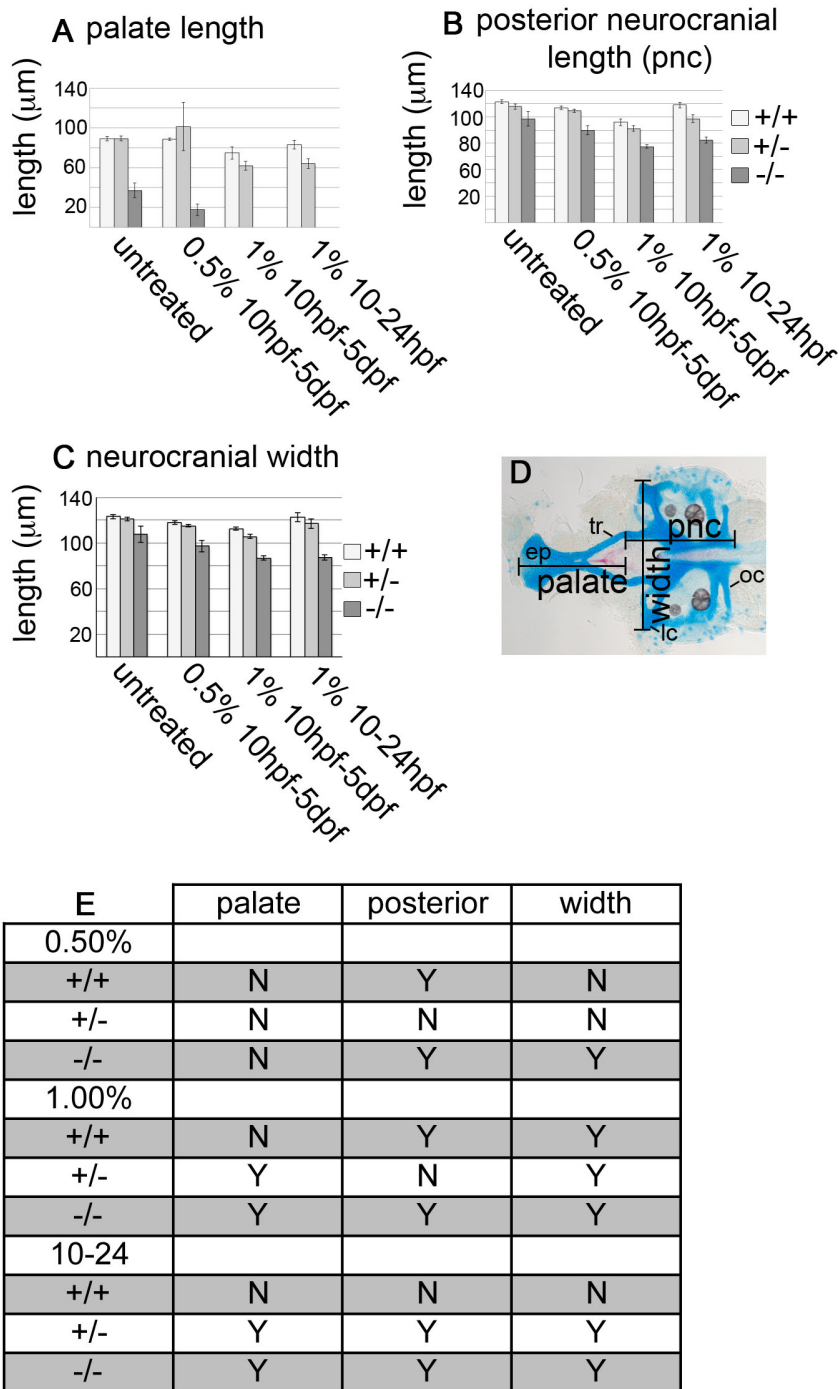


Figure 2.5: Ethanol-treatment causes a decrease in overall neurocranial length and width in *pdgfra* mutants. Graphs depict the average (A) palate length, (B)

posterior neurocranial length, and (C) neurocranial width in micrometers. X-axis on all graphs denote either untreated, 0.5% ethanol from 10 hpf-5dpf, 1% ethanol from 10 hpf to 5 dpf, or 1% ethanol from 10 hpf to 24 hpf (standard error bars are depicted at 1.5 SEM, non-overlapping bars indicate significant differences; Moses, 1987). Wild-type, light bar; *pdgfra* heterozygote, gray bar; mutant, dark bar. (D) Depicts alcian and alizarin stained 5 dpf untreated wildtype neurocranium. Palate length was measured from the most anterior part of the ethmoid plate (ep) to the ends of the trabeculae (tr). The posterior neurocranium was measured from the most posterior part of the occipital arches (oc) to the ends of the trabeculae (tr). Neurocranial width was measured between the most lateral edges of the lateral commissures (lc). (E) Statistical analyses comparing the genotype/ethanol interactions to individual genotype and treatment controls. “Y” denotes a significant difference. Wildtype (+/+) comparisons denote if there is a difference between treated and untreated wild-type embryos. pnc; posterior neurocranium.

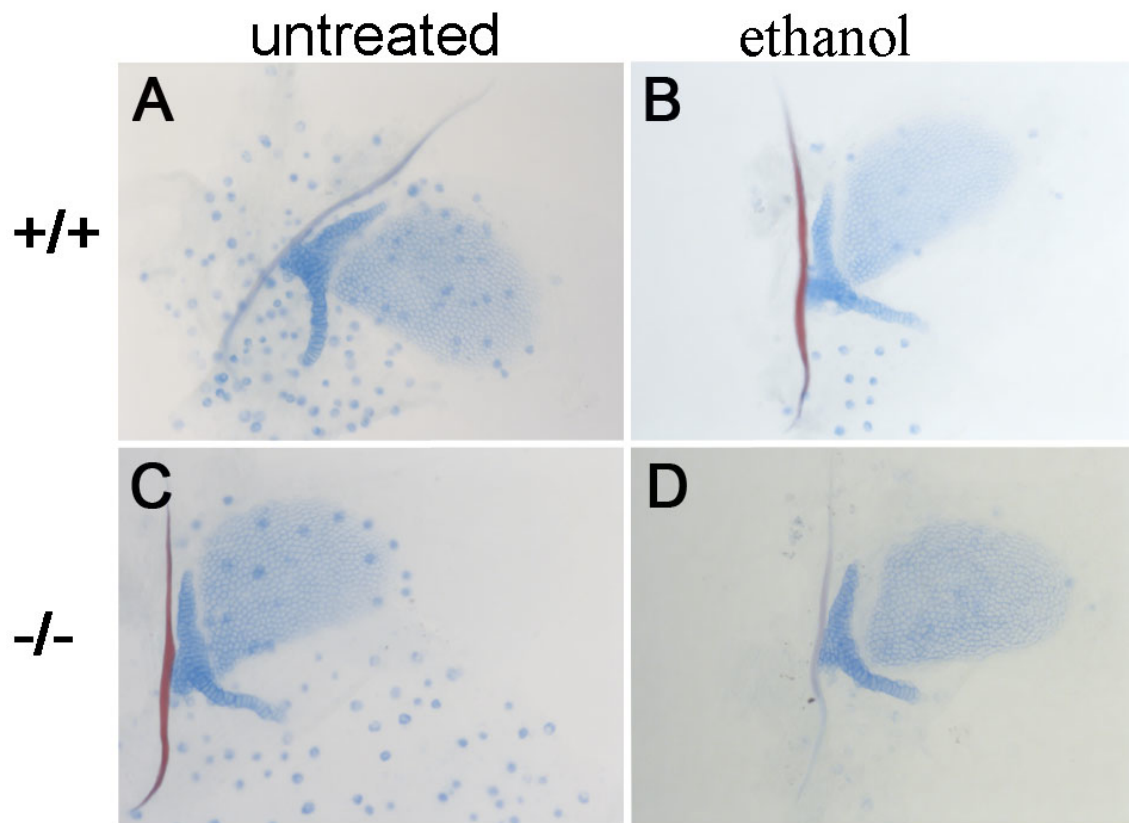


Figure 2.6: Ethanol treatment does not disrupt the pectoral fin in *pdgfra* mutants. Panels A-D depict fin cartilage elements, proximal to the left, stained for cartilage and bone using Alcian Blue and Alizarin Red, respectively. Untreated (A) wildtype and ethanol-treated (B) wildtype. Untreated (C) *pdgfra* mutant and ethanol-treated (D) *pdgfra* mutant. Ethanol treatment of 1.0% from 10 to 24 hpf.

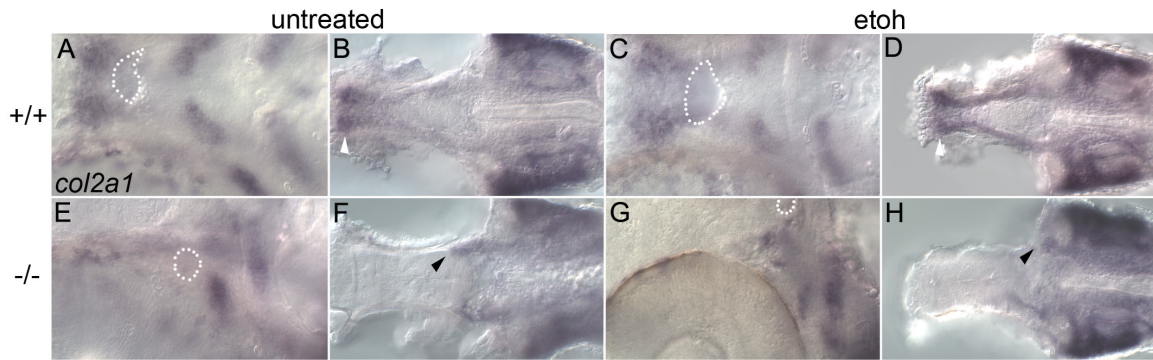


Figure 2.7: *col1a* expression is unaffected in cartilage elements not lost in ethanol-treated *pdgfra* mutants. (A-H) show ventral views of 48 hpf *col1a* *in situ* hybridization images with anterior to the left. (A, C, E, G) show the oral ectoderm (outline in white dots) showing ventral cartilage structures. (B, D, F, H) show the neurocranium. White arrows point the complete neurocranium in untreated and ethanol-treated wildtype siblings. Dark arrows label the most anterior region of the neurocranium in untreated and ethanol-treated mutants. Figure provided by Mary E. Swartz.

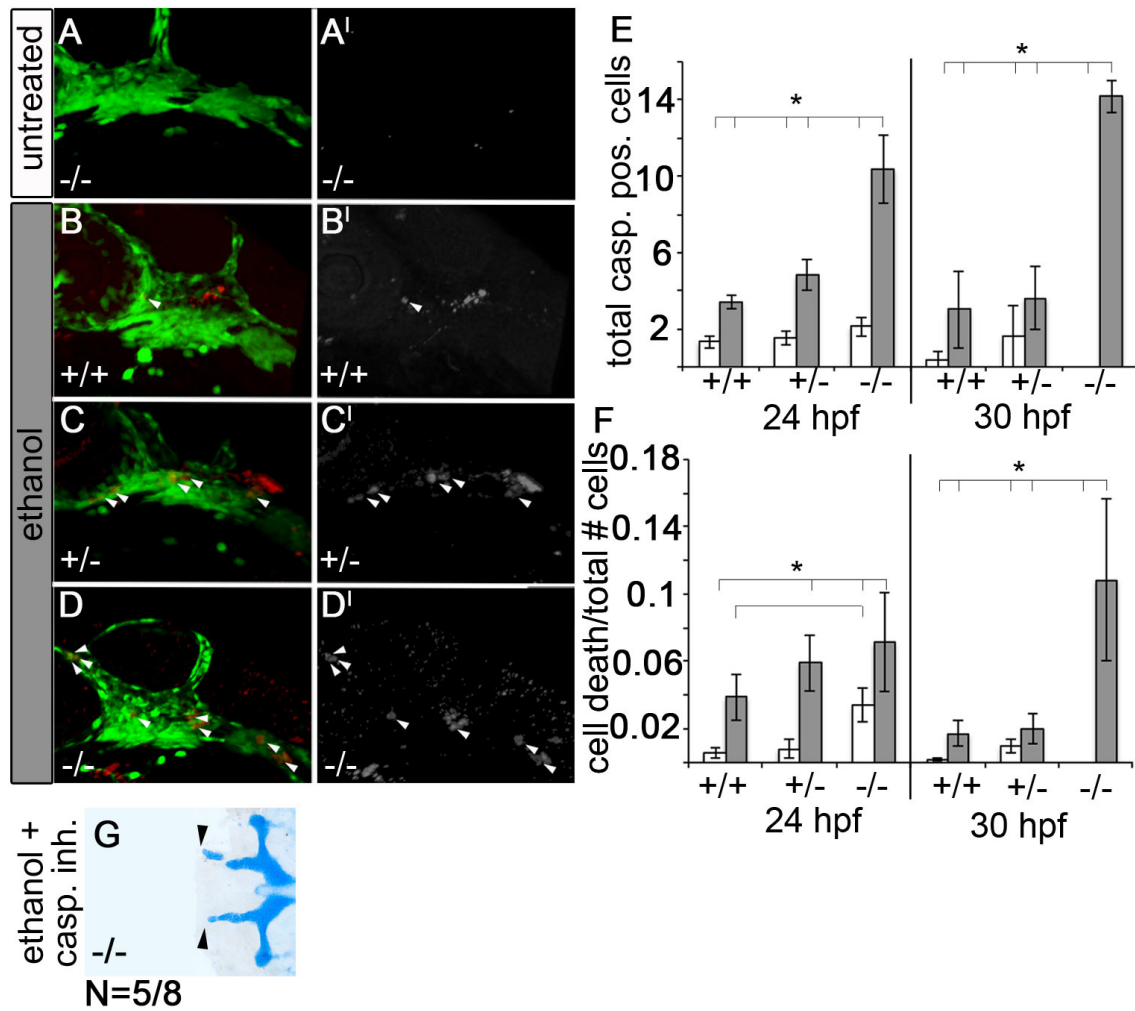


Figure 2.8: Ethanol-treated *pdgfra* mutants exhibit an increase in neural crest cell death. (A-D) are confocal images of 24 hpf anti-active caspase 3-stained *fli1;EGFP* embryos. (A'-D') show the active-caspase 3 staining only. Anterior is to the left. (A-A') Untreated *pdgfra* mutants have low levels of neural crest apoptosis. (B-B') Low levels of neural crest apoptosis are also present in ethanol-treated wild-type embryos treated with 1.0% ethanol from 10-24 hpdf. (C-C') Ethanol treatment causes a slight increase in neural crest cell death in

heterozygotes. (D-D') *pdgfra* mutants have greatly elevated levels of neural crest apoptosis. (E) Graph depicts quantification of cell death across genotypes at 24 hpf and 30 hpf after ethanol was removed at 24 hpf (Untreated control=dark bars, ethanol=light bars). Ethanol-treated *pdgfra* mutants show significant cell death compared to all other genotypes (One-way ANOVA, $*p < .05$). (F) Graph depicts quantification of the ratio of cell death compared to total cell numbers across genotypes (Untreated control=dark bars, ethanol=light bars). (G) 5 dpf *pdgfra* mutant treated with 1.0% ethanol and 25 μ M caspase inhibitor from 10-24 hpf and stained for cartilage and bone using Alcian Blue and Alizarin Red, respectively. Anterior is to the left. Arrowheads denote partial rescue of the trabeculae (compare 4F with 1C and 1F).

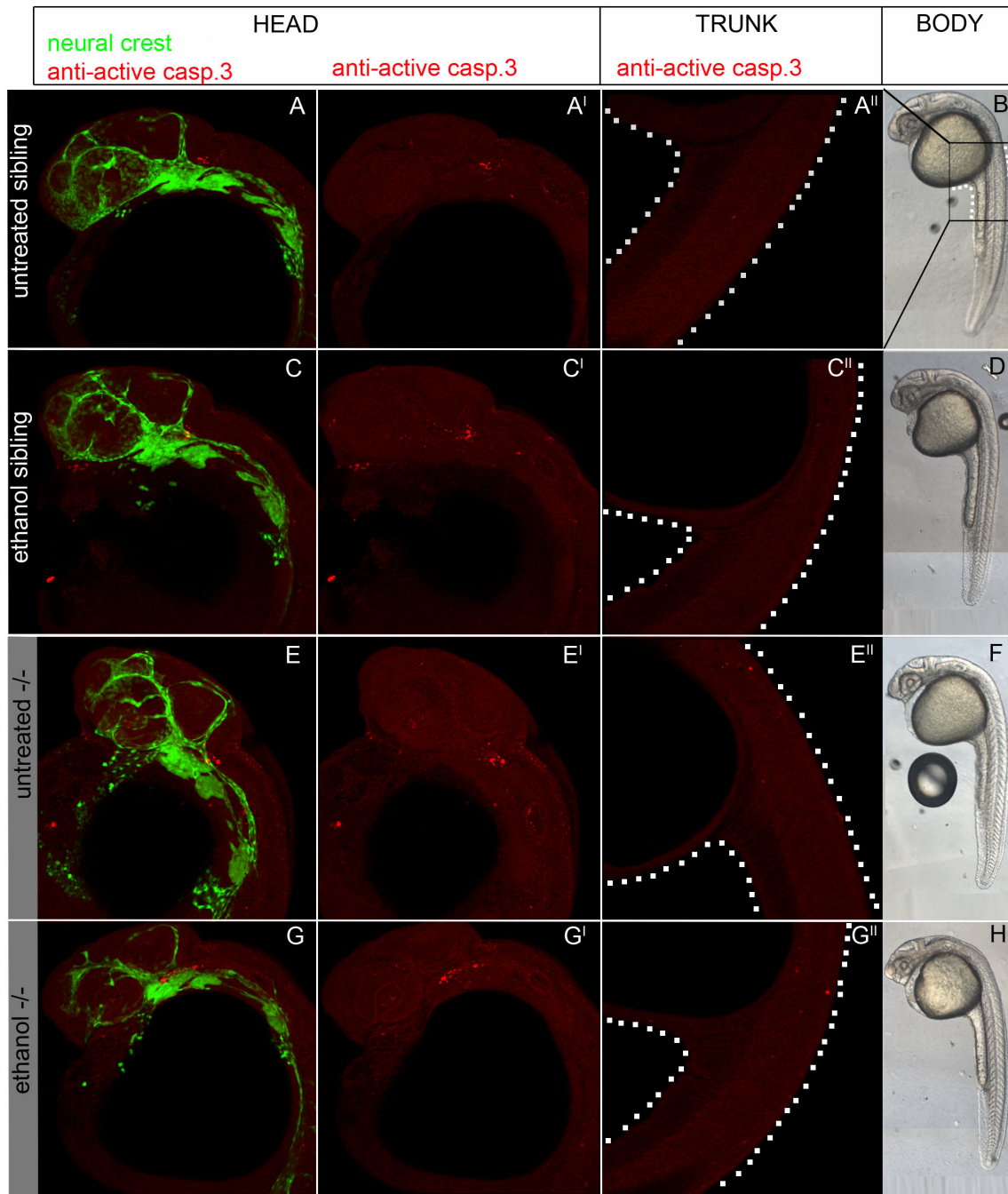


Figure 2.9: Ethanol treatment does not cause developmental delay or global increases in cell death in *pdgfra* mutants. (A,C,E,G, A',C',E',G') show 24 hpf embryos, anterior to the left, stained for active caspase 3. There is no

widespread elevation of apoptosis in the head or trunk of ethanol treated *pdgfra* mutants as compared to other groups. The trunk and yolk are outlined by white dots in A",B",C" and D". (B,D,F,H) DIC images of ethanol treated and untreated *pdgfra* mutants and siblings show that ethanol treated *pdgfra* mutants are not developmentally delayed and have no gross morphological defects at 24 hpf. With the exception of the ethmoid plate and the trabeculae, all precartilaginous condensations are present in ethanol-treated *pdgfra* mutants.

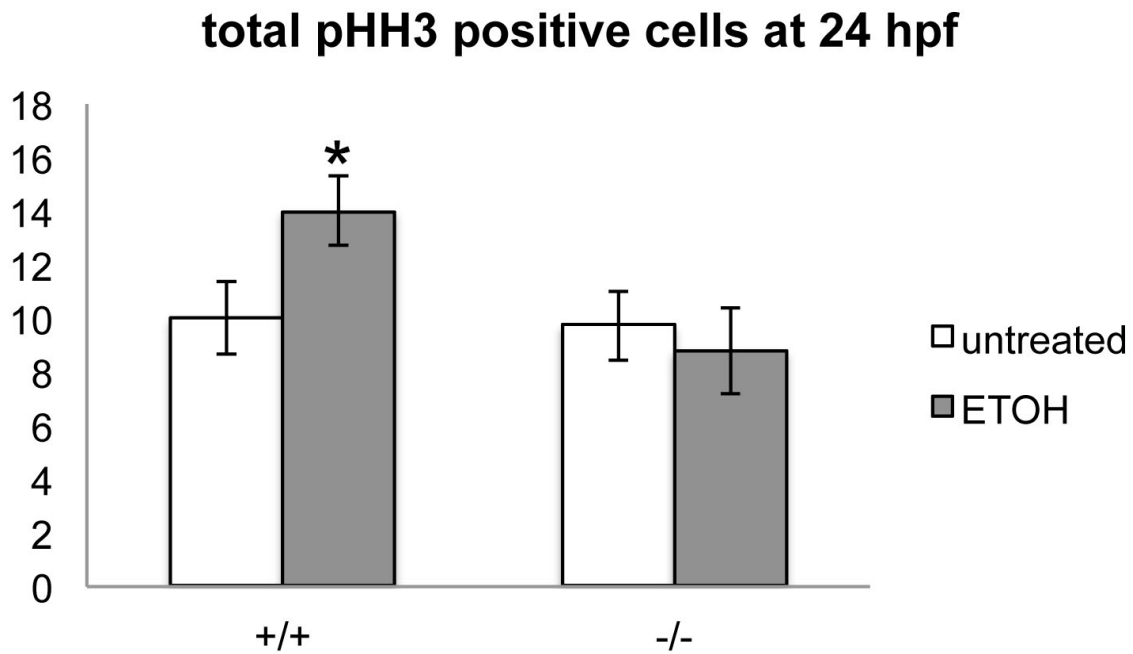


Figure 2.10: Neural crest-specific proliferation is not reduced in ethanol-treated *pdgfra* mutants. Graph depicts average number of pHH3-positive neural crest cells in untreated (white bar) versus ethanol-treated (gray bar) wild-type (+/+) and mutant (-/-) embryos.

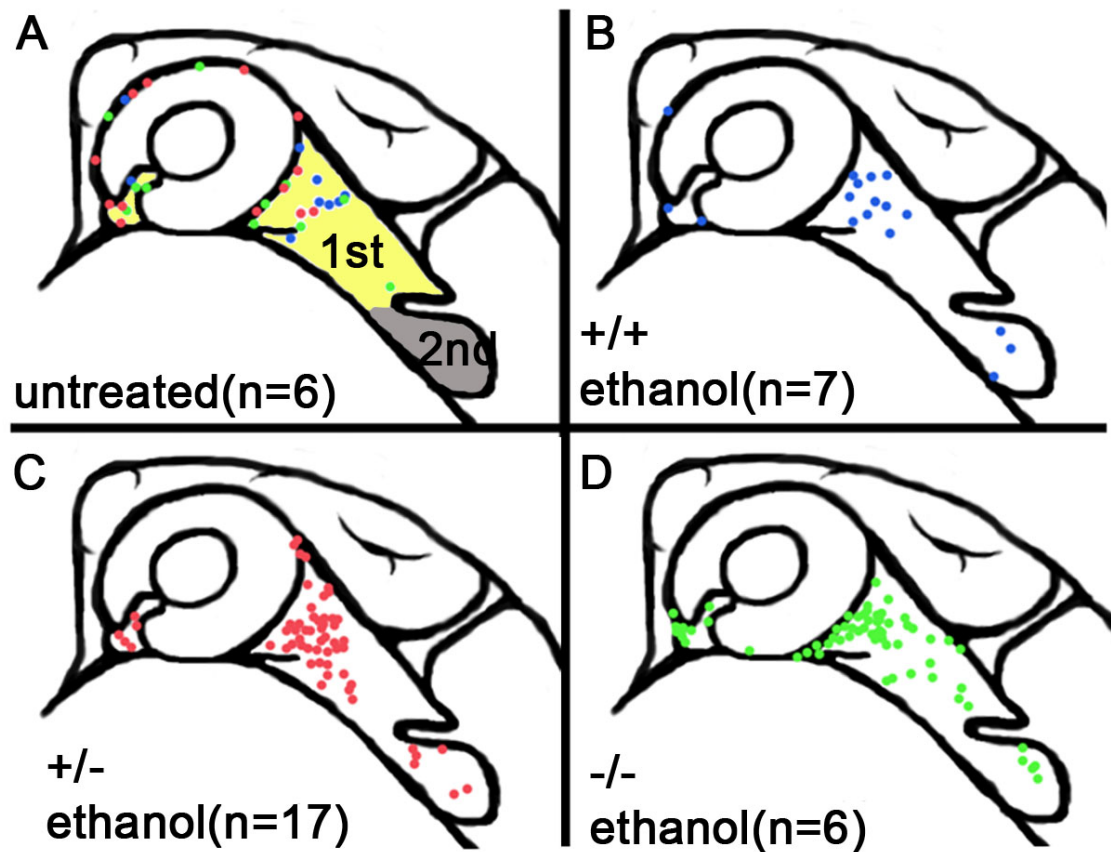


Figure 2.11: At 24 hpf ethanol-induced cell death occurs in pharyngeal arch areas destined to contribute to the jaw and jaw support elements. (A-D) depict 24 hpf embryos, anterior to the left. Each dot marks the relative position of an apoptotic neural crest cell. (A) Untreated controls, yellow marks the first pharyngeal arch, grey marks the second pharyngeal arch. (B-D) 1.0% ethanol-treatment from 10-24 hpf in (B) wild-types, (C) *pdgfra* heterozygotes, and (D) *pdgfra* mutants. Cell death is enriched in areas fated to become the palatal

skeleton and dorsal pharyngeal arch skeletal elements. Wild-type, blue dots;
pdgfra heterozygote, red dots; *pdgfra* mutant, green dots.

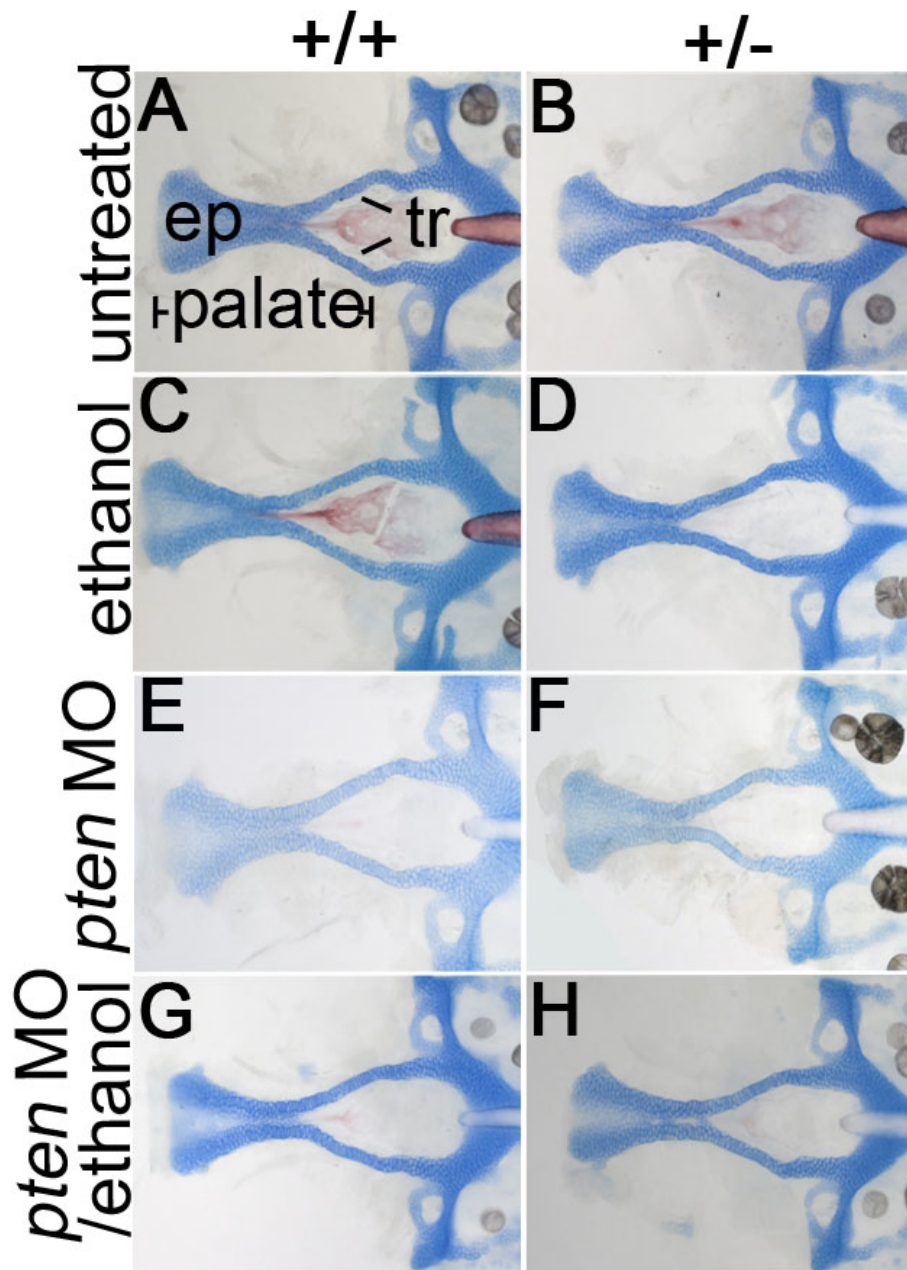


Figure 2.12: *pten* morpholino injection does not alter neurocranial development in untreated and ethanol-treated wild-type and *pdgfra* heterozygotes. (A-H) show dorsal views of 5 dpf zebrafish neurocrania, stained for cartilage and bone using Alcian Blue and Alizarin Red, respectively. Anterior is to the left. (A-B) Untreated

controls. (C-D) 1.0% ethanol treatment from 10-24 hpf. (E-F) *pten* morpholino injections. (G-H) *pten* morpholino injections with 1.0% ethanol treatment from 10-24 hpf. The palate consists of the ethmoid plate, ep and trabeculae, tr.

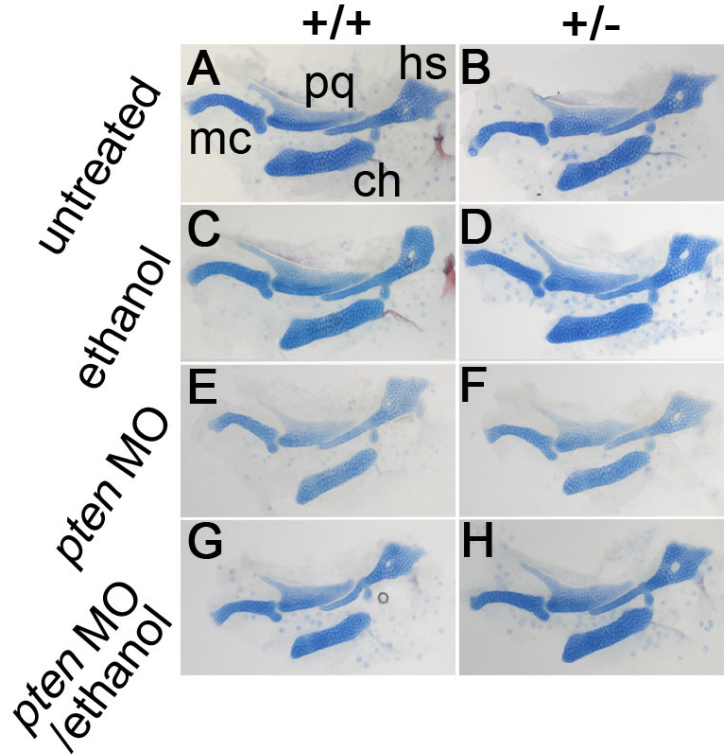


Figure 2.13: *pten* morpholino injections do not alter jaw and jaw support development in untreated and ethanol-treated wild-type and *ptdgfra* heterozygotes. (A-H) Flat mount views of 5 dpf zebrafish jaw and jaw supports, stained for cartilage and bone using Alcian Blue and Alizarin Red, respectively. Anterior is to the left. (A-B) Untreated controls. (C-D) 1.0% ethanol treatment from 10-24 hpf. (E-F) *pten* morpholino injections. (G-H) *pten* morpholino injections with 1.0% ethanol treatment from 10-24 hpf. Meckel's cartilage, mc; palatoquadrate, pq; hyosymplectic, hs; ceratohyal, ch.

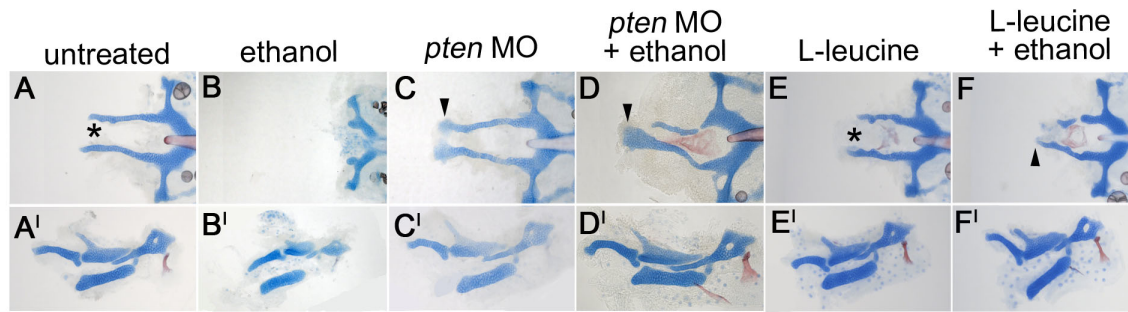


Figure 2.14: Injection of *pten* morpholino rescues the craniofacial defects in ethanol-treated *pdgfra* mutants. (A-D) show 5 dpf *pdgfra* mutant (-/-) neurocrania and (A'-D') are the corresponding pharyngeal skeletal elements, stained for cartilage and bone using Alcian Blue and Alizarin Red, respectively. Anterior is to the left. (A-A') Untreated mutants have clefting of the ethmoid plate, asterisk. (B, B') Treatment with 1.0% ethanol from 10-24 hpf causes loss of the palatal skeleton and hypoplasia of the pharyngeal skeleton. (C-D') Injection of *pten* morpholino (MO) rescues the craniofacial phenotypes of both (C-C') untreated and (D-D') ethanol exposed *pdgfra* mutants. Arrowheads mark the partially rescued ethmoid plates.

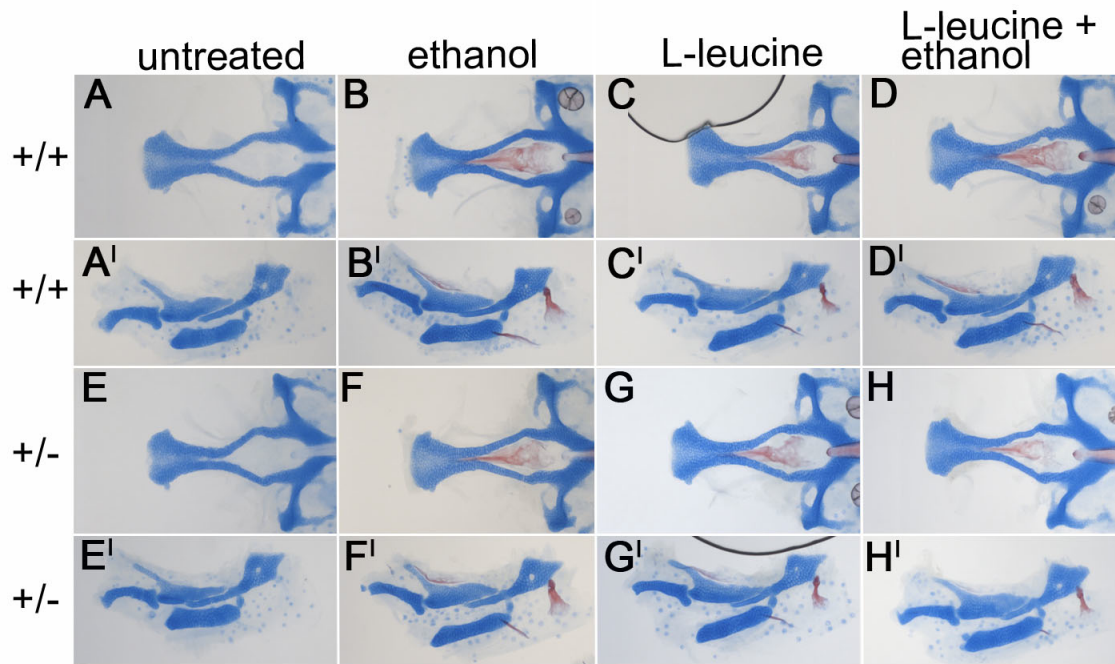


Figure 2.15: L-leucine does not alter the craniofacial skeleton of untreated and ethanol-treated wild-type and *pdgfra* heterozygotes. 5 dpf Alcian Blue and Alizarin Red stained flat mounted (A-H) neurocrania and (A'-H') jaw and jaw supports. (A,A',E,E') Untreated controls. (B,B',F,F') 1.0% ethanol treatment from 10-24 hpf. (C,C',G,G') 50 mM L-leucine treatment from 10-24 hpf. (D,D',H,H') 50 mM L-leucine with 1.0% ethanol treatment from 10-24 hpf. Anterior is to the left.

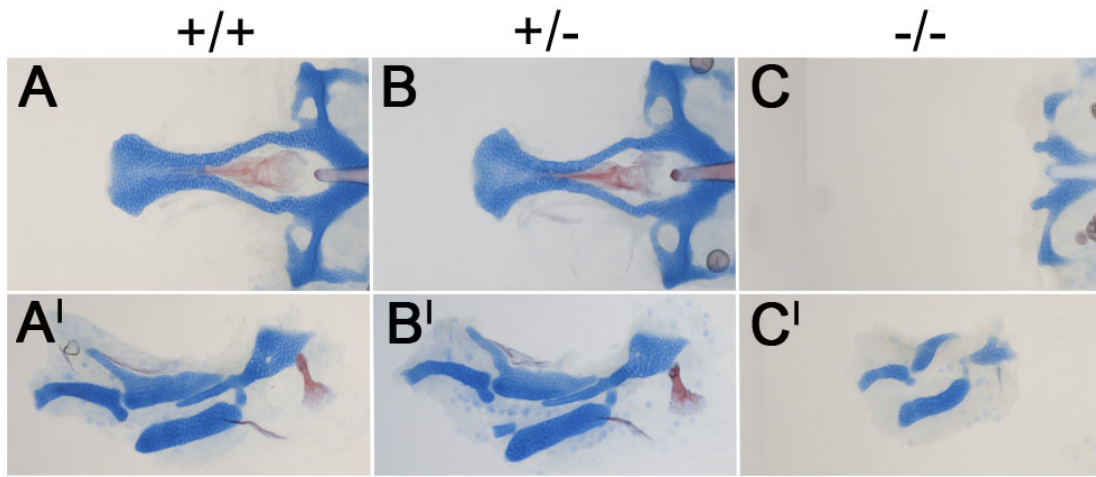


Figure 2.16: L-leucine treatment from 24 to 48 hpf does not rescue the ethanol-induced defects in 10-24 hpf treated mutants. Flat mounted 5 dpf Alcian Blue and Alizarin Red stained (A-C) neurocrania and (A'-C') jaw and jaw supports, Ethanol was administered from 10-24hpf and 50mM L-leucine was added from 24-48 hpf. (A, A') wildtype; (B,B') heterozygote; (C, C') mutant. Anterior is to the left.

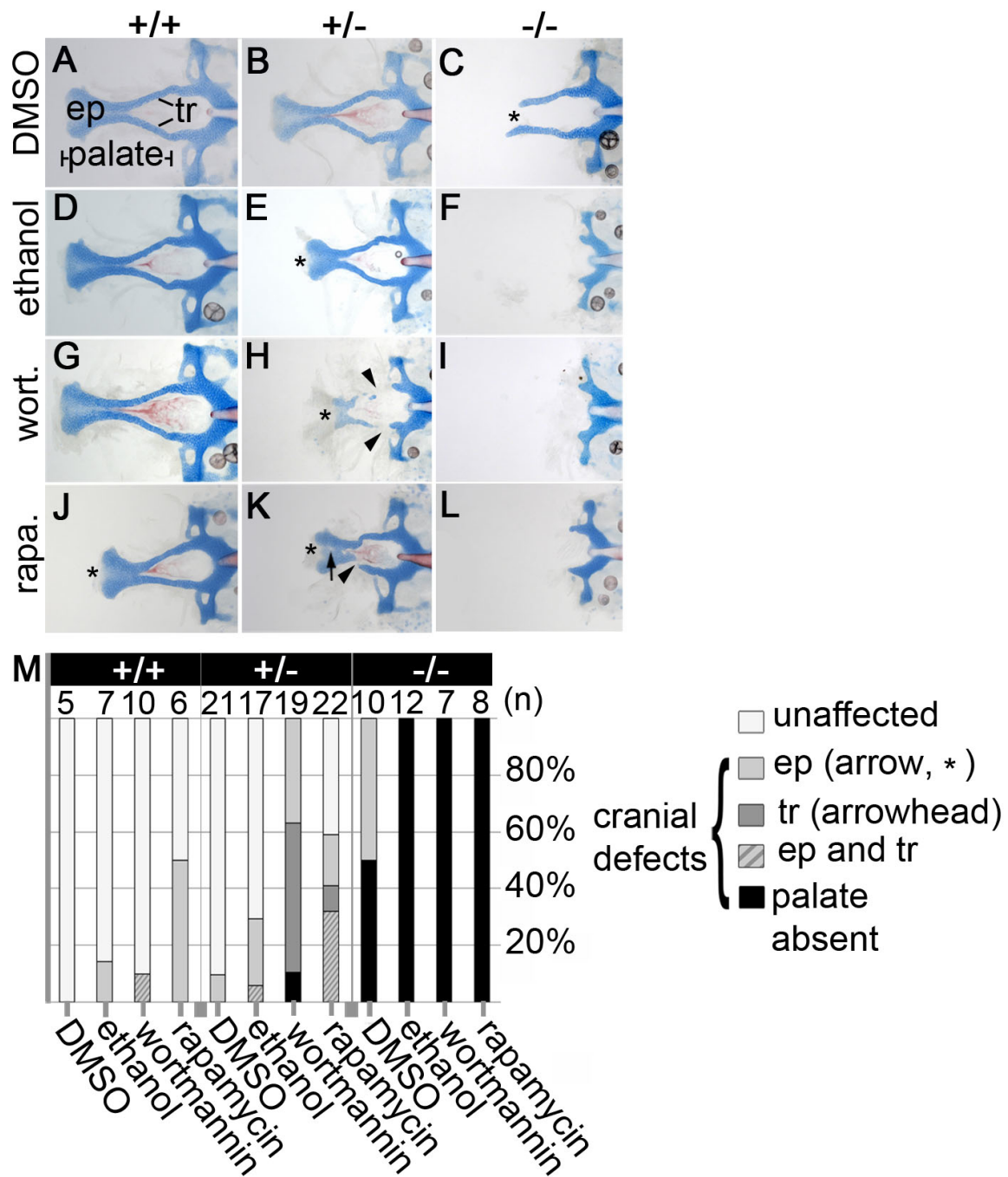


Figure 2.17: Both wortmannin and rapamycin phenocopy the effects of ethanol on *pdgfra* mutants. (A-L) show 5 dpf zebrafish neurocrania stained for cartilage and bone using Alcian Blue and Alizarin Red, respectively. Anterior is to the left.

Embryos were treated from 10-24 hpf with (A-C) DMSO, (D-F) 1.0% ethanol, (G-I) 1.5 μ M wortmannin or (J-L) 3 μ M rapamycin. Asterisks denote ethmoid-plate defects (ep), arrowheads denote trabeculae defects (tr). (M) Graph of percent defects found in all three genotypes, across treatments. Unaffected denotes a wild-type phenotype, ep denotes ethmoid-plate defects (e.g. arrow and asterisk in K), tr denotes trabeculae defects (e.g. arrowhead in H). The zebrafish palate consists of the ethmoid plate, ep and trabeculae, tr.

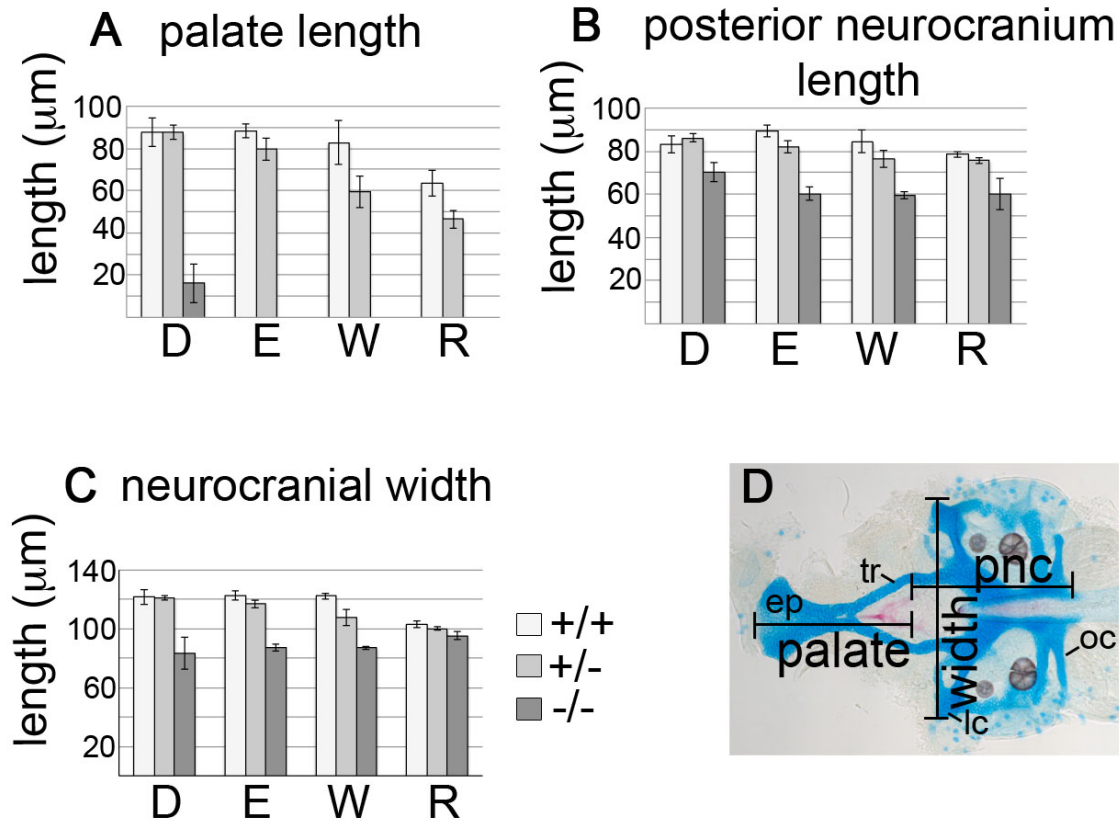


Figure 2.18: Both wortmannin- and rapamycin-treated *pdgfra* mutants show a decrease in overall neurocranial length and width. Embryos were treated from 10-24 hpf with either DMSO, 1.0% ethanol, 1.5 μ M wortmannin or 3 μ M rapamycin. Inhibition of either PI3K or mTOR phenocopies the effects of ethanol. Graphs depict the average (A) palate length, (B) posterior neurocranial length, and (C) neurocranial width in microns (standard error bars are 1.5 SEM, non-overlapping bars indicate significance; Moses, 1987). Wild-type, light bar; *pdgfra* heterozygote, gray bar; mutant, dark bar. (D) An Alcian Blue and Alizarin Red stained 5 dpf untreated wildtype neurocranium. Palate length was measured from the most anterior part of the ethmoid plate (ep) to the ends of the trabeculae (tr).

The posterior neurocranium was measured from the most posterior part of the occipital arches (oc) to the ends of the trabeculae (tr). Neurocranial width was measured between the most lateral edges of the lateral commissures (lc). D, DMSO; E, ethanol; W, wortmannin, R, rapamycin.

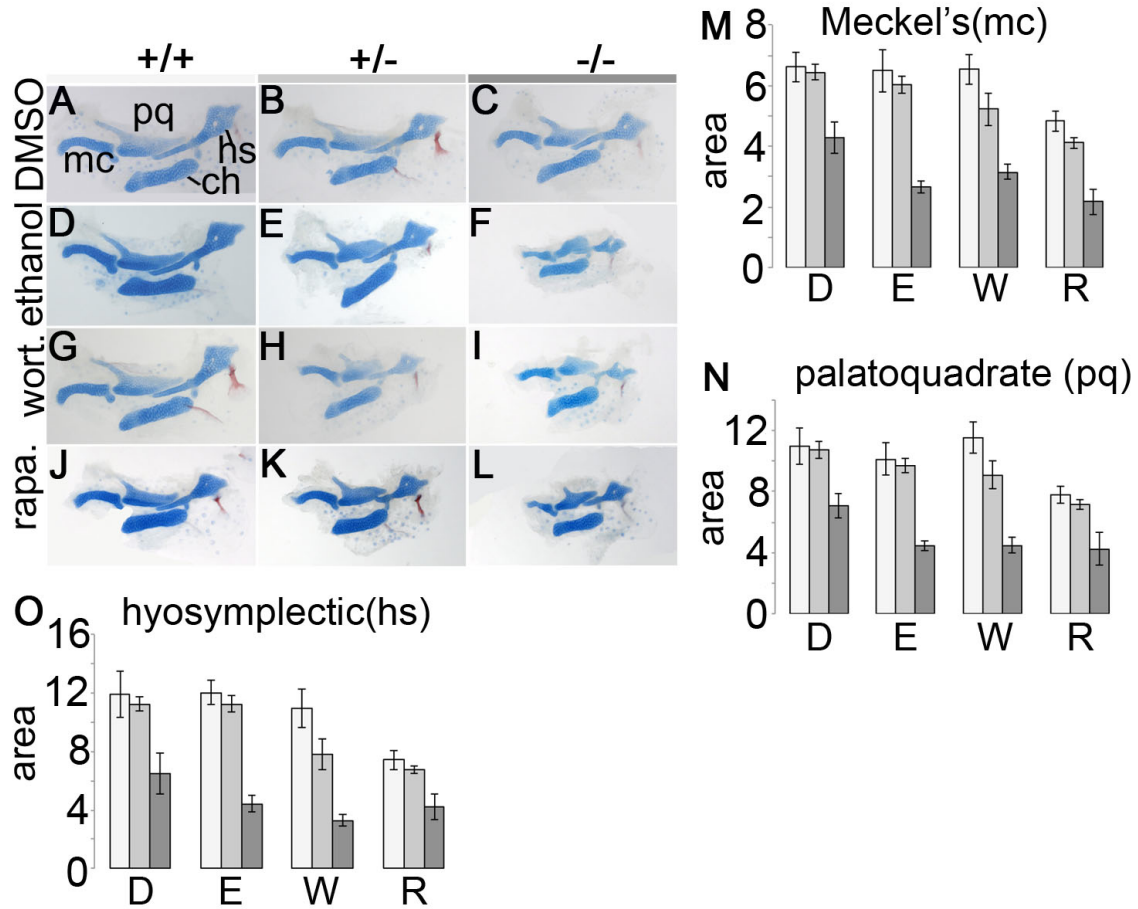


Figure 2.19: Treating *pdgfra* mutants with wortmannin or rapamycin induces pharyngeal skeleton hypoplasia. (A-L) show jaw and jaw support elements, anterior to the left, stained for cartilage and bone using Alcian Blue and Alizarin Red, respectively. Embryos were treated from 10-24 hpf with either (A-C) DMSO, (D-F) 1.0% ethanol, (G-I) 1.5 μ M wortmannin or (J-L) 3 μ M rapamycin. Inhibition of either PI3K or mTOR phenocopies the effects of ethanol. (M-O) Graphs depict the average area sizes of (M) the Meckel's, mc (N) palatoquadrate, pq and (O) hyosymplectic, hs cartilages. X-axis on all graphs denote D, DMSO; E, ethanol; W, wortmannin, R, rapamycin (standard error bars are depicted at 1.5 SEM, see

Supplemental Table 1 for full ANOVA statistical analysis). Wild-type, light bar; *pdgfra* heterozygote, gray bar; mutant, dark bar. Meckel's cartilage, mc; palatoquadrate, pq; hyosymplectic, hs; ceratohyal, ch.

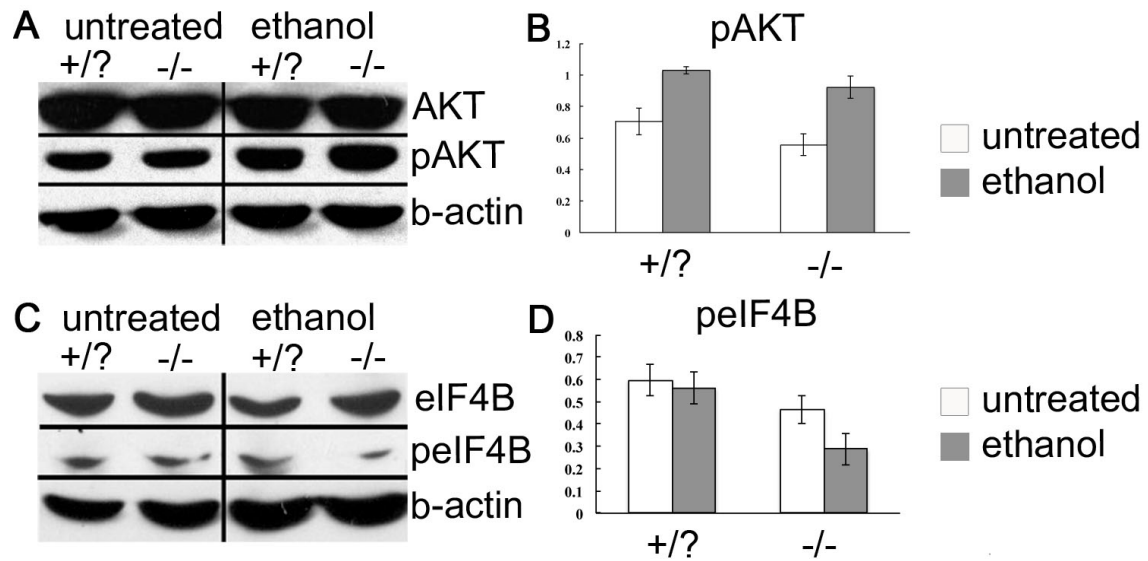


Figure 2.20: Ethanol affects phosphorylation of AKT and pEIF4B in ethanol-treated *pdgfra* mutants. Tissue samples consist of 24 hpf harvested *pdgfra* mutant (-/-) and mixed *pdgfra* heterozygote/wild-type (+/?) heads in either untreated control or 1.0% ethanol treatment from 10-24 hpf. (A) Immunoblot was stripped and reprobed for total AKT, phospho-AKT (pAKT), and b-actin for total loading control. Both ethanol-treated *pdgfra* heterozygote/wildtype and *pdgfra* mutants have elevated levels of phospho-AKT compared to untreated counterparts. (B) Immunoblot was stripped and reprobed for total eIF4B (tEIF4B), phospho-eIF4B (pEIF4B), and b-actin for loading control. *pdgfra* mutants have decreased levels of phospho-eIF4B compared to untreated mutants and both untreated and ethanol-treated heterozygote/wildtype samples.

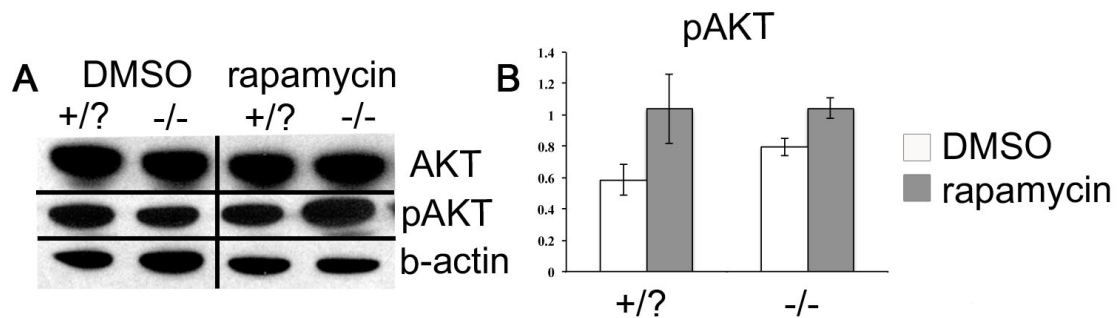


Figure 2.21: Rapamycin-treatment leads to an increase in phosphorylated AKT in both *pdgfra* mutants and siblings as compared to DMSO-treated controls. Tissue samples consist of 24 hpf harvested *pdgfra* mutant (-/-) and sibling (+/?) heads from embryos of either DMSO or 3mM rapamycin treatment from 10-24 hpf. (A) Immunoblot was stripped and reprobed for total AKT, phospho-AKT (pAKT), and b-actin as a loading control. Rapamycin treatment caused elevated levels of phospho-AKT compared to untreated counterparts. (B) Graph of the quantification of pAKT to total AKT across 3 immunoblots.

2.VIII. Tables

	Mc	pq	hs
0.50%			
+/+	N	N	N
+/-	N	N	N
-/-	N	N	N
1.00%			
+/+	N	N	Y
+/-	N	N	Y
-/-	Y	Y	Y
10-24			
+/+	N	N	N
+/-	N	N	N
-/-	Y	Y	Y

Table 2.1: ANOVA statistics describing significant differences of skeletal elements across genotype and treatments. Tables are categorized by skeletal elements Meckel's (mc), palatoquadrate (pq), and hyosympletctic (hs). "Y" denotes a significant difference between the genotype/ethanol interaction relative to the genotype and ethanol treatment alone. wt, wild type; het, heterozygous; mut, mutant. Treatments are: unt, untreated; 0.5%, 0.5% ethanol from 10 hpf-5 dpf; 1%, 1% ethanol from 10 hpf-5 dpf; 10-24, 1% ethanol from 10-24 hpf.


GENE	SNP	GENE	SNP	GENE	SNP	GENE	SNP
PDGFRA:	rs7678144	PDGFC:	rs1425486	PDGFD:	rs1471936	PDGFD:	rs361315
	rs7677751		rs4691377		rs10895548		rs361262
	rs4358459		rs983473		rs901782		rs361266
	rs7656613		rs6834932		rs2220377		rs10502025
	rs1547904		rs17035257		rs6591063		rs615290
	rs2228230		rs10023148		rs10502023		rs361281
	rs3733540		rs4691381		rs12282189		rs361283
PDGFRB:	rs165979		rs10517653		rs2047698		rs590216
	rs246391		rs10033375		rs10791658		rs603781
	rs246395		rs2974254		rs260836		rs488753
	rs17656204		rs2911941		rs10895555		rs361291
	rs2304061		rs17035367		rs1872902		rs11226159
	rs1075846		rs342317		rs651979		rs168636
	rs919751		rs342308		rs11226106		rs11226185
	rs3756309		rs6812101		rs10895558		rs1532673
	rs1864971		rs17231377		rs12574463		rs361268
	rs740750		rs11728198		rs629720		rs10895586
	rs740751		rs4691383		rs732451		rs10791670
	rs9324641		rs17231573		rs12146566		rs10791671
	rs4358508		rs10517660		rs260862		rs11226207
	rs3776081		rs10010472		rs260864		rs2128806
	rs2302273		rs4382082		rs1386751		rs10895595
			rs6845322		rs260865		rs7943011
PDGFB:	rs4416326	PDGFD:	rs1053861		rs12363710	SNP x ethanol interaction significance 	
	rs9611117		rs11226057		rs17421481		
	rs4821877		rs1872901		rs260852		
	rs11704525		rs541150		rs260858		
	rs9622979		rs545643		rs11226125		
	rs2247128		rs1994450		rs1818106		
	rs879180		rs11226082		rs260815		
	rs5757573		rs4384362		rs9326345		
	rs5750781		rs4145958		rs260818		

Table 2.2: Human SNP-ethanol interactions produce craniofacial measurement changes. Significant SNP-ethanol interactions associated with changes in craniofacial measurements are highlighted in yellow. Chr, chromosome; SNP, single-nucleotide polymorphism identification number; BP, base-pair; MAF, minor

allele frequency; ICW, inner canthal width; OCW, outer canthal width; LFH, lower facial height; LFD, lower facial depth; MFD, mid-facial depth (Mattson et al., 2010; Moore et al., 2007). Analysis by Leah Wetherill and Tatiana M. Foroud.

Chapter 3: An Fgf-Shh signaling hierarchy regulates early specification of the zebrafish skull.¹

3.1. Abstract

The neurocranium generates most of the craniofacial skeleton and consists of prechordal and postchordal regions. Although development of the prechordal is well studied, little is known of the postchordal region. Here we characterize a signaling hierarchy necessary for postchordal neurocranial development involving Fibroblast growth factor (Fgf) signaling for early specification of mesodermally-derived progenitor cells. The expression of *hyaluron synthetase 2* (*has2*) in the cephalic mesoderm requires Fgf signaling and Has2 function, in turn, is critical for postchordal neurocranial development. While Hedgehog (Hh)-deficient embryos also lack a postchordal neurocranium, this is due to a later defect in chondrocyte differentiation. Inhibitor studies demonstrate that postchordal neurocranial development requires early Fgf and later Hh signaling. Collectively, our results provide a mechanistic understanding of early postchordal neurocranial development and demonstrate a hierarchy of signaling between Fgf and Hh in the development of this structure.

¹ Authors: Neil McCarthy¹, Julien Y. Bertrand³, and Johann K. Eberhart^{1,2}.

¹Department of Molecular Biosciences; Institute of cell and molecular biology, Waggoner Center for Alcohol and Alcohol Addiction Research, University of Texas, Austin, Texas.

²Department of Molecular Biosciences; Institute of Neurobiology, University of Texas, Austin, Texas.

³Department of Pathology and Immunology, University of Geneva Medical School, Geneva, Switzerland.

3.II. Introduction

The neurocranium is an embryonic structure that generates essential craniofacial structures including the skull vault, skull base, and palate. The palate and skull base are connected and demarcate the prechordal, or anterior, and postchordal, or posterior, regions of the neurocranium, respectively. Extensive fate mapping in tetrapod species demonstrate that the neural crest and mesoderm contribute to the prechordal and postchordal neurocranium, respectively (Couly et al., 1992 and 1993; Crump et al., 2004; Eberhart et al., 2006; Gross et al., 2008; Koentges and Lumsden, 1996; McBratney-Owen et al., 2008; Wada et al., 2011). Despite our knowledge of the tissue origins of the neurocranium, mechanistic studies of development have overwhelmingly focused on the prechordal neurocranium, while the postchordal region has been left largely neglected.

For proper formation, the neurocranium requires the orchestration of numerous signaling and morphogenetic events, and is dependent on interactions with surrounding neural as well as non-neural ectoderm, mesoderm, and endoderm (Alexander et al., 2011; Kimmel et al., 2001; Marcucio et al., 2011; Noden and Trainor, 2005; Richtsmeier and Flaherty, 2013). The complexity of these interactions implicates the involvement of multiple signaling molecules in neurocranial development. Much progress has been made in elucidating those factors that induce craniofacial formation and patterning. These factors include many signaling pathways, including Shh, Fgf, Bmp, and Wnt (Alexander et al., 2014; Marcucio, 2005; Richtsmeier et al., 2013; Wada et al, 2005; Wilson and

Tucker, 2004). No one single factor can direct craniofacial formation; instead, they interact in spatial and temporal hierarchies that coordinate craniofacial growth and development.

While we know of many of the signaling hierarchies in the neural-crest derived-portions of the craniofacial skeleton, little is known of the mesoderm-derived portions. Hosokawa et al showed that development of the posterior skull vault, a mesoderm-derived structure, involves a signaling hierarchy between TGF- β and Msx2 (Hosokawa et al., 2007). In mouse, chick, and zebrafish, Shh is a critical midline signal necessary for chondrocyte differentiation in the postchordal neurocranium, as well as other regions of the skull (Balczerski et al., 2012; Eberhart et al., 2006; Wada et al., 2005). Specification of the early cephalic mesoderm, however, is refractory to sonic hedgehog signaling (Balcezerski et al., 2012), suggesting that other signals are necessary for early cephalic mesoderm specification. Due to their proximity to the postchordal neurocranium and their importance in numerous aspects of craniofacial development, the Fibroblast growth factor (Fgf) family is a prime candidate for this function.

Fgfs are part of a large family of intercellular signaling molecules (Itoh, 2007) that emanate from multiple tissue sources in the head. They are also crucial in numerous aspects of craniofacial development, including the proper migration, survival, and patterning of the neural crest (Creuzet et al., 2004; Crump et al., 2006; Hu et al., 2009; Wilson and Tucker, 2004) as well as cranial suture formation (Nie et al., 2006; Rice et al., 2000). Furthermore, Fgfs are

implicated in a number of congenital craniofacial disorders with reported skull base defects including Aperts and Crouzon (Aggarwal et al., 2006; Tokumaru et al., 1996). In a screen for gene-ethanol interactions, it was found that *fgf8a* and ethanol interact to affect postchordal neurocranial structures that could be recapitulated with rapamycin, an inhibitor of mTOR which is a constituent of growth factor signaling (Fig 3.1C and 3.1D compared to 3.1B; McCarthy et al., 2013). Ethanol seems to broadly attenuate growth factor signaling (McCarthy et al., 2013), suggesting that the postchordal defects in the *fgf8a*-ethanol interaction are due to attenuated Fgf signaling. However, it is unclear what role Fgfs play in early postchordal neurocranial development in the absence of ethanol.

Here, we characterize a signaling hierarchy required for proper postchordal neurocranial development involving Fgf and Shh signaling. Loss of function of both *fgf3* and *fgf8a* lead to a striking loss of the postchordal neurocranium that can be rescued by restoring Fgf3 and Fgf8a signaling centers in the brain and mesoderm. We go on to precisely describe, for the first time, the dual tissue origins of the zebrafish neurocranium. The zebrafish postchordal neurocranium has small pockets of neural crest-derived areas occurring in a mostly mesodermally-derived structure. *In situ* analysis reveals that both the early cephalic mesoderm marker *hyaluron synthetase 2 (has2)* and markers for chondrocytes are lost in *fgf3;fgf8a* knockdown embryos, and that *has2* is required for postchordal neurocranial development in an Fgf-dependent manner. Examination of Hh loss-of-function embryos reveals that Hh signaling is

dispensable for specification of head mesoderm. These results provide evidence of an early signaling interaction required for proper postchordal neurocranial development.

3.III. Results

3.III.a. The postchordal neurocranium requires *fgf8a* and *fgf3*.

The neurocranium can be split into anterior and posterior halves (dashed line in Fig. 3.2A). While much research has been directed at the development of the neural crest-derived prechordal neurocranium (Fig. 3.2A, prech.), little is known of the development of the postchordal neurocranium (Fig. 3.2A, postch.). The postchordal neurocranium includes the parachordal cartilages (pc), which abut the notochord (n); as well as the anterior and posterior basicapsular commissures (abc & pbc, respectively) which encircle the developing ear, the lateral commissures (lc), and the occipital arches (oc) (Fig. 3.2A; de Beer, 1937). Due to its development adjacent to the notochord and the hindbrain, we reasoned that signals from one or both of these structures could influence posterior neurocranial development.

Fgf8 and Fgf3 signal cooperatively to pattern the hindbrain, making these two Fgfs prime candidates for our analyses. We used a combination of genetic and morpholino-based loss of function of these Fgf ligands, each of which resulted in similar results (Fig. 3.2 and 3.3). Whereas neither *fgf8a* nor *fgf3* single-mutants show any profound postchordal neurocranial defects (Fig. 3.2B

and 3.2C compared to 3.2A), the vast majority of the postchordal neurocranium is absent in double *fgf8a;fgf3* mutants (Fig. 3.2E, arrowhead), with only the prechordal neurocranium and occipital arches remaining. Furthermore, even the loss of a single allele of *fgf3* in an *fgf8a* mutant background gives rise to variable postchordal neurocranial defects, including anterior basicapsular and parachordal cartilage loss (Fig. 3.2D, arrowheads). These mutants also have severe viscerocranial defects (not shown, Crump et al., 2004). Because, at least, *fgf8a* is maternally expressed (Reifers et al., 1998), we extended our analyses using the well-characterized morpholinos against each of these Fgfs (Crump et al., 2004; Liu et al., 2003; Maves et al., 2002).

Morpholinos targeting either *fgf8a* or *fgf3* injected into *fgf3* or *fgf8a* mutants, respectively, recapitulated postchordal neurocranial defects observed in the double mutants (Fig. 3.3). Embryos injected with *fgf3* morpholinos display infrequent loss of the anterior basicapsular commissure (24%, n=6/24, Fig. 3.3), however the remainder of the neurocranium in these embryos is well developed. Embryos injected with *fgf3* morpholinos also consistently display fused otoliths (Fig. 3.2) as well as variable viscerocranial defects, including fusions of Meckel's cartilage and the palatoquadrate, and loss of the ceratobranchial cartilages (data not shown; Crump et al., 2004). As in our mutant analysis, we found strong synergy between *fgf8a* and *fgf3* in development of the postchordal neurocranium.

In contrast to phenotypes in single mutants, the postchordal neurocranium is lost in *fgf3* morpholino-injected *fgf8a* mutants (100%, n=21/21, Fig. 3.2). The

ethmoid plate and trabeculae are retained, albeit reduced, in these embryos (n=21/21). Viscerocranial defects also occur in these embryos, including variable hyosymplectic loss, severe reductions and fusions of Meckel's cartilage and the palatoquadrate (data not shown; Crump et al. 2004). Lastly, we could recapitulate the postchordal neurocranial loss in *fgf8a* morpholino-injected *fgf3* mutants (Fig. 3.2). Together, these data show *fgf3* and *fgf8a* synergize during postchordal neurocranial development.

Fgf signaling occurs through four receptors (Itoh et al., 2002); however, they are expressed in multiple tissues throughout development (Sivak et al., 2005; Thisse and Thisse, 2005). To understand which receptor is involved in postchordal neurocranial development, we used the *fgf8a* mutant line and a suboptimal dose of morpholino to target each receptor individually. While *fgfr1*, *fgfr2*, and *fgfr4* knockdowns in the *fgf8a* mutant background caused variable ear and viscerocranial defects, no postchordal neurocranial defects were found (not shown). However, a suboptimal dose of *fgfr3* morpholino injected into *fgf8a* mutants showed variable defects to the postchordal neurocranium that mirrored those seen in *fgf8a;fgf3* double loss-of-function embryos (Fig. 3.4). These data suggest that Fgfr3 is a strong candidate for Fgf-mediated postchordal neurocranial development.

3.III.b. The mesoderm and neural ectoderm are Fgf sources required for postchordal neurocranium formation.

Fgf signaling is required throughout development, forming numerous centers of activity including the mesoderm and neural ectoderm early, and the endoderm and otic placode later (Crump et al., 2004; Sivak et al., 2005; Thisse and Thisse, 2005). To investigate the required Fgf signaling source for postchordal formation, we generated genetic chimeras to re-introduce Fgf signaling from wild-type donor tissues in *fgf3;fgf8* knockdown hosts. We tested four tissue sources: the mesoderm, neural ectoderm, endoderm, and otic placode (Fig. 3.5). While neither endoderm nor otic placode transplants restored the neurocranium (n=0/12 for endoderm, n=0/9 for otic placode, Fig. 3.5A-A'', 3.5B-B''), we observed a partial rescue of the postchordal neurocranium in embryos receiving either mesoderm or neural ectoderm transplants (n=4/7 for mesoderm, n=8/16 for neural ectoderm, Fig. 3.5C-C'', 3.5D-D'', 3.5H). In these transplants most of the parachordal cartilage and anterior basicapsular commissure were present, but rescue was incomplete, suggesting that both tissues might be required. To test this dual requirement, double mesoderm and neural ectoderm transplants were performed, and indeed, complete rescue of the postchordal neurocrania on the transplanted side in *fgf3;fgf8a* loss-of-function hosts was attained (n=4/12 for full rescue, n=3/12 for partial rescue, Fig. 3.5E-E'', 3.5H). Together, these data suggest that Fgf signaling from the mesoderm and neural ectoderm cooperate during formation of the postchordal neurocranium.

The otic placode is induced by Fgf signaling from the neural ectoderm (Leger and Brand, 2002; Sai and Ladher, 2015), so it is possible that we restored these signals by our neural ectoderm transplants. Thus, the partial rescue by neural ectoderm could be due to the otic placode. To directly test this possibility, we injected embryos with *dlx3b* and *foxi1* morpholinos which results in the loss of the otic placode (Solomon et al., 2002; Solomon et al., 2003). While injection of both *dlx3b* and *foxi1* caused complete loss of the otic placode at 24 hpf (Fig. 3.6), only the anterior basicapsular commissure was missing or reduced in these embryos (Fig. 3.6). These data show that while the otic placode may provide signals required for the anterior basicapsular commissure, defects to the otic placode itself do not explain the extensive loss of the postchordal neurocranium found in *fgf3;fgf8* loss of function embryos.

3.III.c. The postchordal neurocranium is primarily mesoderm-derived.

Deeper analysis of the role of Fgf signaling in postchordal development requires a detailed characterization of the precursors to this structure. However, the origins of the postchordal neurocranium are unknown in zebrafish. To fully characterize any neural crest contribution to the postchordal neurocranium, we utilized three neural-crest labeling transgenic lines, *sox10:KikGR*, *sox10:Kaede*, and *sox10:Cre;ubi:RSG* (Balczerski et al., 2012; Dougherty et al., 2013; Kague et al., 2012). The *sox10:KikGR* and *sox10:Kaede* embryos were photoconverted at 24 hpf to label all neural crest cells, while the *sox10:Cre;ubi:RSG* line genetically

labels neural crest cell descendants (Kague et al., 2012). Results in all 3 lines were identical, with extensive labeling in the ethmoid plate (ep) and trabeculae (tr) of the prechordal neurocranium (Fig. 3.7A-D, 3.7G, data not shown; Eberhart et al., 2006; Kague et al., 2012; Wada et al., 2005). We also observed highly localized labeling within postchordal structures. Labeled areas included the lateral auditory capsule as well as the lateral and anterior-most region of the anterior basicapsular commissure (Fig. 3.7A-D, 3.7G). It is of interest that this precise region articulates with the second arch crest-derived hyosymplectic of the viscerocranium (Crump et al., 2004).

The first and second arches are composed of Hox-negative and Hox-positive neural crest cells, respectively (Crump et al., 2006). These arches undergo dynamic morphogenetic movements that involve numerous neural crest-specific cellular rearrangements (Crump et al., 2004; Crump et al., 2006; Eberhart et al., 2006). To elucidate which pharyngeal arch contributes neural crest cells to the postchordal neurocranium, we performed fate mapping with *sox10:Kaede* embryos. We photoconverted either the first or second arch at 26 hpf (Fig. 3.8; Crump et al., 2006), and found that the second arch crest contributed to the lateral auditory capsule (Fig. 3.8), while the first arch crest contributed to the lateral and anterior most region of the anterior basicapsular commissure (Fig. 3.8). Together, these results show that Hox-negative and Hox-positive neural crest cells contribute to adjacent regions of the postchordal neurocranium.

In both mouse and chicken, mesoderm contributes significantly to the posterior neurocranium. We used the mesoderm-labeling *drl:CreERT2;ubi:switch* line to track mesoderm derivatives in zebrafish (Fig. 3.9; Mosimann et al., 2011). Tamoxifen was added from 6 hpf to 24 hpf to induce Cre- excision. We find a pattern of labeling perfectly complimentary to that generated by the neural crest (Fig. 3.7E–G). The parachordal cartilages, posterior basicapsular commissures, and occipital arches appear to be completely of mesoderm origin (Fig. 3.7E–G). The regions of the anterior basicapsular commissure that were not labeled by neural crest are also of mesoderm origin (Fig. 3.7E–G). The lateral commissure was the only structure where neural crest and mesoderm cells appear to mix (Fig. 3.7). Collectively, these data provide a high-resolution fate map of neural crest and mesoderm contribution to the neurocranium and suggest that, even in regions of dual origin, there is little mixing between these cell types.

In order to determine what happens to this mesoderm population in Fgf loss-of-function embryos, a detailed fate map of these postchordal progenitor cells was necessary. We used Kaede photoconversion to label and track groups of cells from 24 hpf to 4 days post fertilization (dpf), when the postchordal neurocranium is well formed in zebrafish (Fig. 3.10A–D). We injected *fli1:EGFP* embryos with *Kaede* mRNA and labeled head mesoderm just dorsal to the pharyngeal arches for our analyses (Schilling and Kimmel, 1994). In the images, the intense EGFP fluorescence masks the much dimmer green Kaede fluorescence so only the red, photoconverted, Kaede is apparent. We find that at

24 hpf, the progenitors of the postchordal neurocranium are positioned within the head in relative accord to their location at 4 dpf (Fig. 3.10E and 3.10E', see Fig. 3.11 for individual data). Overall, no relative change in position of these labeled cells occurred between 24 hpf and 4 dpf. Cells labeled anterior of the otic capsule (o.c.) maintain this position at 4 dpf (Fig. 3.10E and 3.10E', dark grey shade). Those cells labeled more medial and posterior to the otic capsule at 24 hpf populate areas medial and posterior 4 dpf (Fig. 3.10E and 3.10E', gray and light gray shades). During this same time period, neural crest cells appear to undergo extensive cell rearrangements in forming skeletal structures (Crump et al., 2006; Le Pabic et al., 2014). We find little dispersion of labeled mesoderm cells, suggesting a lack of similar rearrangements in the mesoderm-derived skeleton. Together, these data show that the progenitors of the postchordal neurocranium are appropriately positioned along the anterior to posterior axis at 24 hpf.

3.III.d. Proper specification of the head paraxial mesoderm requires Fgf signaling.

Our fate map of the postchordal neurocranium shows that these cartilage precursors are in place by 24 hpf. To investigate whether these precursors are present in embryos lacking *fgf3* and *fgf8a*, we analyzed the expression of the prechondrogenic marker *sox9a* and the cartilage marker *col2a1a*. Compared to un-injected and control morpholino-injected *fgf8a* mutants, *fgf3;fgf8a* double loss

of function embryos display a loss of *col2a1a* in the cephalic mesoderm (Fig. 3.12D, compared to 3.12A-C, asterisks; Piotrowski et al. 2000). The notochord staining for *col2a1a* is retained in double loss-of-function embryos, demonstrating specificity of the effect (Fig. 3.12D, arrowheads denote anterior notochord). Furthermore, the pre-cartilage marker *sox9a* is also lost in these *fgf3* morpholino-injected *fgf8a* mutants (Fig. 3.12H, compared to 3.12E-G). Together, these data suggest that the head paraxial mesoderm that will generate these cartilages is either mislocalized or improperly specified when Fgf signaling is attenuated.

To directly address if head paraxial mesoderm is mislocalized in Fgf loss-of-function embryos, we tracked endomesoderm progenitor cells from the initiation of gastrulation (6 hpf) to the end of gastrulation (10 hpf) via Kaede photoconversion. We elaborated on established fate-maps of the mesoderm to label and track postchordal progenitor cells (Kimmel et al., 1990; Schilling and Kimmel, 1994). We injected embryos with Kaede mRNA, photoconverted endomesoderm cells adjacent to the shield at 6 hpf (Fig. 3.13A-B), and imaged their progression adjacent to the notochord at 10 hpf (Fig. 3.13C). These labeled cells were then confirmed to contribute to the postchordal neurocranium at 4 dpf (Fig. 3.13D). Similar to control and Fgf single loss-of-function embryos, mesoderm cells in *fgf3;fgf8a* morpholino-injected embryos migrated to the notochord by 10hpf (Fig. 3.13H compared to 3.13E-G). These results demonstrate that head paraxial mesoderm does migrate to its location lateral to the notochord in Fgf loss-of-function embryos and suggest that the postchordal

neurocranial defects may be due to a failure in specification of this population of head mesoderm cells.

Because the head paraxial mesoderm expresses *sox9a* and *col2a1a* relatively early in development, we hypothesized that some genes important in chondrocyte maturation would be early markers of this population of head paraxial mesoderm. *Hyaluronan synthetase 2 (has2)* is required for hyaluronic acid synthesis (Bakkers et al., 2003; Moffatt et al., 2011; Necas et al., 2008; Weigel et al., 1997; Yoshida et al., 2000). Hyaluronic acid is an important extracellular glycosaminoglycan involved in numerous cellular processes including chondrocyte maturation (Moffatt et al., 2011; Necas et al., 2008). Mouse *Has2* knockouts display cephalic mesoderm defects (Camenisch et al., 2000) and in chick limb mesodermal cells, fetal bovine chondrocytes, mouse ear placodal cells, and breast cancer cells, *Has2* is positively regulated by Fgf signaling (Bohrer et al., 2014; Hamerman et al., 1986; Munaim et al., 1991; Urness et al., 2010). These data suggest that *has2* might not only be a marker of head paraxial mesoderm, but may also be important in the generation of the Fgf loss-of-function phenotype.

Our earlier analysis revealed that localization of the head paraxial mesoderm was unperturbed in *fgf3;fgf8* knockdown embryos at 10 hpf. However, by 10 hpf, *has2*-positive cells abutting the notochord in the most anterior region, where the postchordal neurocranium is developing, are lost in *fgf3;fgf8* knockdown embryos (Fig. 3.14D-D', compared to 3.14A-C, 3.14A'-C'). No gross

alterations in earlier *has2* expression, at 6 hpf, could be ascertained in *fgf3;fgf8* knockdown embryos (Fig. 3.15). This suggests that early cephalic mesoderm is not properly specified when Fgf signaling is attenuated.

Chondrocyte maturation has been shown to rely on *has2* function, however, it was unclear whether loss of *has2* contributed directly to the postchordal neurocranial defects in *fgf3;fgf8* knockdown embryos. Utilizing a previously published morpholino targeting *has2* (Bakkers et al., 2004), we injected *fgf8a* mutants with a suboptimal dose of the *has2* morpholino. Wildtype siblings are largely unaffected in the posterior neurocranium (Fig 3.14G compared to 3.14E), as are control morpholino-injected *fgf8a* mutants (Fig 3.14F compared to 3.14E). However, *has2* morpholino-injected *fgf8a* mutants display partial loss of the postchordal neurocranium (Fig. 3.14H, arrowheads). These data suggest that the exacerbated postchordal neurocranial defects observed in *fgf3;fgf8* knockdown embryos is, at least, partially due to loss of *has2*.

The major function of Has2 is in the synthesis of hyaluronic acid (Bakkers et al., 2003; Moffatt et al., 2011; Necas et al., 2008; Weigel et al., 1997; Yoshida et al., 2000). To test the requirement of this function of *has2*, we treated *fgf8a* mutants with a suboptimal concentration of 4-methylumbelliferon (4-MU; Sigma-Aldrich), which is known to inhibit hyaluronic acid production (Garcia-Vilas et al., 2013). Treating *fgf8a* mutants with 4-MU between 6 and 10 hpf did not result in appreciable postchordal neurocranial defects (not shown). However, when treated between 10 and 30 hpf, 4 MU-treated *fgf8a* mutants display loss of

col2a1a expression at 30 hpf and, at 5 dpf, disruption of mesodermal-derived portions of the postchordal neurocranium, as compared to control-treated *fgf8a* mutants and 4 MU-treated wildtype siblings (Fig. 3.16). Collectively, these data suggest that the postchordal neurocranial defects found in Fgf-compromised embryos is dependent on hyaluronic acid production following gastrulation.

Due to the loss of *has2* expression at 10 hpf in *fgf3;fgf8a* knockdown embryos, we reasoned that Fgf signaling would be required early for postchordal neurocranial development. Using a suboptimal dose of SU5402 (Tocris Biosciences) from 6 to 10 hpf on *fgf8a* mutants and siblings, we found that, while SU5402-treated wildtypes showed normal neurocranial development (Fig. 3.17B compared to 3.17A and 3.17E), both heterozygote and mutant *fgf8a* zebrafish showed postchordal neurocranial defects, affecting the anterior basicapsular commissure in heterozygotes, and the entirety of the postchordal neurocranium in mutants (Fig. 3.17D compared to 3.17A-C, 3.17E). Furthermore, *has2* expression at 10 hpf in SU5402-treated *fgf8a* mutants is completely absent in the region of the developing postchordal neurocranium (compare Fig. 3.17I to 3.17F and 3.17G). These data strongly suggest that Fgf signaling is required during gastrulation, between 6 and 10 hpf, for postchordal neurocranial formation and specification.

3.III.e. The notochord is dispensable in the formation of the postchordal neurocranium

Our data shows that Fgf signaling, originating from the mesoderm and neural ectoderm, is required in the development of the postchordal neurocranium.

Previous reports have shown the importance of Shh signaling from the notochord in this process (Balczerski et al., 2012). Considering our data, Fgf and Shh together may form a signaling hierarchy required for postchordal neurocranial development. Thus, we investigated the function of the notochord and Shh in the formation of the postchordal neurocranium.

To directly ask whether the maintenance of a notochord is necessary for cephalic mesoderm induction and postchordal neurocranial formation, we analyzed *brachyury* mutants (previously known as *no tail*), which transfect the notochord early in development (Amacher et al., 2002). However, *brachyury* mutants express *has2* at 10 hpf (Fig. 3.18B-B', compared to 3.18A-A'), *col2a1a* at 24 hpf (Fig. 3.18D), and retain a postchordal neurocranium (Fig. 3.18F, compared to 3.18E). These data show that notochord maintenance is dispensable for the formation of the postchordal neurocranium.

In *brachyury* mutants, midline sources of Hh remain. To directly test the involvement of Hh signaling in posterior neurocranial development, we analyzed *smo* mutants, which lack all Hh signaling and a postchordal neurocranium (Varga et al., 2001). In *smo* mutants, we find that *has2* expression in the region of the postchordal neurocranium is present (Fig. 3.19B-B' compared to 3.19A-A'), but

there are severe reductions in cells expressing the chondrocyte marker *col2a1a* (Fig. 3.19D compared to 3.19C, Eberhart et al., 2006; Wada et al., 2005). Our *smo* data suggests that Hh signaling is required for differentiation of chondrocytes in the mesoderm-derived postchordal neurocranium after 10 hpf.

To directly test the temporal requirement of Hh in the formation of the posterior neurocranium, we utilized the pan-Hh inhibitor cyclopamine (Toronto Research Chemicals; Hirsinger et al., 2004). Treating wildtype embryos from 6 to 10 hpf with cyclopamine did not alter *has2* expression at 10 hpf in the anterior region of the embryo (Fig. 3.20B and 3.20B' compared to 3.20A and 3.20A'). In these same embryos, *col2a1a* expression at 24 hpf remained as well (Fig. 3.20D compared to 3.20C), albeit to a potentially lesser degree. However, blocking Hh signaling between 10 and 24 hpf resulted in the complete loss of *col2a1a* expression (Fig. 3.20E). Together, these data demonstrate that Hh signaling is required for cartilage differentiation, but not early specification of mesoderm-derived postchordal neurocranial progenitors.

3.IV. Discussion

Here we describe a hierarchy of genetic signaling required for the specification and differentiation of the postchordal neurocranium in zebrafish. The postchordal neurocranium is a structure primarily derived from mesoderm, and is lost in embryos with attenuated Fgf or Shh signaling. Fgf signaling plays an early role in the specification of head mesoderm via *has2*, and the loss of *has2* and

subsequent hyaluronic acid production is at least partly causative of the postchordal neurocranial defects. Shh signaling is then required for the later differentiation of *sox9a* and *col2a1a*-expressing chondrocytes in the postchordal neurocranium. Together, these results reveal a previously unknown genetic signaling hierarchy required in the development of the postchordal neurocranium.

3.IV.a. The dual origin of the zebrafish neurocranium

The zebrafish neurocranium originates from the neural crest and mesoderm. Frog, mouse, and chick fate-maps show similar neurocranial contributions (Couley et al., 1993; Gross and Hanken, 2008; Jiang et al., 2002; Koentges and Lumsden, 1996; McBratney-Owen et al., 2010). Our results strongly suggest that the ancestral pattern of neurocranial contribution is neural crest being largely restricted to prechordal regions, and mesoderm only providing contributions to postchordal regions. The prechordal neurocranium is exclusively of neural-crest origin. This region of the neurocranium has received a good deal of characterization in zebrafish (Eberhart et al., 2006; Kague et al., 2012; Mongera et al., 2013; Wada et al., 2005), therefore, here we will focus on the postchordal neurocranium.

Using a pan-mesodermal Cre-transgenic line driven by *draculin*, we found that the majority of the postchordal neurocranium is mesoderm derived. In mouse and chick, the postchordal neurocranium is also primarily mesoderm-derived (Couley et al., 1992 and 1993; Koentges and Lumsden, 1996; McBratney-Owen

et al., 2008). This data is lacking in frog, however, in neural-crest labeling fate-map studies, non-neural crest derived cartilages are all positioned in the postchordal neurocranium (Gross and Hanken, 2008).

More effort has been spent in mapping the neural crest-derived portions of the skull (Couley et al., 1993; Gross and Hanken, 2008; Kague et al., 2012; Koentges and Lumsden, 1996; Jiang et al., 2002; McBratney-Owen et al., 2010). Our fate mapping has defined the precise postchordal structures that neural crest cells contribute to in zebrafish, including the most lateral regions of the basicapsular commissures, the lateral auditory capsule, and the parts of the lateral commissures. These areas are important for articulations with the jaw support element the hyosymplectic, as well as muscle attachment sites (Koentges and Lumsden, 1996). Furthermore, Hox-negative and Hox-positive neural crest contribute to distinct regions of the postchordal neurocranium. Along with results in chick (Koentges and Lumsden, 1996), this finding suggests an evolutionarily conserved function of neural crest in forming attachment sites in the postchordal neurocranium with the neural crest-derived jaw, jaw supports, and muscle attachment sites (Koentges and Lumsden, 1996).

3.IV.b. Fibroblast growth factor signaling in the zebrafish neurocranium

The vertebrate neurocranium is the product of the mesoderm and the cranial neural crest, yet requires interactions between multiple tissues. An important regulator of the development of the neural crest-derived portion of the

neurocranium is Fibroblast growth factor signaling (Creuzet et al., 2004; Crump et al., 2006; Monsoro-Burq et al., 2003). Our data reveals a second, and much earlier, role for Fgf signaling in the mesoderm-derived postchordal neurocranium.

We show that loss of function of both *fgf3* and *fgf8a* causes a severe defect in postchordal neurocranial development. The phenotypic differences between the *fgf8a;fgf3* double mutant and the *fgf3* morpholino-injected *fgf8a* mutants may be explained by the retention of maternally-supplied Fgfs early in development in the *fgf8a;fgf3* double mutants (Reifers et al., 1998). Analysis of downstream constituents of Fgf signaling, including *sprouty* genes, may show the phenotypic differences are due to genotypic ones. However, these analyses show that loss of function of Fgf signaling causes defects to the postchordal neurocranium.

The root of this defect lies in the misspecification of cephalic mesoderm at the end of gastrulation via downregulated expression of the chondrocyte-regulator *hyaluronan-synthetase 2 (has2)*, which is essential for hyaluronic acid production. In *fgf8a* mutants, loss of *has2* or hyaluronic acid, led to perturbed postchordal neurocranial defects similar to *fgf3;fgf8* loss of function embryos. How Fgfs function to activate *has2* expression remains to be elucidated. Fgf signaling could maintain *has2* expression directly, via STAT3 activation (Saavalainen et al., 2005). Indeed, Fgf receptors have been shown to activate HAS2 function in breast cancer cells via STAT3 (Bohrer et al., 2014). Our analysis suggests *Fgfr3* could work in this capacity, as knockdown in an *fgf8a*-

mutant recapitulates postchordal neurocranial defects. Elucidating the pathway that activates *has2* in an *fgfr3*-dependent fashion will be of ongoing interest.

3.IV.c. A signaling hierarchy orchestrates the specification and differentiation of the postchordal neurocranium

Proper craniofacial development relies on complex hierarchies of signaling pathways. Our analysis implicates Fgf signaling from the mesoderm and neuroectoderm is a major regulator of postchordal neurocranial development. Otic placode development is dependent upon signals from the neuroectoderm (Leger and Brand, 2002; Sai and Ladher, 2015), which could confound our otic placode transplantation results. However, loss of the otic placode itself only results in variable anterior basicapsular commissure loss, not the severe postchordal neurocranial loss phenotype observed in *fgf3;fgf8* knockdown embryos. Thus, the mesoderm and neuroectoderm appear to be the most important sources of Fgf for postchordal development.

Other studies have purported that the notochord is also vital in postchordal neurocranial formation and that *shh* emanating from this structure mediates the formation of the postchordal neurocranium via chondrogenesis of the paraxial mesoderm (Balzcerski et al., 2012). Consistent with this report, we find a loss of differentiated chondrocytes in the postchordal neurocranium. In contrast, *has2* expression was retained in both *smoothened* mutants, which completely lack Hh signaling (Varga et al., 2001), and in embryos treated with cyclopamine from 6-

10 hpf. This shows that, unlike Fgf signaling, Hh signaling is dispensable in early specification of postchordal neurocranium precursors, but is important in their terminal differentiation.

The notochord has been thought to be a critical source of Shh for posterior neurocranial development (Balzcerski et al., 2012). Analysis of *brachyury* mutants, which transfect the notochord during gastrulation (Amacher et al., 2002; Halpern et al., 1993), showed that the postchordal neurocranium was fully developed and included a chondrocytic region expanded into the area where the notochord develops. Due to the retention of *shh* expression in *brachyury* mutants, this suggests that the notochord is not a structural requirement for postchordal neurocranial development, but instead serves purely a signaling function, either through maintenance of the *shh* signal or by some other unexplained mechanism.

Our findings now place Fgf signaling prior to Hh in the formation of the postchordal neurocranium. Cephalic mesoderm is first specified in an Fgf-dependent manner beginning at 10 hpf via activation of *has2*. Temporal-loss of Fgf signaling via SU5402 treatment also shows that Fgf signaling is required early, from 6 to 10 hpf, for *has2* activation. Loss of *has2* ultimately results in the loss of the chondrogenic program resulting in postchordal neurocranial defects in Fgf loss-of-function embryos. Shh, on the other hand, is not required for this early activation of *has2*, but supports proper chondrogenic differentiation of this group

of cells. Together, these results clarify the temporal and genetic control required for proper postchordal neurocranial development in zebrafish.

3.V. Materials and Methods

3.V.a. Fish husbandry and care

All embryos were raised and cared for using established protocols (Westerfield, 1993) with IACUC approval from the University of Texas at Austin. The *fgf8a*^{ti282a} (Brand et al., 1996), *fgf3*^{t24149} (Herzog et al., 2004), *brachyury*^{b195} (Schulte-Merker et al., 1994), *smoothened*^{b577} (Varga et al., 2001), *sox10:Cre* (Kague et al., 2012), *sox10:KikGR* (Balczerski et al, 2012), *sox10:kaede* (Dougherty et al., 2013), *ubi:switch* (Mosimann et al., 2011), and *ubi:RSG* (Kikuchi et al., 2010) alleles have all been described previously. The *drl:CreERT2* line was generated using a 3.8kb *draculin* promoter upstream of the ATG start site. Primers used to amplify this promoter were:

for1: ATTGCGGCCGCTTCAATTGTGGTTGAGCAGTC

rev1: ATTACTAGTCCAAGTGTGAATTGGGATCG. The 3.8KB fragment was amplified with iProof polymerase (BioRad), then cloned into TOPO-Blunt (Invitrogen). After verification, the promoter was sub cloned into the Tol2 vector (Kawakami et al., 2004) upstream of the CRE-ERT2 (Feil et al, PNAS 1996). The Tol2-drl-creert2 vector was co-injected with Tol2 mRNA into AB* in order to establish a founder line. Tamoxifen was added from 10-24 hours post fertilization on the *drl:CreERT2* line, and the *sox10:KikGR* and *sox10:kaede* lines were UV-

activated at 24 hours post fertilization using DAPI-filter attached to a Zeiss LSM 710. Embryos were treated in embryo media with 5 μ M SU5402 (Tocris Biosciences) from 6 to 10 hpf, and 100 μ M cyclopamine (Toronto Research Chemicals) or 1 mM 4-methylumbiferone (Sigma-Aldrich) from 6 to 10 and 10 to 24 hpf.

3.V.b. Morpholino and RNA injection

Approximately 5 nl of morpholinos (Gene Tools), working concentrations of 5 mg/ml of a combination of *fgf3b* and *fgf3c* morpholinos with sequences 5'GGTCCCATCAAAGAAGTATCATTTG3' and 5'TCTGCTGGAATAGAAAGAGCTGGC3', respectively (Maves et al., 2002), of a combination of *fgf8aE212* and *fgf8aE313* with sequences 5'TAGGATGCTCTTACCATGAACGTCG3' and 5'CACATACCTTGCCAATCAGTTTCCC3' (Draper et al., 2001), and control morpholinos with sequence 5'CCTCTTACCTCAGTTACAATTTATA3' were injected into one- or two-cell stage embryos of *fgf8a* and *fgf3* lines.

Approximately 3 nl of a working concentration of 3 mg/ml of *fgfr3* morpholino with sequence 5'AAATGAGGTGTAATGTCTGACCTGT3' was injected into *fgf8a* mutants. This dose was suboptimal, as it did not cause any defects to wildtype-injected embryos. This is a splice-blocking morpholino targeting the first exon-intron boundary of *fgfr3*. To validate the targeting of this morpholino, whole embryo RNA extracts were isolated from uninjected and *fgfr3* morpholino-injected zebrafish at 24 hpf using Trizol extraction (Invitrogen). cDNA pools were

then synthesized using Superscript First-Strand Synthesis System (Invitrogen).

To detect changes in mRNA transcripts in morphant embryos, PCR was performed on cDNA pools using the gene-specific primers spanning the morpholino-targeted exon-intron boundary ForTACAGTGCACACCTGCTGTC and revAGCCAATGGATACTGGGCG giving a final size of 491 bp in wildtype.

Other morpholinos used that were previously described: *fgfr1*: 5'-

GCAGCAGCGTGGTCTTCATTATCAT-3'(Scholpp et al., 2004); *fgfr2*: 5'-

GTCGAACCTCGAACGGGAAAGCGTA-3'(Nakayama et al., 2008); *fgfr4*: 5'-

ATATCTGCTGGAGTAAAAAATGAGG-3'(Nakayama et al., 2008); *dlx3b*: 5'-

ATATGTCGGTCCACTCATCCTTTAAT-3' (Solomon et al., 2002); *foxi1*: 5'-

TAATCCGCTCTCCCTCCAGAAACAT-3' (Solomon et al., 2003)

; and, *has2*, which required dual injection of two morpholinos: 5'-

AGCAGCTCTTTGGAGATGTCCCGTT-3' and 5'-

CGTTAGTTGAACAGGGATGCTGTCC-3' (Bakkers et al., 2004).

Kaede mRNA was injected into one-cell stage embryos, with or without morpholinos, and UV activated at either 6 or 24 hpf using a Zeiss LSM 710 Confocal microscope.

3.V.c. Cartilage and bone staining

Five and four day postfertilization (dpf) zebrafish embryos were stained with Alcian blue and Alizarin Red (Walker and Kimmel, 2007), and then were either flat mounted (Kimmel et al., 1998) or had the viscerocrania removed for imaging.

Images were taken with a Zeiss Axio Imager-AI microscope. Graphs were made in Microsoft Excel 2011.

3.V.d. Confocal Microscopy and figure processing

Confocal z-stacks were collected on a Zeiss LSM 710 using Zen software.

Images were processed in Adobe Photoshop CS. Kaede and tissue fate maps were generated in Adobe Photoshop CS by overlaying images gathered on the Zeiss confocal. Graphs were generated using Microsoft Excel 2011.

3.V.e. In Situ Hybridization

RNA in situ hybridization was performed as reported in Miller et al. (2000). AB wildtype, *fgf8a*, *fgf3;fgf8a* morpholino, *brachyury*, and *smoothened* embryos were treated with 0.0015% PTU (1-phenyl 2- thiourea) to inhibit the production of melanin (Westerfield et al., 1993). Probes used were *sox9a* (Yan et al., 2002), *col2a1a* (Yan et al., 1995), and the *has2* probe was generated using primers For:ACAAGTCACTGGCCCTATGC and Rev:GGTAGGTAATGGGCGTCTCG (NCBI ref# NM_153650.2). DIC images of *in situ* hybridizations were collected on a Zeiss Axioimager.

3.V.f. Cell transplants

Genetic mosaics were generated as described elsewhere (Crump et al., 2004; Maves et al., 2002; Stafford et al., 2006). For neural and otic placode tissue transplants, embryos were injected at the 1-2 cell stage with 2.5% Rhodamine Alexa 568 dextran. At shield stage (6 hpf), donor cells were removed and placed into corresponding areas in *fgf3;fgf8* morpholino-injected hosts using previously

described fate maps (Kimmel et al., 1990 and Woo and Fraser, 1995). Mesoderm transplants were performed at shield stage (4 hpf) using donor tissue cells located at the margin and moved to the margins of *fgf3;fgf8* morpholino-injected hosts (Kimmel et al., 1990). For endoderm transplants, donor 1 cell stage embryos were injected with a mixture of 2.5% Rhodamine Alexa 568 dextran and *sox32* mRNA and donor cells located at the margin at shield were transplanted into the margin of *fgf3;fgf8* morpholino-injected hosts (Stafford et al., 2006). For double mesoderm and neural transplants, donor tissue from 2.5% Rhodamine Alexa 568 dextran injected hosts was transplanted at both sphere (taking cells from the margin) and shield (taking cells from the neural ectoderm-forming region) into *fgf3;fgf8* morpholino-injected hosts. At 24 hpf, all hosts were screened using a LeicaM216F fluorescence stereomicroscope for substantial and tissue-specific contributions of donor tissue for subsequent analysis.

3.VI. Acknowledgments

We wanted to thank the following people for their kind contributions of fish lines, embryos, and morpholinos in this work: Sharon Amacher for the *brachyury* embryos; Gage Crump for the *sox10:Kikgr* line; Sharon Fischer for the *sox10:Cre* line; Eric Liao for the *sox10:Kaede* line; Alex Neichoporuk for the *fgf3* line; and Bruce Riley for the *dlx3b* and *foxi1* morpholinos. We would also like to thank Georgy Koentges, Ben Lovely, Patrick McGurk, Anna Percy, Alfire Sidic, and Mary Swartz for reviewing the manuscript. We would also like to thank Anna Percy for the maintenance and care of all zebrafish lines. This work was

supported by NIH/NIDCR grant R01DE020884 and NIH/NIAAA grant U24AA014811 (Riley PI) to JKE; endorsed by a Gabriella Giorgi-Cavaglieri Chair for life sciences and by the Swiss National Fund #31003A_146527 to JYB and NIH/NIAAA F31AA020731 to NM. No competing interests to disclose.

3.VII. Figures

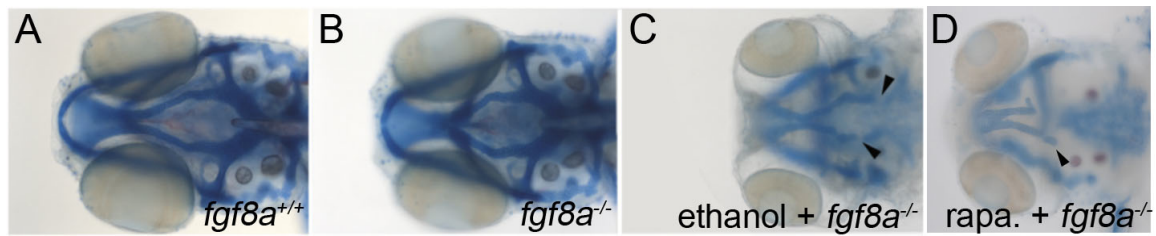


Figure 3.1: *fgf8a* mutants interact with ethanol to cause postchordal neurocranial defects. (A-D) Wholemounted zebrafish neurocrania at 5 days post fertilization. Anterior is to the left. Untreated (A) wildtype and (B) *fgf8a* mutants showing normal neurocranial development, compared to an (C) *fgf8a* mutant treated with ethanol showing variable postchordal neurocranial defects (arrowheads) and (D) *fgf8a* mutant treated with rapamycin showing variable postchordal neurocranial defects (arrowheads).

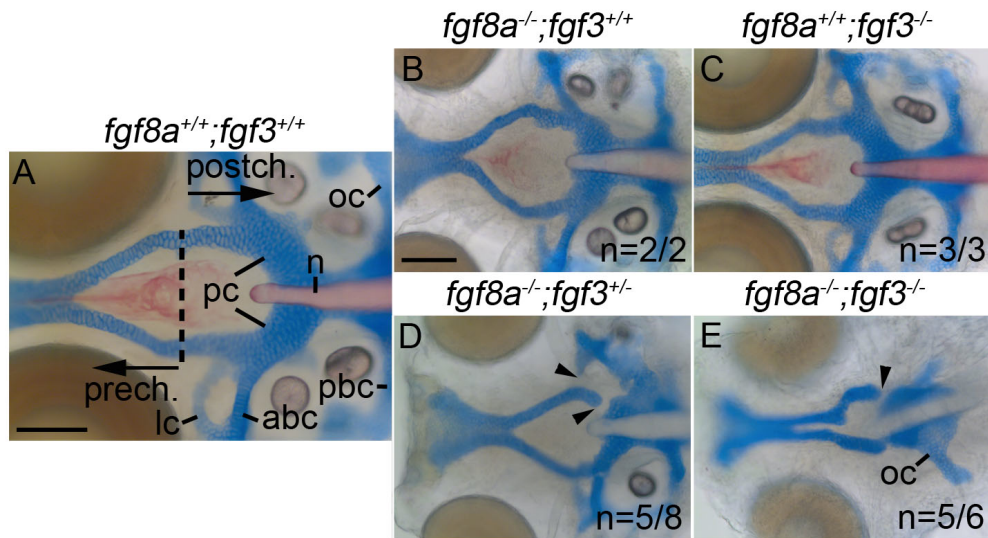


Figure 3.2: The postchordal neurocranium requires Fgf signaling. (A-E) Wholemounted zebrafish neurocrania with the viscerocrania removed at 5 days post fertilization. Anterior is to the left. (A) Wildtype, showing the prechordal versus postchordal regions of the neurocranium demarcated by a dashed line, (B) *fgf8a* mutant, (C) and *fgf3* mutant embryos display normal neurocrania. (D) Variable neurocranial defects occur in 63% (n=5/8) of *fgf8a*^{-/-};*fgf3*^{+/-} embryos (arrowheads). (E) The postchordal neurocranium in *fgf8a*^{-/-};*fgf3*^{-/-} embryos is almost completely absent in 83% (n=5/6) of embryos, including the parachordals, anterior and posterior basicapsular commissure and the lateral commissures (arrowhead). abc- anterior basicapsular commissure, lc- lateral commissure, n- notochord, oc- occipital arch, pbc- posterior basicapsular commissure, pc- parachordals, prech.=prechordal neurocranium, postch.= postchordal neurocranium. scale bar=20 μm.

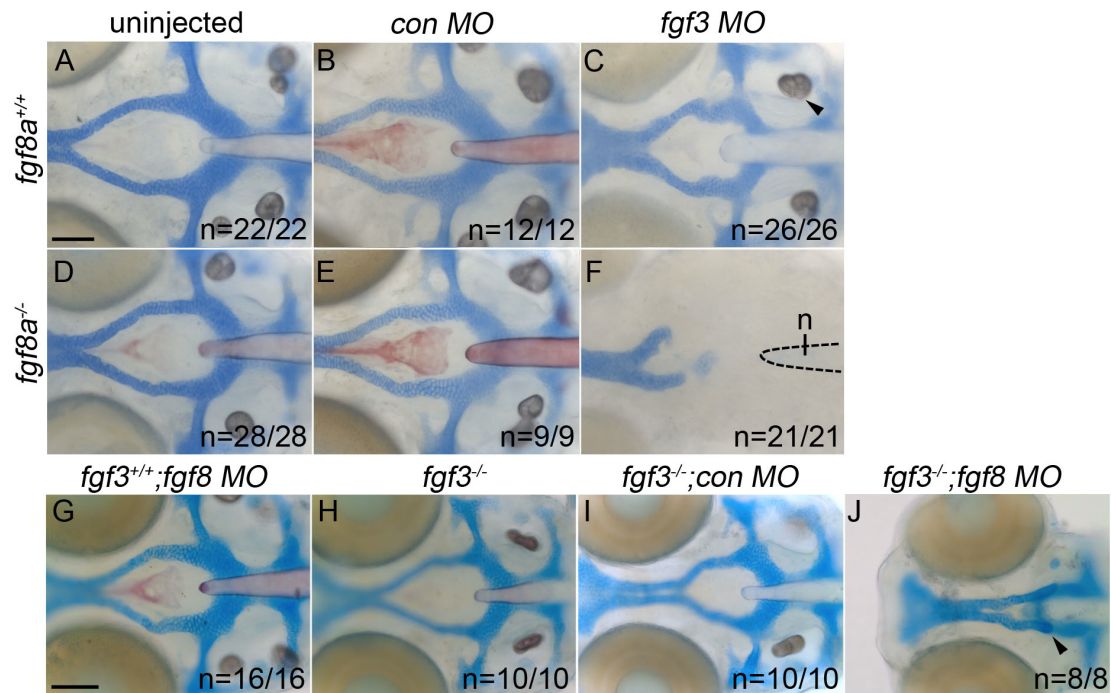


Figure 3.3: Loss of Fgf signaling causes postchordal neurocranial defects. (A-J) Wholemount zebrafish neurocrania at 5 days post fertilization, with the viscerocrania removed. Anterior is to the left. Wildtype embryos injected with (B) control or (C) *fgf3*-morpholinos develop normal posterior neurocranial structures compared to (A) uninjected controls. (D and E) Un-injected and control morpholino-injected *fgf8a* mutants display normal posterior neurocranial development compared to (A) wildtype controls, but (F) develop severe posterior neurocranial loss when injected with *fgf3* morpholino. (G) Wildtype injected with *fgf8* morpholino, (H) *fgf3* mutants, and (I) control morpholino-injected *fgf3* mutants display normal neurocranial development however, (J) *fgf8* morpholino-injected *fgf3* mutants display severe postchordal neurocranial scale bar=20 μm.

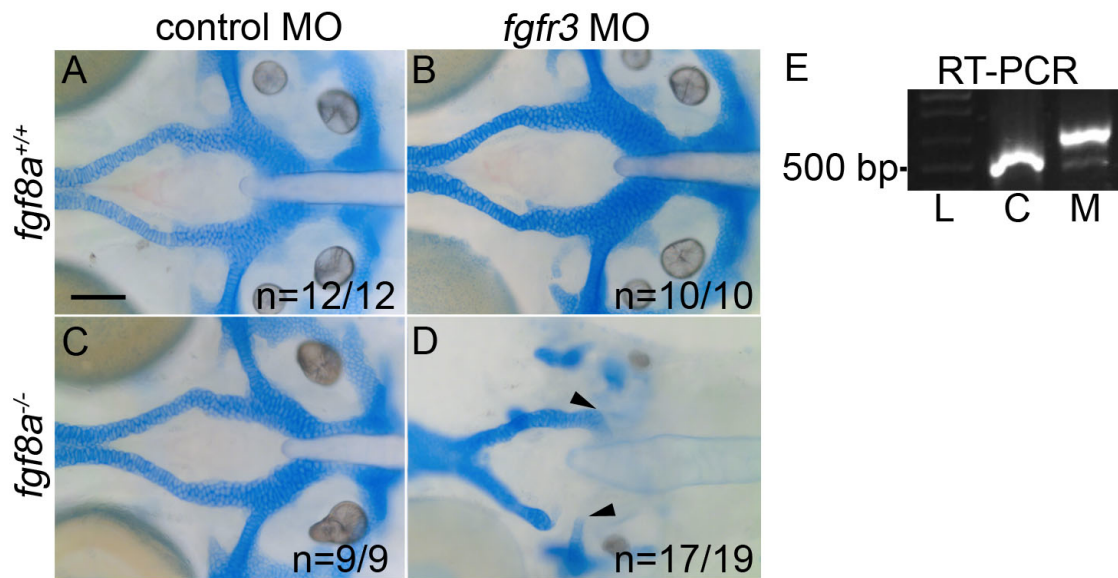


Figure 3.4: Fgfr3 and Fgf8 interact in postchordal neurocranial development. (A-D) Wholemounted zebrafish neurocrania with viscerocrania removed at 5 days post fertilization. Anterior is to the left. (A and C) Control morpholino-injected wildtypes and *fgf8a* mutants display normal craniofacial development. (B) Injecting a suboptimal dose of *fgfr3* morpholino does not affect craniofacial development in wildtype, however, (D) in *fgf8a* mutants causes variable postchordal neurocranial defects (arrowheads). (E) Gel showing RT-PCR analysis of the exon-intron boundary of *fgfr3* targeted by the splice-blocking morpholino with cDNA isolated from either uninjected (C) or *fgfr3*-morpholino (M) injected embryos at 24 hours post fertilization (L denotes ladder). scale bar=20 μm .

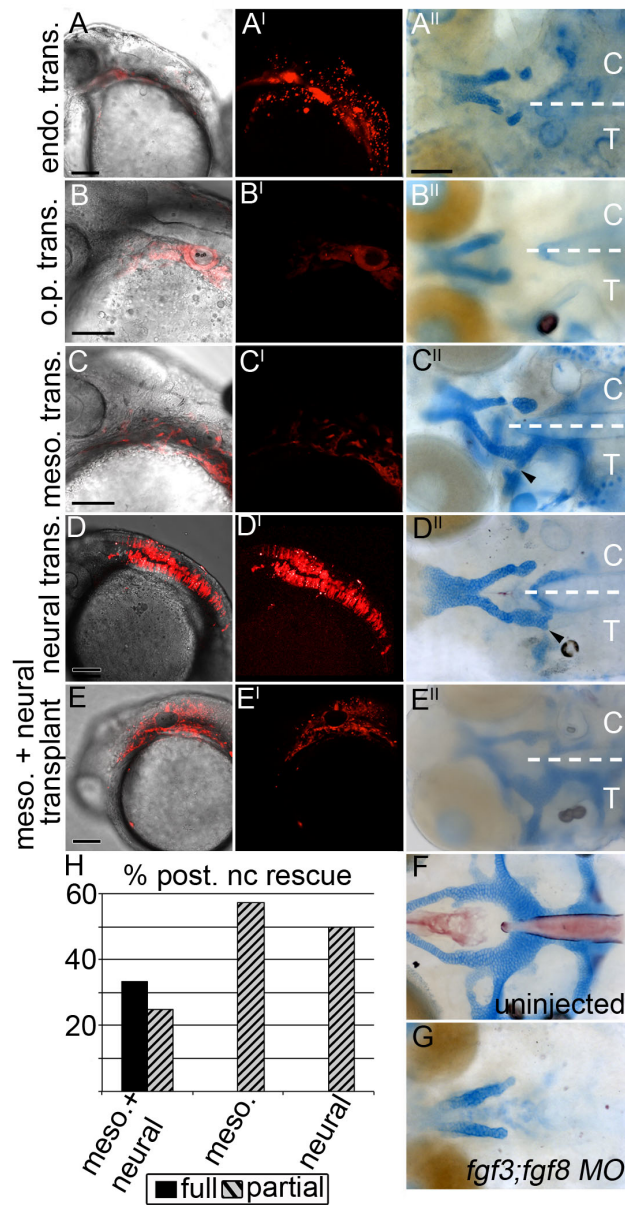


Figure 3.5: The mesoderm and neural ectoderm are Fgf sources required for postchordal neurocranial formation. (A-E, A'-E') 24 hours post fertilization confocal images of transplanted wildtype tissues into *fgf3;fgf8* morpholino-injected hosts with and without DIC, respectively; (A''-E'') corresponding 4 days

post fertilization (dpf) neurocranial wholemounts with viscerocrania removed. Transplanted side of neurocrania is marked with a T, and control side with a C. (F and G) 4 dpf postchordal neurocrania of uninjected and *fgf3;fgf8* morpholino injected embryos respectively. Anterior is to the left. (A,A',A'') Endoderm transplants, (B,B',B'') otic placode transplants, (C,C',C'') mesoderm only, (D,D',D'') neural ectoderm only, and (E,E',E'') mesoderm and neural ectoderm double-transplants. Endoderm and otic placode transplants fail to rescue the posterior neurocranium (compare A'' and B'' to F and G). Transplantation of mesoderm or neural ectoderm alone partially rescues the postchordal neurocranium (compare C'' and D'' to F and G). Transplantation of mesoderm and neural ectoderm together can fully rescue the postchordal neurocranium on the side of the embryo receiving the transplant (compare E'' to F and G). Quantification of partial or full rescue is shown in graph H. scale bars=100 μm in A-E and scale bar=20 μm in A''.

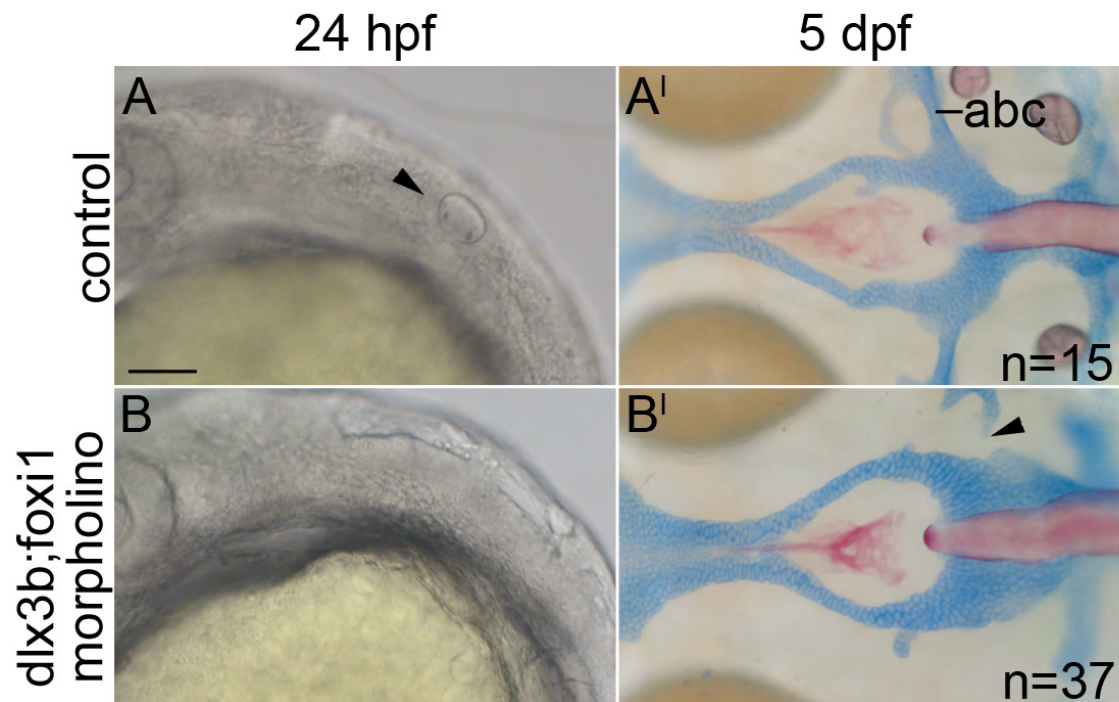


Figure 3.6: The postchordal neurocranium is primarily intact in *dlx3b;foxi1* knockdown embryos. (A-B) DIC images of 24 hpf embryos and (A'B') the same embryo at 5 dpf wholemounted neurocrania with viscerochromia removed. Anterior is to the left. (A-A') Un-injected control embryos show an otic placode at 24 hpf (arrowhead) and normal posterior neurocranium at 5 dpf. (B-B') *dlx3b;foxi1* double morpholino-injected embryos lack an otic placode at 24 hpf, but retain most of the posterior neurocranium at 5 dpf (arrowheads point to missing anterior basicapsular commissure). abc- anterior basicapsular commissure, scale bar= 20 μm .

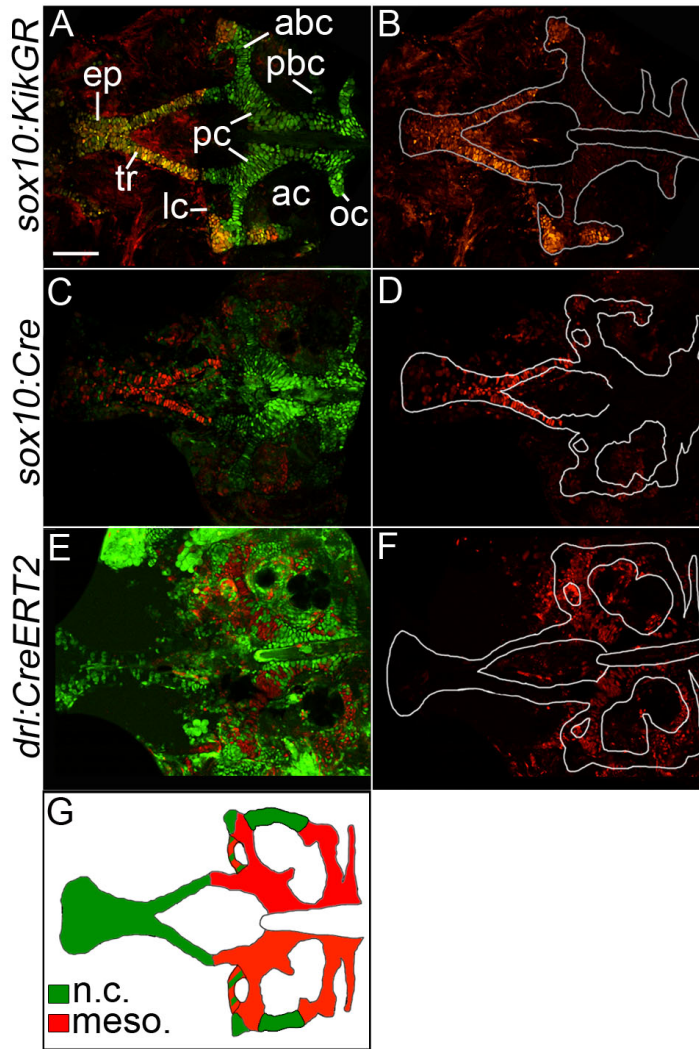


Figure 3.7: The zebrafish postchordal neurocranium is derived from both mesoderm and neural crest tissues. (A-F) Confocal images of 5 days post fertilization flatmounted zebrafish neurocrania of (A,B) *sox10:KikGR*, (C, D) *sox10:Cre;ubiRSG*, and (E,F) *drl:CreERT2;ubi:switch*. Anterior is to the left. In C-D the red and green channels have been switched for clarity in comparisons to

A & B. (B, D, F) Lineage-traced cells only, neurocrania outlined in white. (A-D) Neural crest contributes to the prechordal elements the ethmoid plate and trabeculae, as well as the lateral and anterior regions of the anterior basicapsular commissures and the lateral auditory capsules. (E-F) Mesoderm contributes the parachordals, anterior and posterior basicapsular commissure, the occipital arch, and the lateral commissures. Schematic of results shown in G (n>10 for each transgenic line). abc- anterior basicapsular commissure, ac- auditory capsule, ep- ethmoid plate, lc- lateral commissure, n- notochord, oc- occipital arch, pbc- posterior basicapsular commissure, pc- parachordals, tr-trabeculae. scale bar=50 μ m.

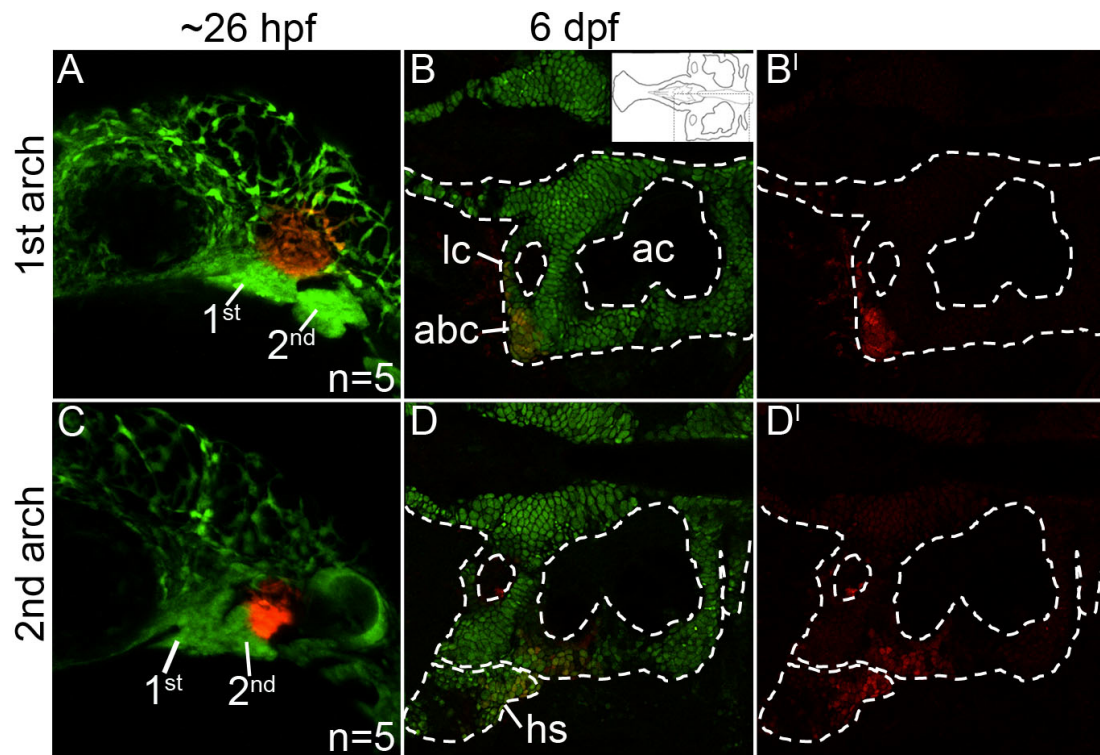


Figure 3.8: Mandibular- and hyoid-specific neural crest contributions to the postchordal neurocranium. (A-D') Confocal images of *sox10:kaede* embryos at (A,C) 24 hours post fertilization and (B,B', D, D') 6 days post fertilization. Anterior is to the left in all images. (A) Photoconverted first arch neural crest cells, red fluorescence, contribute to the lateral anterior basicapsular commissure (B,B', arrowhead, inset in B shows relative region shown in B and D). (C) Photoconverted second arch cells, red fluorescence, contribute to the lateral auditory capsule, with cells also labeled in the hyosymplectic, a second arch viscerocranial structure (D,D'). abc- anterior basicapsular commissure, ac- auditory capsule, hs- hyosymplectic, lc- lateral commissure.

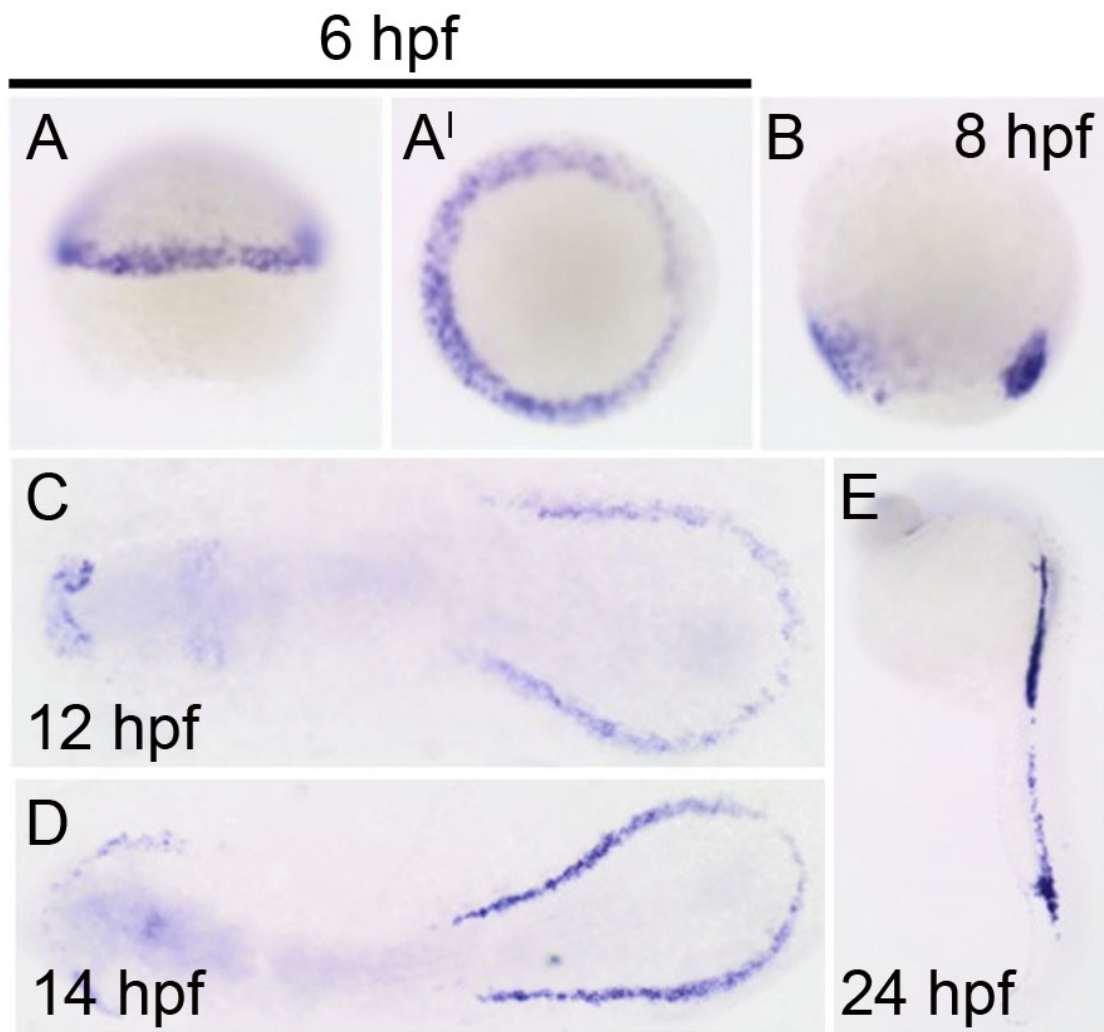


Figure 3.9: *cre* expression in the *drl:CreERT2* line confirms mesoderm-specific labeling at 6 hours post fertilization (hpf). All panels show Cre expression in *drl:CreERT2* line at (A-A') 6 hpf (lateral and dorsal views, respectively), (B) 8 hpf, (C) 12 hpf, (D) 14 hpf, and (E) 24 hpf. Figure by Julien Y. Bertrand.

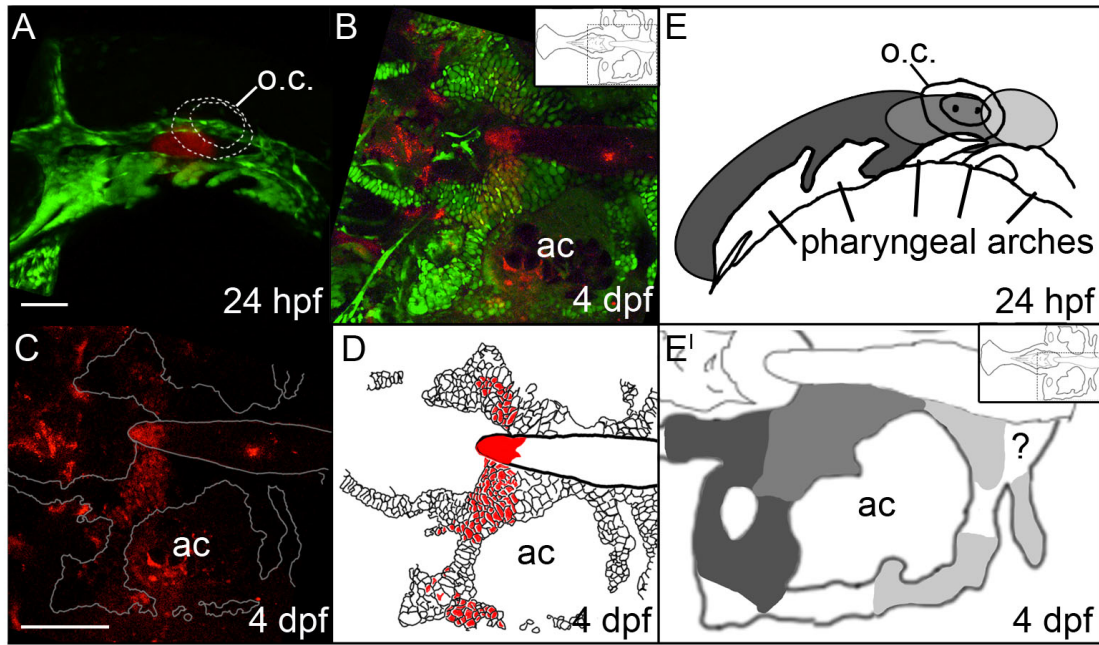


Figure 3.10: Fate-mapping of head mesoderm shows the anterior/posterior organization of postchordal cells is set by 24 hours post fertilization (hpf). (A-C) Confocal images of a Kaede-injected embryo at (A) 24 hpf and (B,C) 4 days post fertilization (dpf). Anterior is to the left. (A) At 24 hpf Kaede was photoconverted, shown in red (the remaining green Kaede is not evident due to the intense green fluorescence from the *fli1:EGFP* transgene), and (B) at 4 dpf, this same embryo shows labeling in the postchordal neurocranium (inset shows relative position in the neurocranium of magnified view). (C) Red channel only, the neurocrania is outlined in white. (D) Schematic of panel C, with red cells depicting the photoconverted region. (E and E') Graphical representation of Kaede-mediated

fate mapping at 24 hpf and 4 dpf. Inset in E' shows relative position of magnified neurocrania. Question mark denotes a region that remained unlabeled in our analyses. ac- auditory capsule, o.c.-otic capsule. Scale bars=10 μm in A and 20 μm in C.

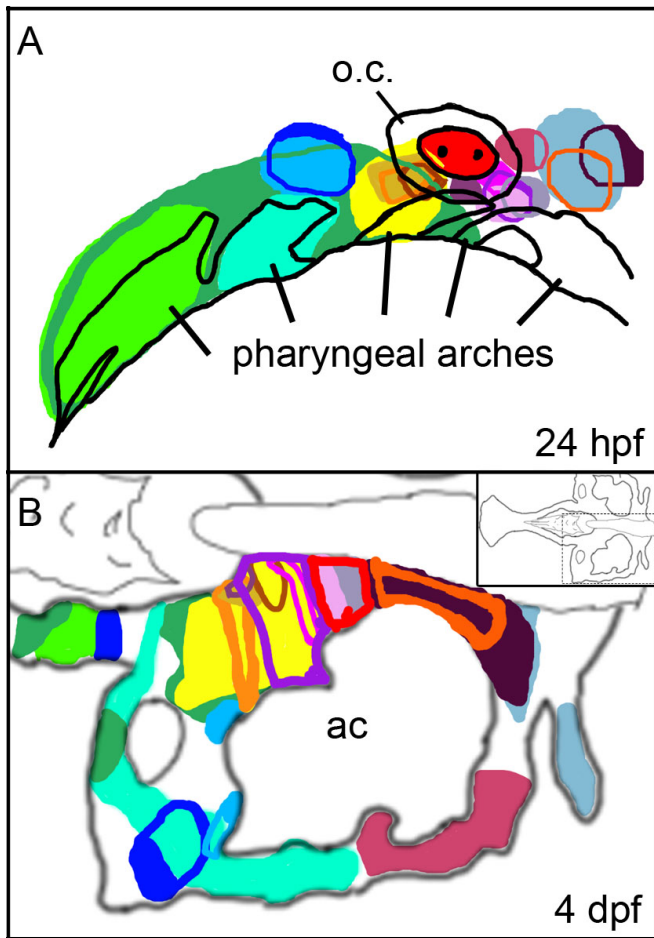


Figure 3.11: Individual kaede photoconversion fate mapping data points. (A and B) Graphical representation of data points of Kaede photoconversion. Anterior is to the left. (A) Circles denote photoconverted regions of Kaede-injected embryos at 24 hours post fertilization. (B) Corresponding colors demonstrate the location of converted cells at 5 days post fertilization. ac-auditory capsule, o.c.-otic capsule.

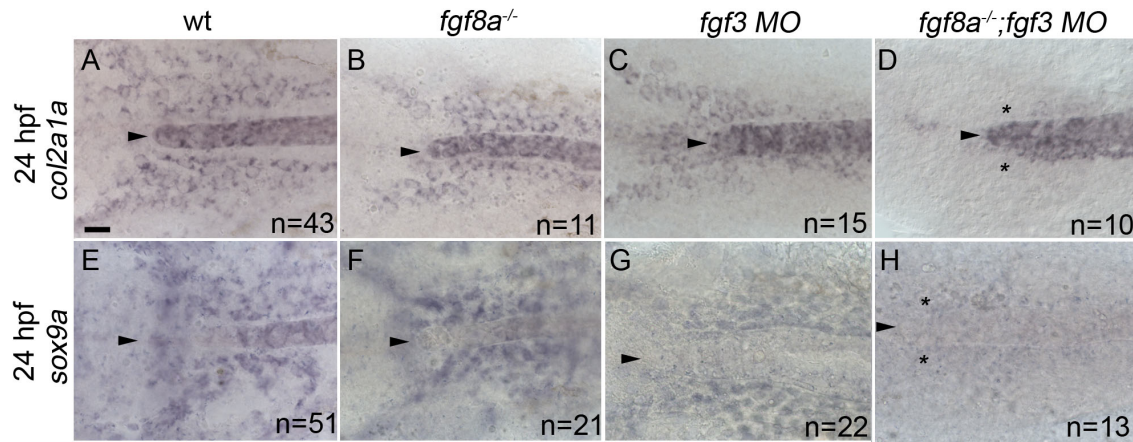


Figure 3.12: Cartilage and pre-cartilage markers *col2a1a* and *sox9a* are absent at 24 hours post fertilization (hpf) in *fgf3;fgf8a* knockdown embryos. (A-H) Images of 24 hpf embryos labeled with (A-D) *col2a1a* and (E-H) *sox9a* riboprobe. Dorsal view with anterior to the left, arrowhead denotes the anterior limit of the notochord. (A,E) Wildtype, (B,F) *fgf8a* mutant, and (C,G) *fgf3* morpholino embryos display normal expression of both *col2a1a* and *sox9a*. However, (D,H) *fgf3* morpholino-injected *fgf8a* mutants lose the expression of both *col2a1a* and *sox9a* (asterisk). scale bar=20 μ m.

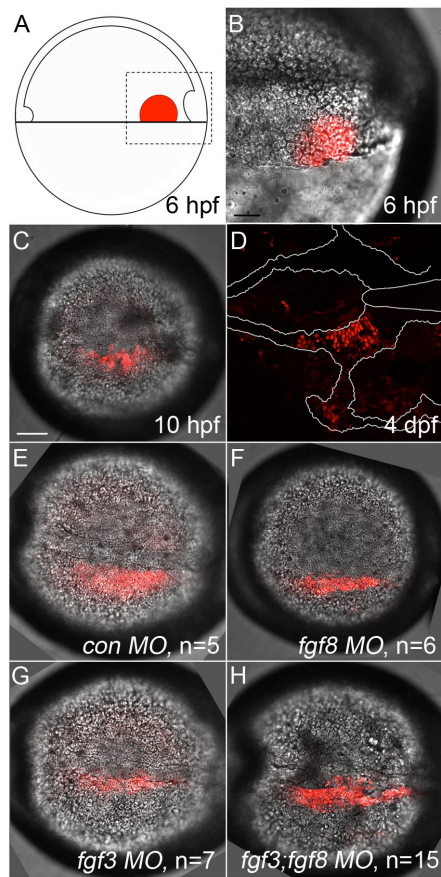


Figure 3.13: Kaede photoconverted endomesoderm postchordal-progenitor cells migrate appropriately in *fgf3;fgf8a* knockdown embryos. (A) Schematic of 6 hours post fertilization (hpf) zebrafish embryo showing the region of the embryo photoconverted in all subsequent experiments, dorsal to the right. (B-D) DIC confocal images showing the photoconverted area at 6 hpf (B, magnified region outlined in A), 10 hpf (C), and 4 days post fertilization (dpf) (D). Cells have migrated adjacent to the notochord by 10 hpf and contributed to the postchordal neurocranium at 4 dpf. At 10 hpf, cells in (E) control, (F) *fgf8*, (G) *fgf3*, and (H)

fgf3;fgf8 double morpholino-injected embryos are appropriately positioned
(compared to C). scale bar= 20 μ m.

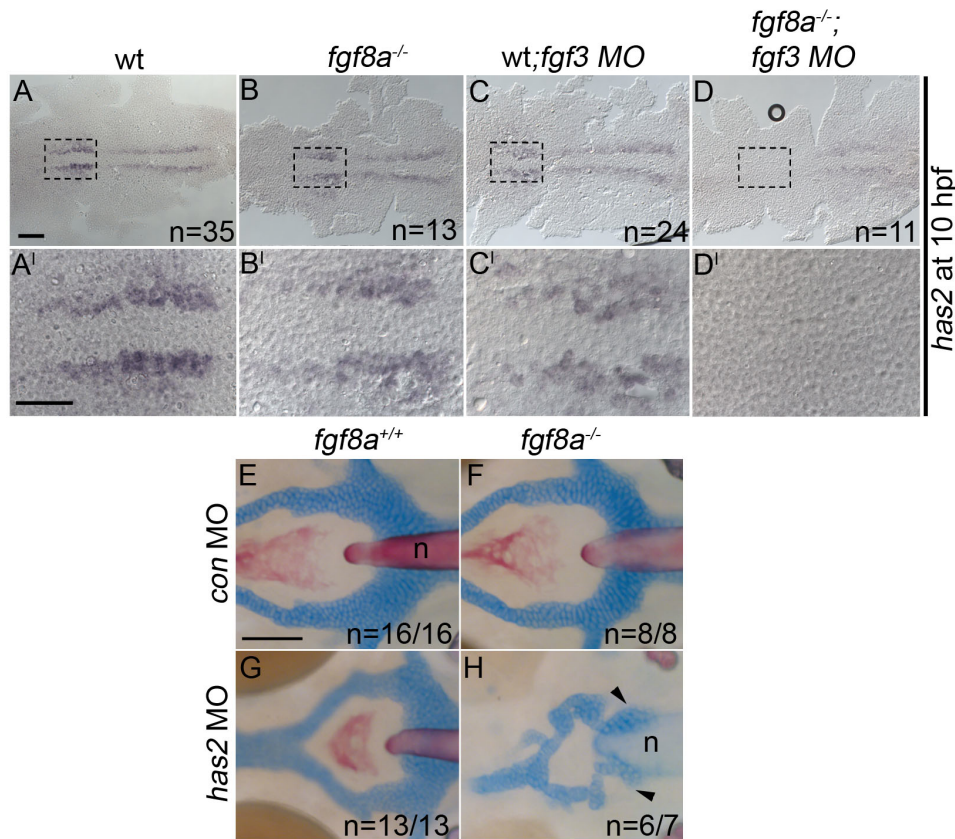


Figure 3.14: Loss of *has2* in Fgf knockdown embryos contributes to the postchordal neurocranial loss phenotype. (A-D, A'-D') Images of 10 hours post fertilization embryos labeled with *has2* riboprobe. Dorsal view and anterior to the left in all images. (E-H) Wholemounted zebrafish neurocrania with the viscerocrania removed at 5 days post fertilization. Anterior is to the left. (A'-D') Magnified areas of region outlined in (A-D). (A,A') Uninjected wildtype, (B,B') *fgf8a* mutants, and (C,C') *fgf3* morpholino-injected wildtype display normal expression of *has2*, however, (D,D') *fgf3* morpholino-injected *fgf8a* mutants exhibit loss of expression of *has2* in the presumptive postchordal neurocrania (D

and D'). (E) Control morpholino-injected wildtype and (F) *fgf8a* mutants, as well as (G) *has2* morpholino-injected wildtypes retain the postchordal neurocranium. However, (H) *has2* morpholino-injected *fgf8a* mutants have a substantial loss of the postchordal neurocranium (arrowheads). n=notochord. scale bar=10 μm in A and 50 μm in A' and 20 μm in E.

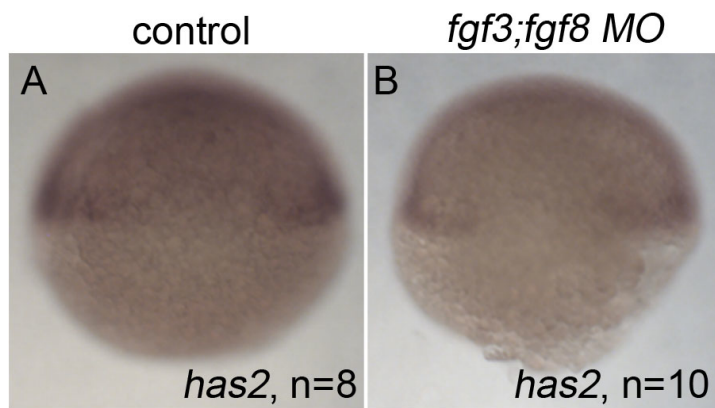


Figure 3.15: Expression of *has2* at 6 hours post fertilization does not require *fgf3;fgf8* function. (A,B) *has2* expression at 6 hpf in (A) control and (B) *fgf3;fgf8a* morpholino-injected embryos. Dorsal view.

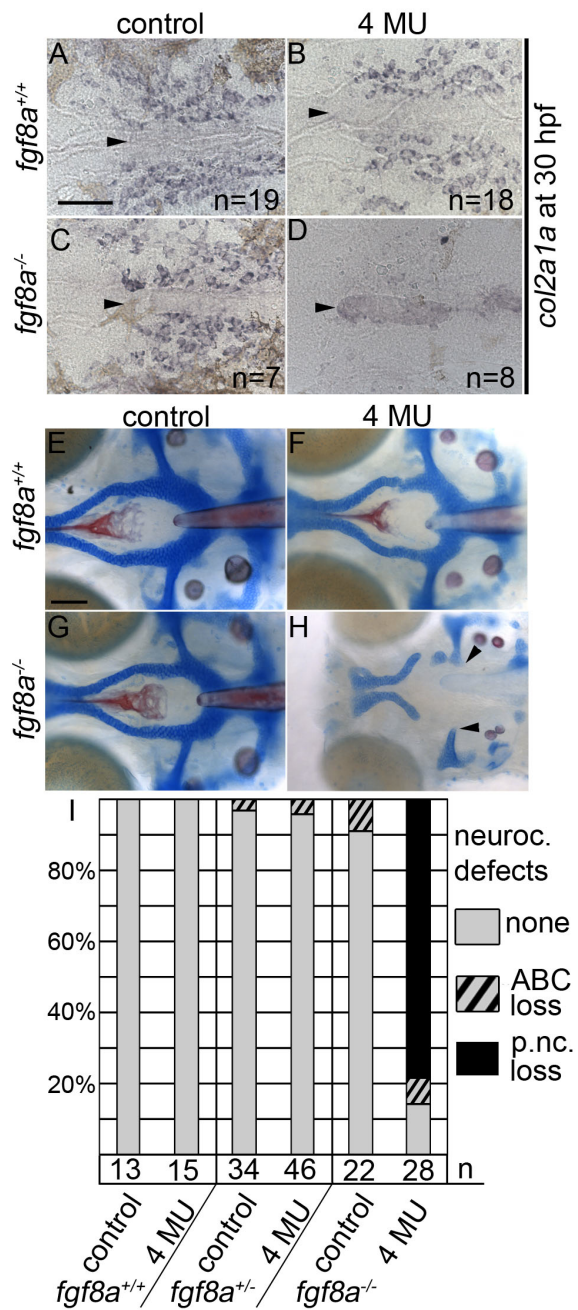


Figure 3.16: Inhibition of hyaluronic acid in *fgf8a* mutants causes postchordal neurocranial defects. (A-D) Images of 30 hpf embryos stained with *col2a1a* riboprobe. Dorsal view, with anterior to the left. (E-H) Wholemount zebrafish

neurocrania at 5 days post fertilization, with the viscerocrania removed. Anterior is to the left. (A) Control-, (B) 4-MU-treated wildtype and (C) control-treated *fgf8a* siblings display normal *col2a1a* staining in the pre-postchordal neurocranium, however, (D) 4-MU-treated *fgf8a* mutants show a loss of *col2a1a* expression at the end of the treatment window (10-30 hpf). (E) Control- and (F) 4-MU-treated wildtype from 10 to 30 hours post fertilization, and (G) untreated *fgf8a* mutants have normal posterior neurocrania. However, (H) the mesoderm-derived regions of the neurocrania are lost in 4-MU treated *fgf8a* mutants (arrowheads). (I) Quantification of postchordal neurocranial defects including none (see E), ABC loss, or variable postchordal neurocranial loss (p. nc. loss) in control and 4-MU-treated wildtype (*fgf8a*^{+/+}), heterozygous (*fgf8a*^{+/-}) and mutant (*fgf8a*^{-/-}) embryos. abc- anterior basicapsular commissure, n- notochord, oc- occipital arch, pc- parachordals, pbc- posterior basicapsular commissure. Scale bar= 50 μ m in A, 20 μ m in E.

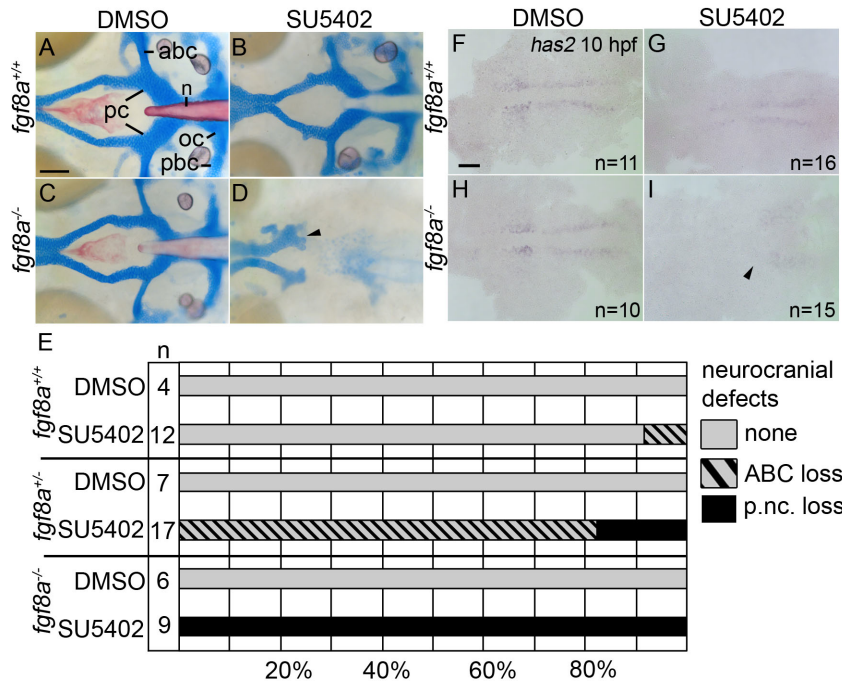


Figure 3.17: Postchordal neurocranial development requires Fgf signaling during gastrulation. (A-D) Wholemount zebrafish neurocrania, anterior is to the left. (A and B) Wildtype neurocrania treated with DMSO or SU5402 develop normally. (C) DMSO-treated *fgf8a* mutants are also unaffected, however, (D) those treated with SU5402 from 6 to 10 hpf develop severe postchordal neurocranial loss. (E) Quantification of postchordal neurocranial defects including none (see A), ABC loss, or complete postchordal neurocranial loss (p. nc. loss) in DMSO and SU5402 treated wildtype (*fgf8a*^{+/+}), heterozygous (*fgf8a*^{+/-}) and mutant (*fgf8a*^{-/-}) embryos. (F-H) DMSO-treated wildtype and *fgf8a* mutants and SU5402-treated wildtype express *has2* appropriately; however, (I) SU5402-treated *fgf8a* mutants display a loss of expression of *has2* in postchordal neurocranial precursors

(arrowhead denotes most anterior expression). abc- anterior basicapsular commissure, lc- lateral commissure, n- notochord, oc- occipital arch, pc- parachordals, pbc- posterior basicapsular commissure. scale bar=20 μm in A and scale 10 μm in F.

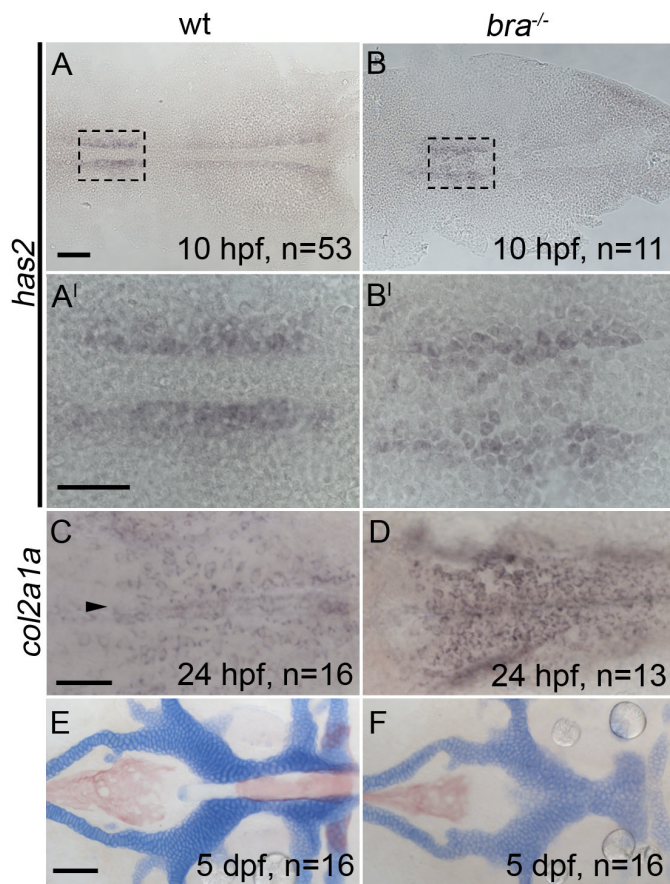


Figure 3.18: Postchordal neurocranial development does not require *brachury* function or a notochord. Anterior is to the left in all panels. (A-B, A'-B') *hyaluronan synthetase 2* (*has2*) is expressed in cephalic regions at 10 hours post fertilization (hpf) in both wildtypes and *brachury* mutants. (C and D) The late chondrogenic marker *col2a1a* at 24 hpf appears in both *brachury* mutants and siblings in the forming postchordal area of the developing embryo (compare D to C, arrowhead in C denotes anterior notochord). (E and F) At 5 days post fertilization, postchordal neurocrania of *brachury* mutants are normal, *sans*

notochord, compared to siblings (compare F to E). scale bar=10 μm in A and 50 μm in A' and C and 20 μm in E.

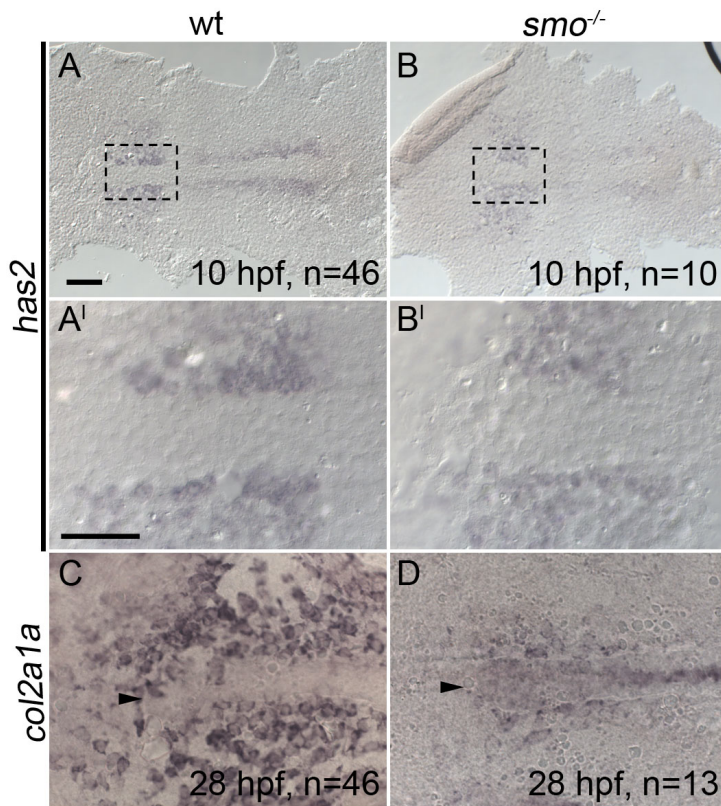


Figure 3.19: Chondrocyte differentiation but not early cephalic mesoderm specification requires Hh signaling. All panels are anterior to the left. (A-B, A'-B') At 10 hours post fertilization (hpf), the early mesoderm marker *has2* is expressed similarly in the anterior region of *smoothened* mutants and wildtypes (Compare B to A, B' to A'). (C and D) However, *smoothened* mutants display a marked reduction in *col2a1a* expression in the forming postchordal neurocranium at 28 hpf compared to siblings (compare D to C, arrowhead denotes anterior notochord). scale bar=10 μm in A and 50 μm in A'.

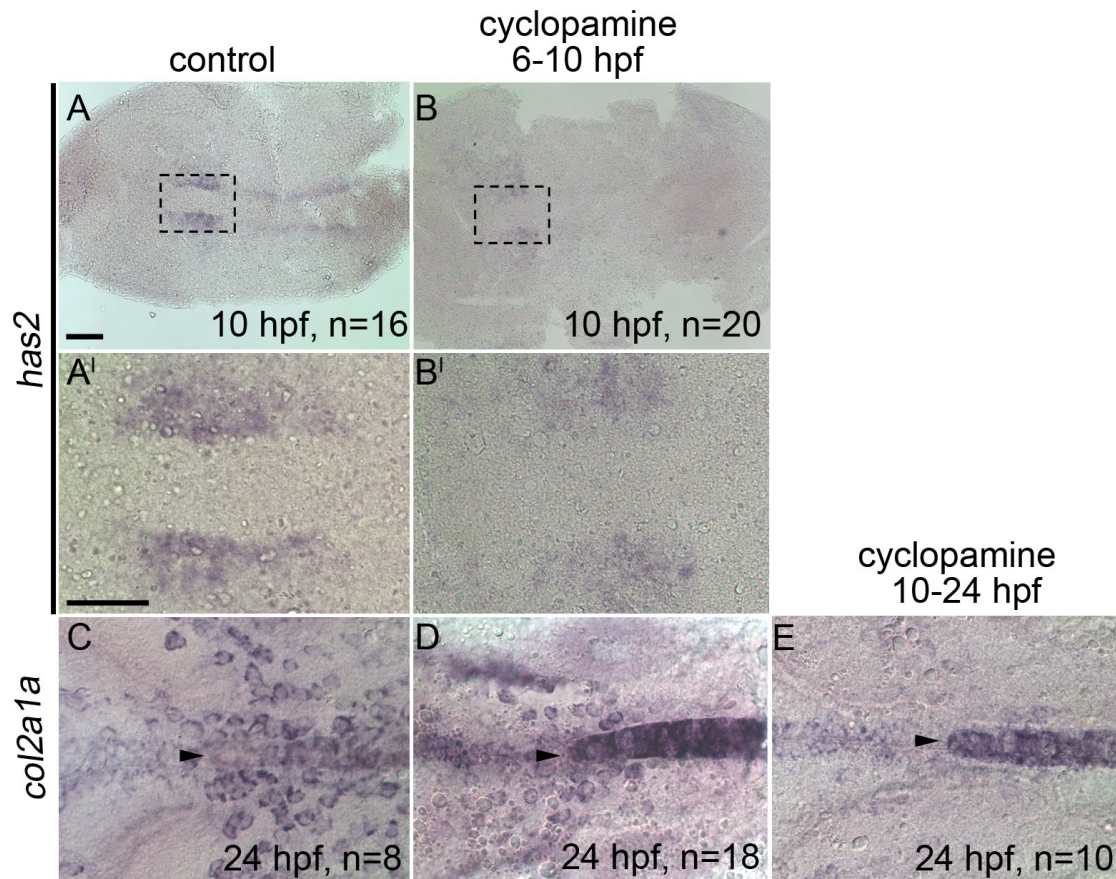


Figure 3.20: Hh signaling is required after Fgf signaling for postchordal neurocranial development. The expression of *has2* is retained following either (A-A') DMSO or (B-B') cyclopamine treatment from 6-10 hours post fertilization (hpf). (C-D) DMSO- and cyclopamine-treated embryos from 6-10 hpf show expression of *col2a1a* at 24 hpf, however, (E) cyclopamine-treated embryos from 10-24 hpf show a loss of *col2a1a* expression in the postchordal neurocranium at 24 hpf. Arrowheads denote the anterior limit of the notochord.

Chapter 4: *pdgfra* and *pdgfrb* synergistically interact in craniofacial development.¹

4.I. Abstract

The cranial neural crest is the primary tissue source of the craniofacial skeleton and platelet-derived growth factors (Pdgf) are critically important in neural crest development. The Pdgf signaling family consists of two receptors, alpha and beta, of which *pdgfra* has a primary role in neural crest migration. It is unclear, however, the role *pdgfrb* plays in the neural crest, or whether *pdgfra* and *pdgfrb* have a synergistic role in craniofacial development. Using both pharmacological and genetic analyses, we find that loss of both *pdgfra* and *pdgfrb* in zebrafish results in exacerbated craniofacial phenotypes unobserved in either *pdgfra* or *pdgfrb* knockdown alone. Data in mouse suggests this synergistic relationship is conserved. In zebrafish, this phenotype is attributed to an increase in neural crest cell apoptosis, revealing an uncharacterized role of Pdgf signaling in the neural crest.

¹Authors: Neil McCarthy¹, Jenna Rozacky¹, Michelle D. Tallquist³, and Johann K. Eberhart^{1,2}.

¹Department of Molecular Biosciences; Institute of cell and molecular biology, Waggoner Center for Alcohol and Alcohol Addiction Research, University of Texas, Austin, Texas.

²Institute of Neurobiology, University of Texas, Austin, Texas.

³Department of Medicine, University of Hawaii, Honolulu, Hawaii.

4.II. Introduction

The craniofacial skeleton is derived primarily from the neural crest, and defects involving the neural crest lead to highly prevalent craniofacial abnormalities (Wilkie and Morriss-Kay, 2001; Stanier and Moore, 2004; Trainor, 2010). The neural crest is a pluripotent population of cells that are derived from the dorsal neural tube and migrate in distinct streams to the periphery of the embryo (Baker and Bronner-Fraser, 1997a; Basch et al., 2006). In cranial regions of the embryo, neural crest cells migrate into regions called pharyngeal arches (Baker and Bronner-Fraser, 1997a; Basch et al., 2006). These, in turn, will undergo morphogenetic events that result in the formation of the facial skeleton (Knight and Schilling, 2006). The proper induction, migration, proliferation, and survival of the neural crest require multiple signaling pathways, including the platelet-derived growth factor (Pdgf) pathway (Soriano, 1997; Eberhart et al., 2008; Tallquist and Soriano, 2003).

The Pdgf signaling family consists of two receptors, alpha and beta, and four ligands in human and mouse, and six ligands in zebrafish (Bestholtz et al., 2001; Tallquist and Kazlauskas, 2004; Eberhart et al., 2008). Ligands and receptors both homo- or heterodimerize, and upon ligand binding, autophosphorylation of intracellular receptor tyrosine residues occurs (Tallquist and Kazlauskas, 2004). This phosphorylation triggers the activation of numerous pathways, primarily PI3K and PLC γ , involved in processes including cell migration, proliferation, and survival (Tallquist and Kazlauskas, 2004). Pdgf

signaling is important throughout development in numerous tissues including the gonads, lung, intestine, skin, central nervous system, skeleton, vasculature, and both cardiac and cranial neural crest (Tallquist and Kazlauskas, 2004).

Multiple studies have focused on the role *Pdgfra* plays in the cranial neural crest. *Pdgfra* is expressed in both premigratory and migratory neural crest cell populations in mouse and zebrafish (Eberhart et al., 2008; Liu et al., 2002; Schatteman et al., 1992). In mouse, conditional loss of *Pdgfra* in the neural crest leads to numerous cranial defects including cleft palate, a shortened skull, absent hyoid bone, and incomplete ossification of the basosphenoid, presphenoid, and alisphenoid bones (Tallquist et al., 2003). A hypomorphic mutant of *pdgfra* in zebrafish has cleft palate as well (Eberhart et al., 2008), which is attributed to disrupted migration of neural crest cells. This migratory defect has also been observed in mouse (Vasudevan and Soriano, 2014), highlighting the conserved function of this gene across species. While *pdgfra* is strongly implicated in craniofacial development, *pdgfrb* is currently not.

Pdgfrb knockout mice exhibit kidney, heart, and hematological defects (Soriano, 1994; Mellgren et al., 2008), but no overt craniofacial abnormalities. Mutations specific to the PI3K-domains of both *Pdgfra* and *Pdgfrb* result in craniofacial defects more severe than a *Pdgfra* null (Klinghoffer et al., 2002). Furthermore, in the epicardium, *Pdgfra* and *Pdgfrb* play redundant roles in proper epithelial-to-mesenchymal transition (Smith et al., 2011). Collectively, these

results suggest that, in certain tissues, these receptors have synergistic functions.

Here, we sought to investigate the roles of the Pdgf receptors in neural crest development. While loss of *pdgfrb* does not cause any overt craniofacial defects, *pdgfra* hypomorphic mutant zebrafish show cleft palate. Double *pdgfra;pdgfrb* mutants show exacerbated defects, even when compared to a *pdgfra* hypomorphic mutant. Data in mouse reveals a conservation of this interaction. Using a broad Pdgf Inhibitor, Pdgf Inhibitor V, we show that craniofacial development requires Pdgf activity from the initiation of neural crest migration to early pharyngeal arch formation. Using *in situ* analysis, we observe that neural crest cells express both *pdgfra* and *pdgfrb* as they are populating the pharyngeal arches. The exacerbated phenotype observed in zebrafish double *pdgfra;pdgfrb* mutants may be due to increased neural crest cell death, revealing a previously unknown compensatory role of Pdgf receptors in neural crest cell survival.

4.III. Results

4.III.a. Dual knockdown of *pdgfra* and *pdgfrb* leads to exacerbated craniofacial defects.

To investigate whether *pdgfra* and *pdgfrb* interact synergistically in craniofacial development, we generated *pdgfra;pdgfrb* double mutants. While *pdgfrb*-mutant embryos develop normal craniofacial skeletons (Fig. 4.1B, 4.1F, 4.1I, compared

to Fig. 4.1A, 4.1E), *pdgfra* mutant embryos exhibit cleft palate where the ethmoid plate fails to fuse, resulting in shorter neurocranial lengths (Fig. 4.1E, astericks, 4.1I; Eberhart et al., 2008; McCarthy et al., 2013). Viscerocranial elements are quantifiably smaller as well, including the Meckel's, palatoquadrate, pterygoid process, hyosymplectic, and symplectic cartilages (Fig. 4.1G, Table 4.1).

While loss of a single allele of *pdgfrb* has no effect on the phenotype of *pdgfra* mutants, analysis of double *pdgfra;pdgfrb* mutants reveals a significantly reduced palate (Fig. 4.1D, arrowheads, 4.1I, Table 4.1) compared to all other genotypes. Neurocranial width and symplectic length are also reduced in double *pdgfra;pdgfrb* mutants compared to all other genotypes (Fig. 4.1G, Table 4.1). Other defects observed in double mutants include cartilage loss between the polar cartilages and the posterior basicapsular commissure, and loss of notochord ossification (Fig. 4.1G, arrows and arrowheads). Together, these data show that loss of both Pdgf receptors results in a synergistic interaction affecting the craniofacial skeleton.

Previous reports show conservation of *pdgfra* function across species (Eberhart et al., 2006; Tallquist et al., 2003; Vasudevan and Soriano, 2014). While loss of the PI3K domains of both *Pdgfra* and *Pdgfrb* genetically interact to recapitulate the defects observed in *Pdgfra* null mutants (Klinghoffer et al., 2002), it is unclear whether *Pdgfra* and *Pdgfrb* interact in the neural crest specifically, or the breadth of Pdgf signaling function in craniofacial development. To test this, we generated neural crest conditional *Pdgfra;Pdgfrb* null mice via *Wnt1:Cre*

mediated excision. Indeed, these mice have exacerbated craniofacial defects including reduced basisphenoid, alisphenoid, and hyoid bones (Fig. 4.2C compared to Fig. 4.2A and 4.2B, Fig. 4.2D) compared to either single mutant alone. These data reveal conservation of the *Pdgfra*;*Pdgfrb* interaction in craniofacial development.

4.III.b. Pdgf activity is required between 6 and 30 hours post fertilization for proper craniofacial development.

To determine when craniofacial development requires Pdgf function, we utilized PDGF Inhibitor V (Sigma), which broadly inhibits Pdgf activity. In an initial dose response analysis, three concentrations of inhibitor were tested on wild-type fish, 1, 1.5, and 2 μ M, at a broad time window from 6 hours post fertilization (hpf), or the beginning of gastrulation, to 30 hpf, when most neural crest cells have condensed within the pharyngeal arches. A concentration of 1 μ M did not cause any gross craniofacial defects (data not shown) and 2 μ M resulted in an increase in embryo death (data not shown). The most consistent and penetrant phenotypes occurred at a concentration of 1.5 μ M (Fig. 4.3). At high concentrations, this inhibitor has been shown to inhibit Kit function, required in melanocyte formation. However, we did not observe any gross alterations to melanocytes, suggesting that at this concentration the inhibition is most likely specific to Pdgf (Fig. 4.4).

We next narrowed the window required for Pdgf function in craniofacial development. In these analyses the craniofacial phenotypes were marked as either unaffected, variable neurocranial defects, or complete loss of the palate (see Fig. 4.3A-C). A time window of inhibitor treatment from 12 to 30 hpf shows more severe defects compared to a time window of 18 to 30 hpf (Fig. 4.3). These data suggest that the function of Pdgf is required during a time window that encompasses both neural crest migration and pharyngeal arch formation.

4.III.c. *pdgfra* and *pdgfrb* have overlapping expression in the head beginning at 20 hours post fertilization.

Our previous analyses show that both receptors function synergistically in proper craniofacial development, and that this function is required between 6 and 30 hpf. We know that *pdgfra* is expressed and required cell-autonomously in the neural crest for proper craniofacial development (Eberhart et al., 2008). It was unclear, however, when or where *pdgfrb* was expressed during the crucial time window Pdgf is required. To test whether *pdgfrb* is expressed in the neural crest, we used fluorescence *in situ* of *pdgfrb* in a *fli1:EGFP* transgenic, which labels the neural crest and vasculature, to look for co-localization. Indeed, at both 24 and 36 hpf, *pdgfrb* expression occurs in the neural crest and the vasculature (Fig. 4.5A-A', 4.5B-B'; Wiens et al., 2010). These data show that *pdgfrb* is expressed in the neural crest during the time window that Pdgf signaling is required.

To pinpoint the timing of dual expression of *pdgfra* and *pdgfrb* in the

neural crest, we used double fluorescent *in situ* analysis. Prior to 20 hpf, we detect no overlap in the expression of *pdgfra* and *pdgfrb* (not shown). By 20 and 24 hpf, both *pdgfra* and *pdgfrb* are expressed throughout the first and second arches (Fig. 4.6A-A'', 4.6B-B''). This dual expression remains even at 36 hpf (Fig. 3.6C-C''). The data suggest that neural crest cells express both *pdgfra* and *pdgfrb* during the window that Pdgf function is required for craniofacial development.

4.III.d. Loss of both *pdgfra* and *pdgfrb* results in increased neural crest cell death.

Loss of both *pdgfra* and *pdgfrb* led to markedly more severe craniofacial phenotypes compared to either loss of *pdgfra* or *pdgfrb* alone. Cell death is not observed by a singular loss of *pdgfra* (McCarthy et al., 2013). However, ethanol treatment causes increased neural crest cell death in *pdgfra* mutants (McCarthy et al., 2013), demonstrating that in certain contexts Pdgf signaling is critical for neural crest cell survival. Therefore, we analyzed cell death at 24 hpf in double *pdgfra;pdgfrb* mutants and compared them to the single mutants. Consistent with our previous results, *pdgfra* mutants do not exhibit any increase in cell death (McCarthy et al., 2013), but in the absence of both receptors, we see a synergistic and significant increase in cell death (Fig. 4.7B-B', 4.7A-A', 4.7C). Cell proliferation was not affected when comparing these two groups (data not shown). Loss of *pdgfrb* alone also does not cause any increase in cell death

compared to wildtype siblings (neural crest cell death: *pdgfrb*^{-/-} mean=1.29, *pdgfrb*^{+/+} mean=2.5, p=0.175). At 30 hpf, both cell death and proliferation are unaffected in double *pdgfra;pdgfrb* mutants compared to all other genotypes (not shown). Together, these data suggest that cell death may contribute to the exacerbated craniofacial phenotype observed in double *pdgfra;pdgfrb* mutants.

4.IV. Discussion and future directions

We show that *pdgfra* and *pdgfrb* synergistically interact during craniofacial development. Loss of both receptors leads to exacerbated neurocranial and viscerocranial defects in zebrafish, and neural crest conditional *Pdgfra;Pdgfrb* knockouts in mouse similarly reveal exacerbated craniofacial defects not observed in either single knockout alone. This suggests a high conservation of the *Pdgfra;Pdgfrb* interaction across species. In zebrafish, we go on to show that loss of Pdgf function during a time window when both receptors are expressed in the neural crest, is critical for proper craniofacial development. Finally, we find evidence that implicates neural crest cell death as a possible factor in the exacerbated phenotype observed in *pdgfra;pdgfrb* mutants.

Numerous publications have uncovered the functional role *Pdgfra* plays in craniofacial development (Eberhart et al., 2008; Hoch and Soriano, 2003; Tallquist and Kazlauskas, 2004; Vasudevan and Soriano, 2014). *Pdgfrb*, on the other hand, has never been observed to cause craniofacial defects (Soriano, 1994; Wiens et al., 2010). Loss of the PI3K domains of both *Pdgfra* and *Pdgfrb*

genetically interacted to cause craniofacial defects as severe as a *Pdgfra* null (Klinghoffer et al., 2002). However, it remained unclear to what extent both Pdgf receptors functioned in craniofacial development and in the neural crest specifically. Here, we show that in neural crest-conditional *Pdgfra*;*Pdgfrb* mutant embryos, a more exacerbated craniofacial phenotype is observed compared to either *Pdgfra* or *Pdgfrb* neural crest-conditional knockouts alone. While *Pdgfra* can completely compensate for loss of *Pdgfrb*, our data suggests that in neural crest-conditional *Pdgfra* mutants, *Pdgfrb* has partial compensatory function. It will be of interest to see whether a specific tyrosine kinase residue of *Pdgfrb* allows this partial compensation. Data from Klinghoffer et al. would suggest that the PI3K activating-residue would be a strong contender for this role (Klinghoffer et al., 2002).

Our data implicates Pdgf to be important in craniofacial development in a window encompassing gastrulation to pharyngeal arch condensation. Future studies will aim to further assess the minimal window of Pdgf requirement for craniofacial development. *Pdgfra* is required for proper neural crest migration (Eberhart et al., 2008; Vasudevan and Soriano, 2014), and in zebrafish, this occurs beginning at 12 hpf. Inhibiting Pdgf signaling between 12 and 30 hpf resulted in less severe craniofacial defects compared to the 6 to 30 hpf time window. This could be due to the fact that inhibitor activity is often delayed compared to administration of the inhibitor. Thus, the timing that Pdgf function is

required could be condensed from just prior to migration, beginning at 10 hpf, to 30 hpf.

While the inhibitor analysis suggests a broad time when Pdgf signaling is required in craniofacial development, our *in situ* expression analysis reveals a much more condensed window of time when *pdgfra* and *pdgfrb* are co-expressed in the neural crest. Indeed, our double fluorescent *in situ* analysis reveals *pdgfra* and *pdgfrb* co-expression occurring in the arches beginning at 20 hpf. We know that *pdgfra* is expressed and required in the neural crest beginning at the time of neural crest migration at 12 hpf (Eberhart et al., 2008), while our data shows *pdgfrb* expression in the neural crest beginning around 20 and 24 hpf. Thus, if the synergistic effects of *pdgfra* and *pdgfrb* are specific to the neural crest, it would suggest that *pdgfrb* is dispensable for early neural crest migration. It will be of interest to determine the extent of overlap of expression between *pdgfra* and *pdgfrb* in the neural crest, which may implicate the timing of the interaction between these two receptors.

The craniofacial defects associated with *pdgfra* loss-of-function embryos are due to neural crest migratory defects (Eberhart et al., 2008; Vasudevan and Soriano, 2014). At this point, it is unclear whether there is a further exacerbation of neural crest migration in *pdgfra;pdgfrb* double mutants. However, our *in situ* analysis suggests that *pdgfrb* may be dispensable for early migration of the neural crest. We did observe increased cell death in the neural crest beginning at 24 hpf in our *pdgfra;pdgfrb* double mutants compared to single *pdgfra* mutants.

This is a time when we know both receptors are expressed in the neural crest. In the future, we will test the involvement of cell death in the craniofacial phenotype by blocking apoptosis in *pdgfra*;*pdgfrb* double mutants. Finally, it will be important to investigate whether a similar mechanism in mouse occurs, to lend further support of the conserved nature of Pdgf signaling in the craniofacial skeleton of vertebrates.

4.V. Materials and methods

4.V.a. Zebrafish care and use

All embryos were raised and cared for using established protocols with IACUC approval. Lines used in this study include the *pdgfra*^{b1059} (Eberhart et al., 2008), *pdgfrb*^{um148} (Kok et al., 2014), and the transgenic *Tg(fli1:EGFP)y1* (Lawson and Weinstein, 2002) called *fli1:EGFP* in the text. Embryos were treated with 1, 1.5, and 2 μ M Pdgf Inhibitor V (Calbiochem) from a 10mM stock in DMSO diluted in embryo medium.

4.V.b. Mice

Mouse lines used include *pdgfra*^{fl;fl} (Tallquist et al., 2003), *pdgfrb*^{fl;fl} (Richarte et al., 2007), and *Wnt1:Cre* (Danielian et al., 1998). Skeletal preparations were performed as described (Klinghoffer et al., 2002).

4.V.c. Immunohistochemistry and *In situ* hybridization

Embryos were fixed and processed as described previously (Maves et al., 2002; McCarthy et al., 2013) using anti-active caspase 3 (Promega) and anti-phospho

histone H3 (Sigma) primary antibodies with AlexaFluor 568 secondary antibodies. Fluorescent *in situ* hybridization was performed as described previously (Jowett and Yan, 1996). Were performed, cell death was counted using anti-active caspase 3- positive neural crest cells, marked via *fli:eGFP*, and a students T-test was performed for statistical analysis.

4.V.d. Zebrafish cartilage staining

5 day old embryos were stained with Alcian Blue and Alizarin Red for cartilage and bone (Walker and Kimmel, 2007), then flat mounted (Kimmel et al., 1998). Images were taken with a Zeiss Axio Imager-AI scope and measurements of neurocranial and viscerocranial elements were performed as described (McCarthy et al., 2013). All graphs were made using Microsoft Excel 2011. We used ANOVA and Tukey-Kramer post-hoc test for all statistical analysis.

4.V.e. Confocal microscopy and figure processing

Confocal z-stacks were collected on a Zeiss LSM 710 using Zeb software. All images were processed in Adobe Photoshop CS.

4.VI. Figures

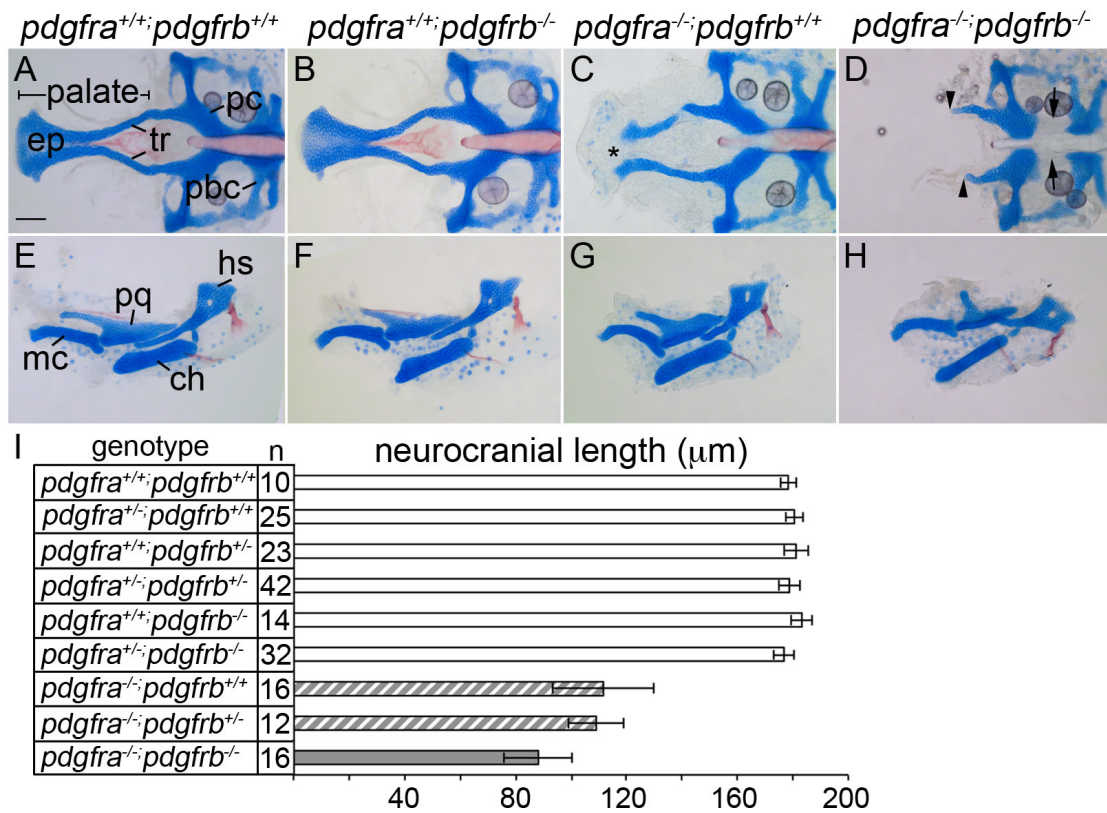


Figure 4.1: *pdgfra* and *pdgfrb* synergistically interact in craniofacial development. (A-D) 5 dpf flatmounted zebrafish neurocrania and (E-H) viscerocrania. Anterior is to the left. (A,E) Wildtype and (B,F) *pdgfrb* mutants display normal craniofacial skeletons, while (C,G) *pdgfra* mutants display a shortened neurocrania, cleft palate (asterisk) and smaller viscerocranial elements. (D,H) *pdgfra*;*pdgfrb* double mutants display synergistic reductions of the neurocranium (arrowheads) and loss of the posterior neurocranium between the parachordals and the posterior basicapsular commissure (arrows) compared to *pdgfra*, *pdgfrb*, and wildtype

siblings.(I) Graph depicting neurocranial length measured from the tip of the anterior palate to the posterior base of the neurocranium. Similar bar shading represents not statistically significant (ANOVA, $p < 0.5$). ep=ethmoid plate, tr=trabeculae, pbc=posterior basicapsular commissure, pc= parachordals. scale bar= 20 μ m.

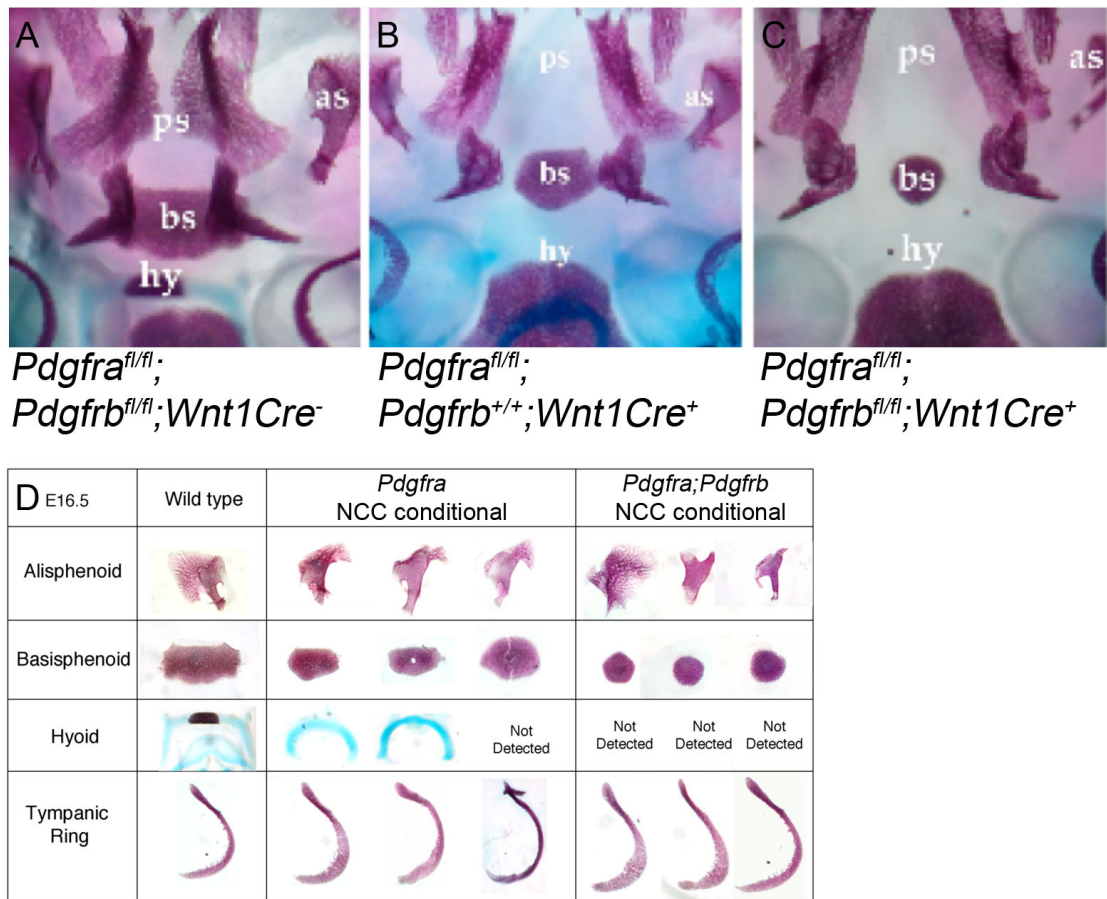


Figure 4.2: Synergistic skeletal abnormalities observed in

pdgfra^{fl/fl};*pdgfrb*^{fl/fl};*wnt1:Cre* mice. (A-C) A ventral view of the skull derived from E16.5 embryos with corresponding genotypes listed below each panel. Anterior is up. (D) Individual craniofacial skeletal elements dissected and flatmounted in one wildtype and three *pdgfra*^{fl/fl};*pdgfrb*^{+/+};*wnt1:Cre*⁺ and *pdgfra*^{fl/fl};*pdgfrb*^{fl/fl};*wnt1:Cre*⁺ mice. In *pdgfra*^{fl/fl};*pdgfrb*^{fl/fl};*wnt1:Cre*⁺ the alisphenoid and basisphenoid is reduced, while the hyoid fails to form compared to

pdgfra^{fl/fl};*pdgfrb*^{+/+};*wnt1:Cre*⁺ mice. as=alisphenoid, bs=basisphenoid, hy= hyoid,
ps=palatal shelf. Figure by Michelle D. Tallquist.

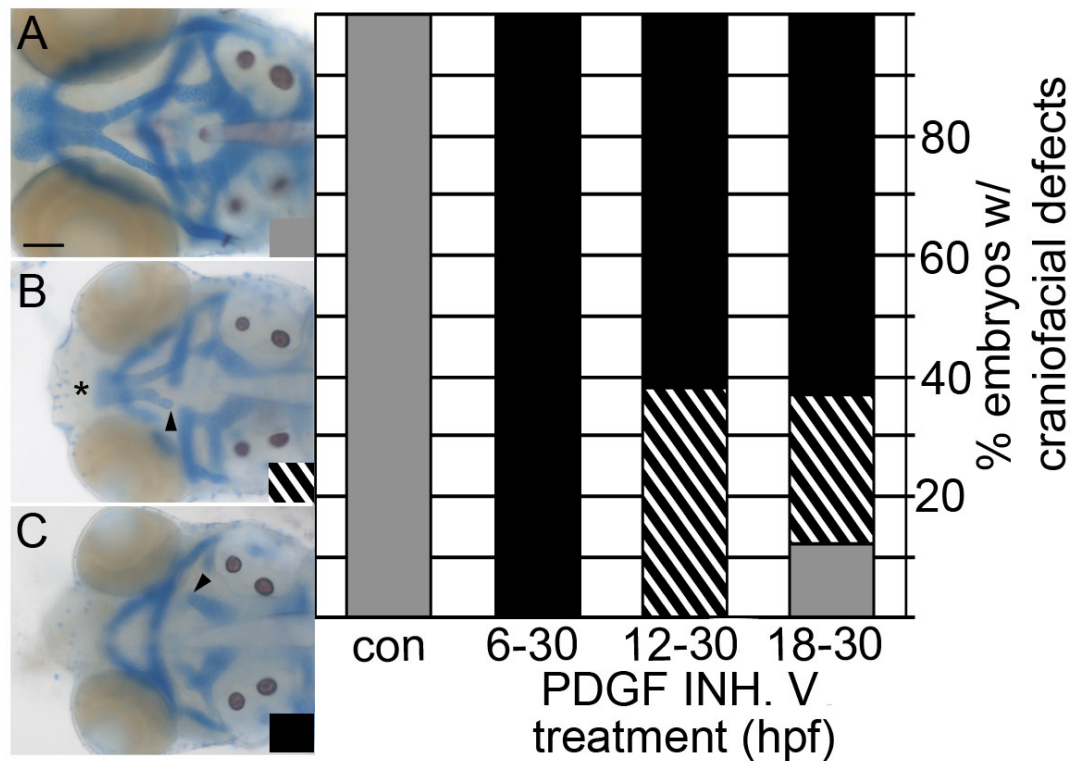


Figure 4.3: Pdgf signaling is required between 6 and 30 hours post fertilization for proper craniofacial development. (A-C) 5 dpf wholemounted zebrafish treated with 1.5 μ M PDGF inhibitor V and stained for cartilage and bone, anterior is to the left. (A) Wildtype, (B) mild, showing reduced palate (asterisk) and broken trabeculae (arrowhead) and (C) severe reductions in the neurocrania (arrowhead) of PDGF inhibitor V treated embryos. Graph depicts percentage of embryos treated with PDGF inhibitor V at varying time windows and resulting phenotypes observed shown in shaded bars that correspond to the phenotypes in A-C.

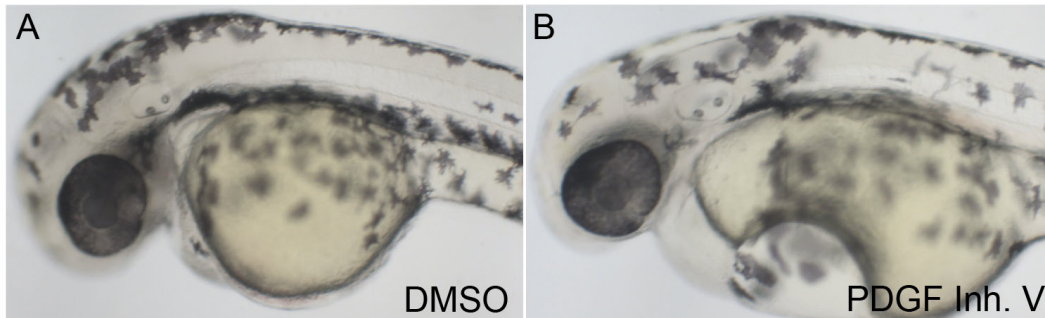


Figure 4.4: PDGF Inhibitor V treatment does not affect melanocyte formation. (A-B) Full-mount DIC images of 40 hpf zebrafish embryos treated with either DMSO or 1.5 μ M PDGF inhibitor V from 6 to 30 hpf, anterior is to the left.

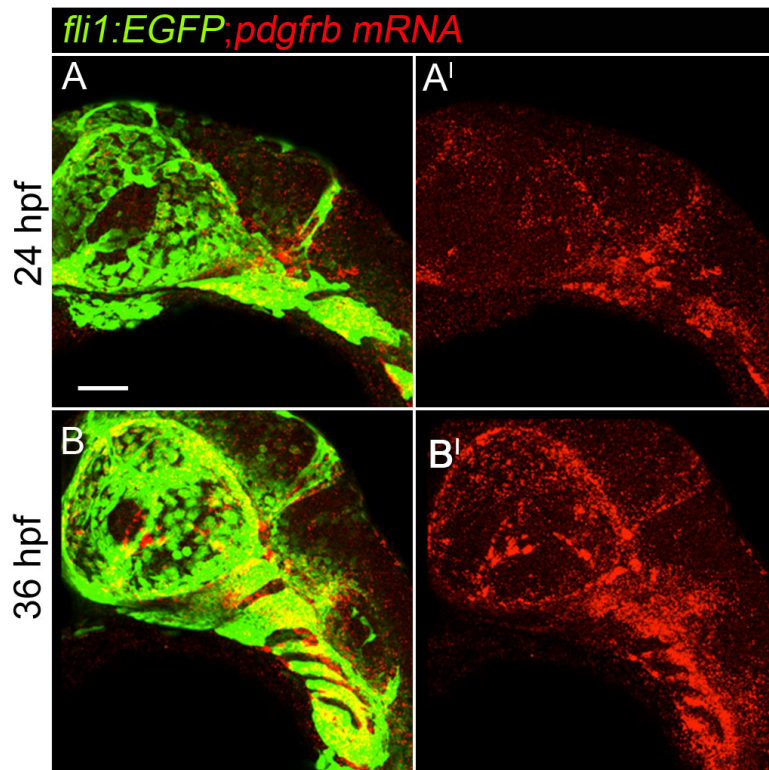


Figure 4.5: The neural crest expresses *pdgfrb* in zebrafish at 24 and 36 hours post fertilization. (A-A') A 24 hpf *fli1:EGFP* transgenic embryo and labeled for *pdgfrb* mRNA via fluorescence *in situ hybridization*, anterior is to the left. (B-B') A 36 hpf *fli1:EGFP* transgenic embryo and labeled for *pdgfrb* mRNA via fluorescence *in situ hybridization*, anterior is to the left. Scale bar= 20 μ m.

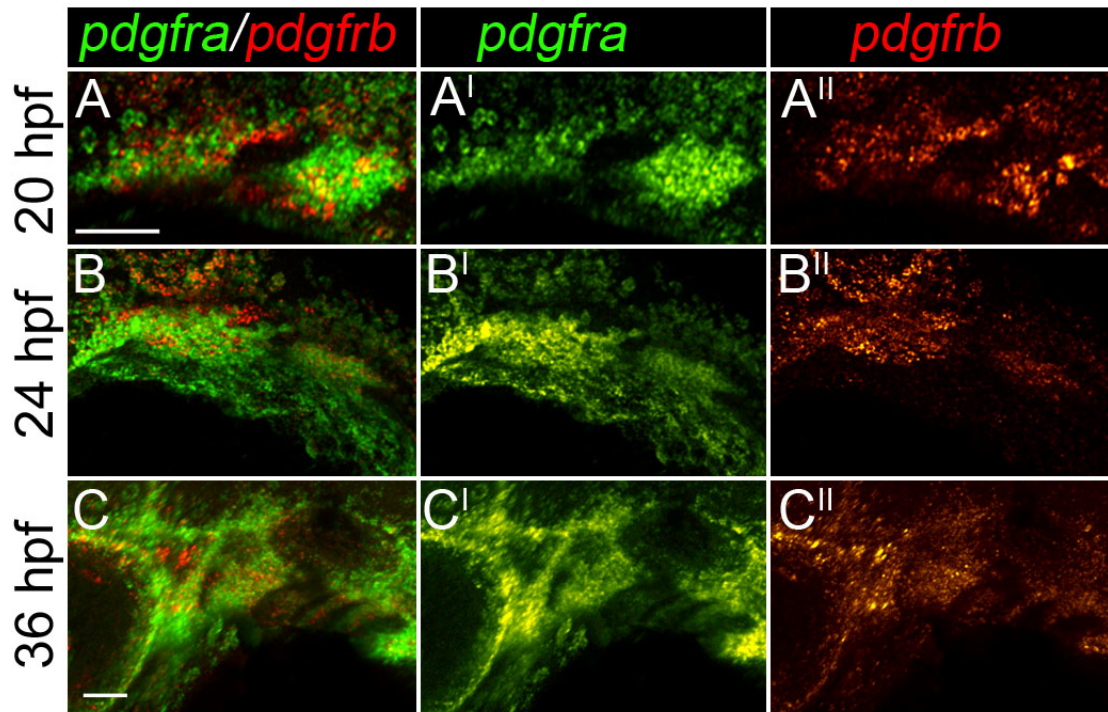


Figure 4.6: Neural crest cells express both *pdgfra* and *pdgfrb* beginning at 20 hours post fertilization. (A-A'') A 20, (B-B'') 24, and (C-C'') 36 hpf embryo stained for both *pdgfra* and *pdgfrb* mRNA via fluorescence in situ hybridization. scale bar= 20 μ m.

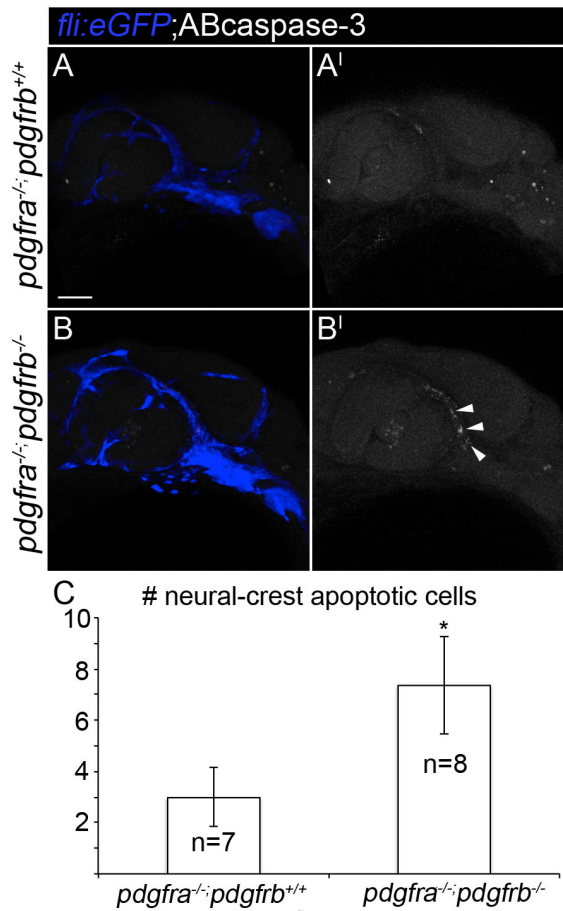


Figure 4.7: *pdgfra*;*pdgfrb* mutants show increased neural crest cell death at 24 hours post fertilization. (A-A', B-B') 24 hpf *fli1:EGFP* (pseudo-colored blue) zebrafish embryo with corresponding genotypes listed left of panels, stained for active caspase 3 (shown in grey). Anterior is to the left. (C) Graph representing number of active caspase 3 positive neural crest cells in corresponding genotypes (Students T-test, $p < 0.05$). scale bar= 20 μ m.

4.VII. Tables

Significant difference compared to all other genotypes*

	nc length	nc width	Mc	pq	ptergoid process	hs	symplectic length	ch
pdgfra ^{-/-} ;pdgfrb ^{+/+}	Y	Y	Y	Y	Y	Y	Y	N
pdgfra ^{-/-} ;pdgfrb ^{+/-}	Y	Y	Y	Y	Y	Y	Y	N
pdgfra ^{-/-} ;pdgfrb ^{-/-}	Y	Y	Y	Y	Y	Y	Y	N

*excluding pdgfra^{-/-};pdgfrb^{+/+}, pdgfra^{-/-};pdgfrb^{+/-}, and pdgfra^{-/-};pdgfrb^{-/-} genotypes

significant difference compared to

pdgfra^{-/-};pdgfrb^{+/+} and pdgfra^{-/-};pdgfrb^{+/-} genotypes

	nc length	nc width	symplectic length
pdgfra ^{-/-} ;pdgfrb ^{-/-}	Y	Y	Y

Table 4.1: *pdgfra*;*pdgfrb* double mutants show statistically significant differences in craniofacial measurements. Compared to all other genotypes, excluding *pdgfra*^{-/-};*pdgfrb*^{+/+}, *pdgfra*^{-/-};*pdgfrb*^{+/-}, and *pdgfra*^{-/-};*pdgfrb*^{-/-} genotypes, *pdgfra*^{-/-};*pdgfrb*^{+/+}, *pdgfra*^{-/-};*pdgfrb*^{+/-}, and *pdgfra*^{-/-};*pdgfrb*^{-/-} genotypes have statistically significant differences in neurocranium (nc) length, nc width, Meckels cartilage area (Mc), palatoquadrate area (pq), length of pterygoid process, hyosymplectic area, and symplectic length, but not in ceratohyal (ch) area. *Pdgfra*^{-/-};*pdgfrb*^{-/-} genotypes have significantly different nc length, nc width, and symplectic length when compared to *pdgfra*^{-/-};*pdgfrb*^{+/+} and *pdgfra*^{-/-};*pdgfrb*^{+/-} genotypes. Y= statistically significant, N= not statistically significant (ANOVA, p<0.5).

Chapter 5: Summary and future directions

The variability and severity of birth defects are modulated by both genetics and the environment (Carinci et al., 2007; Das et al., 2004; Green et al., 2004; Jacobson et al., 2006; Wu et al., 2014). A highly prevalent and variable birth defect is FASD. Although it is environmentally induced, genetics contributes to the risk for FASD (Das et al., 2004; Green et al., 2004; Jacobson et al., 2006). My work has provided important insight into the role genetics plays in the variability and susceptibility to ethanol-induced craniofacial defects.

I helped develop a zebrafish model to uncover gene-ethanol interactions and apply these findings to humans. In chapter 2, I showed that *pdgfra* interacts with ethanol in zebrafish and found support for this interaction in a human dataset. In zebrafish, not only does ethanol increase the severity of the mutant phenotype, it causes haploinsufficiency in heterozygous siblings. My findings demonstrated that *pdgfra* and ethanol synergistically interact, due to a role for Pdgfra in protecting against ethanol-induced neural crest apoptosis. I showed that the mechanism of the interaction was due to combinatorial inhibition of the PI3K/mTOR pathway. Collectively, how *pdgfra* functioned in an optimal (control) environment did not translate to how it functioned in a less desirable environment (ethanol). Thus, phenotypes generated by synergistic gene-ethanol interactions are not readily predicted by mutant phenotypes in other contexts. In fact, it

suggests that the function of a gene can only ever be completely cataloged when tested in multiple environmental contexts, including ethanol.

My work with *pdgfra* suggested that ethanol may interact synergistically with other growth factor pathways and so I tested if *fgf8a* mutants were ethanol sensitive. While the *pdgfra* and ethanol interaction caused defects specific to neural-crest derivatives of the craniofacial skeleton, ethanol disrupted postchordal, mesoderm-derived, structures in *fgf8a* mutants. Because the development of this portion of the skull is very poorly characterized, I focused my efforts to understand Fgf function in the normal development of this structure in chapter 3. I recapitulated the *fgf8a*-ethanol phenotype by blocking both *fgf8a* and *fgf3*. I found that Fgf signaling from the brain and mesoderm was essential to specify the precursors of the postchordal neurocranium. Following this specification, Shh signaling was essential for proper differentiation of the postchordal mesoderm precursors. The neural ectoderm is the most likely source of Shh signaling, as the notochord appears dispensable for proper postchordal neurocranial formation. These results provided clarity into the mechanism of how Fgfs function in proper postchordal neurocranial development, and provided new developmental insights into this relatively neglected organ in research. As the *fgf8a;fgf3* and *fgf8a*-ethanol interactions showed mirroring phenotypes, it suggested that ethanol may broadly attenuate growth factor signaling pathways. Thus, the *pdgfra*-ethanol interaction may, in part, be due to combinatorial loss of signaling across Pdgf receptors. I tested this in chapter 4.

There are two Pdgf receptors and, unlike *pdgfra*, *pdgfrb* has not been implicated in craniofacial development. However, through genetic analysis, I found that double *pdgfra;pdgfrb* mutants have a more severe craniofacial phenotype compared to either a *pdgfra* or *pdgfrb* mutant alone. Conservation of this interaction was shown in mouse. Lastly, data in zebrafish shows that cell death might contribute to the severe craniofacial phenotype found in *pdgfra;pdgfrb* double mutants. The full mechanism of this interaction and whether it fully phenocopies the ethanol-*pdgfra* interaction is still of ongoing interest.

Collectively, my dissertation focuses on how growth factor signaling and the environmental ethanol exposure can synergistically interact during craniofacial development. Specifically, I focused on *pdgfra* and *fgf8a* as ethanol-sensitive genes. While I did uncover a specific mechanism involving PI3K/AKT/mTOR signaling as the target of the *pdgfra*-ethanol interaction, this still needs to be tested in my *fgf8a*-ethanol interaction. Also, I focused on the craniofacial defects associated with these gene-ethanol interactions. Significant neurological defects are present in FASD (Calhoun and Warren, 1997; Hoyme et al., 2005; Jones, 2011; Moore et al., 2014), and we know that both *pdgfra* and *fgf8a* have functions in brain development (Echevarria et al., 2005; Zhu et al., 2014). Future studies will be aimed at elucidating whether these gene-ethanol interactions cause neurological defects. Furthermore, there are numerous genes involved in growth factor signaling that may interact with ethanol. These will need to be tested to further support my hypothesis that genes involved in growth factor

signaling broadly interact with ethanol. Lastly, with the data that I have generated, it would be of high interest to propose therapeutic treatments for FASD specifically targeting growth factor signaling genes in especially prone individuals.

5.I. FUTURE DIRECTIONS

5.I.a. Mechanistic understanding of the *fgf8a*-ethanol interaction

Two main questions remain concerning the *fgf8a*-ethanol interaction: 1) Is the *fgf8a*-ethanol interaction caused by a mechanism similar to the *pdgfra*-ethanol interaction? and, 2) Is the cause of the postchordal neurocranial loss the same between the *fgf8a*-ethanol interaction and the *fgf8a;fgf3* interaction? Based on my *pdgfra*-ethanol work, I hypothesized that ethanol interacts with genes involved in activation of growth factor signaling at the level of mTOR. Similarly, Fgf receptors activate growth factor signaling and so the *fgf8a*-ethanol interaction may impede proper Fgf function at the level of mTOR.

I have already shown that blocking mTOR in *fgf8a* mutants recapitulates the ethanol-induced *fgf8a* defects. This supports my theory that ethanol impedes proper growth factor signaling at the level of mTOR, however, further analysis is required. Direct evidence that mTOR function is disrupted in the *fgf8a*-ethanol would require protein analysis showing decreased phosphorylated forms of downstream constituents. My model predicts that increasing mTOR signaling, via L-Leucine supplementation, would rescue *fgf8a* mutants treated with ethanol. I

would test whether cell death contributes to the ethanol-induced *fgf8a* effects by staining for active caspase-3 in the *Dra:Cre* transgenic background, which labels cephalic mesoderm. If ethanol inhibits growth factor signaling downstream of receptor activation at the level of mTOR, I would expect to observe cell death in cephalic mesoderm. Collectively, these results would support my hypothesis that ethanol broadly interacts with growth factor signaling pathways through synergistic inhibition of mTOR signaling leading to apoptosis.

In the case that mTOR is inhibited, but cell survival appears unaffected, it would suggest that the *fgf8a*-ethanol interaction is due to a similar misspecification defect found in *fgf8a;fgf3* double mutants. My work in chapter 3 showed that the cephalic paraxial mesoderm was misspecified in *fgf3;fgf8a* double mutants, as evidenced by a loss of *has2* expression. I would perform protein analysis on Fgf3 and Fgf8 ligands to determine if they are directly decreased in ethanol, because studies using NIH 3T3 cells suggests that mTOR targets translation of *fgf10* ligand directly (Hertzler-Schaefer et al. 2014). If the mechanism occurs through mTOR, I would expect to see a rescue of specification with increased mTOR activity in ethanol-treated *fgf8a* mutants. Collectively, these results would demonstrate that ethanol can disrupt distinct cellular processes, apoptosis versus specification, via the same mechanism of mTOR inhibition.

The other alternative is that the *fgf8a*-ethanol interaction is independent of mTOR inhibition. Ethanol has been shown to reduce Erk activity (Sanna et al.,

2002), a major effector of Fgf signaling. This could be easily tested via Erk inhibitor analyses recapitulating the *fgf8a*-ethanol interaction. Although my overall hypothesis predicts growth factor signaling genes to interact with ethanol at the level of mTOR, due to the many signaling pathways growth factors feed into, ethanol may in fact interact with them through multiple mechanisms.

5.1.b. Other defects associated with gene-ethanol interactions

My work has focused primarily on craniofacial defects associated with gene-ethanol interactions. However, FASD also causes debilitating neurological defects (Calhoun and Warren, 1997; Hoyme et al., 2005; Jones, 2011; Moore et al., 2014). Furthermore, both *pdgfra* and *fgf8a* have functions in neural tissues. For instance *Pdgfra* is critical in developing oligodendrocytes (Zhu et al., 2014) and *Fgf8* is necessary to pattern brain regions, including the midbrain-hindbrain boundary and rhombomere 4 (Echevarria et al., 2005). Experiments that could be utilized to elucidate whether ethanol disrupts the neurological functions of these genes include histological analysis of brain regions and immunohistochemistry of markers of neural cell types including the oligodendrocyte marker O4+ (Ackerman et al., 2015), and the hindbrain-marker *Kitb* (Staudt et al., 2015). There are also numerous transgenic zebrafish lines labeling neural-specific cell types and regions that could be utilized to investigate neurological defects in 4D in these gene-ethanol interactions, including the oligodendrocyte and purkinje neuron labeling transgenic *olig2:RFP* (Shin et al., 2003) and the neuroepithelial

transgenic *nestin:EGFP* (Kaslin et al., 2009). There is a possibility, however, that more subtle behavioral defects could be caused by these gene ethanol interactions, rather than physical defects.

To test whether gene-ethanol interactions can disrupt behavior, new behavioral analyses that have just recently been characterized in zebrafish FASD models can be utilized (Fernandes et al., 2015a, Fernandes et al., 2015b). In these tests, wild-type zebrafish exposed to a subteratogenic level of ethanol at an early developmental timepoint showed behavioral deficits months later (Fernandes et al., 2015a). Since both *pdgfra* and *fgf8a* mutants are embryonic lethal, only heterozygous siblings exposed to ethanol could be tested for gene-ethanol behavior deficits. Whether genetic background influences enhancement of ethanol-induced behavioral deficits remains to be seen. These experiments are currently underway.

5.I.c. Screening for ethanol sensitivity in other growth factor signaling genes

My dissertation shows genes involved in growth factor signaling interact with ethanol. At least for *pdgfra*, this interaction occurs at the level of mTOR, and so mutations in any gene involved in activating this pathway could potentially show an interaction with ethanol. Furthermore, any gene, which naturally functions to inhibit this pathway, could protect against ethanol teratogenesis. The easiest and

quickest way to uncover these genes would be to perform zebrafish genetic screens.

Many thousand zebrafish mutants are available and genome-editing technologies have advanced to where generating new zebrafish mutants is straightforward. Genes that I would hypothesize to interact with ethanol would be those involved in the transduction of the mTOR pathway, including *mTOR*, *eIF4B*, upstream activator *AKT* as well as the PI3K inhibitor *pten*. There are numerous growth factor signaling genes that should be tested as well, including those implicated in my work, including *pdgfrb* as well as the Pdgf ligands, and *fgfr3* and *fgf3*. Studies, in mostly *in vitro* assays, have implicated ethanol interacting with other growth factor genes, including *insulin-like receptor* (McClure et al., 2011; de la Monte et al., 1999; Sasaki et al., 1994), *BDNF* (de la Monte, 2000), *TGFB* (Jegou et al., 2013), and *VEGF* (Feng et al., 2005). Lastly, our efforts focusing on growth factor genes interacting with ethanol could be focused through our collaboration with the Foroud lab, whom have generated human data on gene by ethanol interactions.

5.1.d. Developing treatments and therapies to mitigate ethanol teratogenesis

A driving motivation in the health sciences is improving health care. FASD affects nearly 1% of the population (Sampson et al., 1997). With unplanned pregnancies accounting for nearly 50% of all pregnancies (Finer and Henshaw, 2006), fetal

exposure to ethanol is a problem that will not likely end soon. How do we mitigate the effects of ethanol on fetus health?

Numerous studies have focused on the importance of nutrition in reducing ethanol effects on the fetus (see review Young et al., 2014). Research has also shown that supplementation with either retinoic acid (Marrs et al., 2010), choline (Hunt, 2012), or *shh* (Aoto et al., 2008; Li et al., 2007) can reduce ethanol-induced defects in various animal models. However, application of *shh* would be difficult to implement, and data on retinoic acid suggests these supplements may not be advisable to use during pregnancy (Arnhold et al., 2002). My work adds L-Leucine to this list of potential therapeutic supplements and is not likely to cause birth defects on its own. Whereas my study focused on L-leucine supplementation rescuing ethanol-induced defects in a genetic-dependent context, these other studies were more general in the supplementation of these nutrients/genes in wildtype genetic backgrounds with high doses of ethanol. Thus, it may be important in the future to consider genetic background in implementing appropriate treatments.

Although my hypothesis that growth factor signaling genes are especially sensitive to ethanol needs to be further tested, it is possible to imagine treatments being implemented in the future to help reduce the effects of ethanol during pregnancy by targeting growth factor genes. The majority of work focusing on growth factors in the clinical setting is in their inhibition, primarily because of their upregulation in cancer (Brooks et al., 2012; Demoulin and Essaghir, 2014).

There are a few cases where growth factors are used therapeutically, namely in wound healing aspects (Finnson et al., 2013; Greenhalgh et al., 1990; Penn et al., 2012). With the coming age of personalized medicine, numerous aspects of health including genetics will be considered to determine appropriate treatments and therapeutics to a given disease or life-state. Given the paucity of information available on gene-environment interactions, continued work in animal models, including zebrafish, will be critical to our understanding of the human condition.

Bibliography

Ackerman, S. D., Garcia, C., Piao, X., Gutmann, D. H. and Monk, K. R. (2015). The adhesion GPCR Gpr56 regulates oligodendrocyte development via interactions with Galpha12/13 and RhoA. *Nat Commun* 6, 6122.

Aggarwal, V. S., Liao, J., Bondarev, A., Schimmang, T., Lewandoski, M., Locker, J., Shanske, A., Campione, M. and Morrow, B. E. (2006). Dissection of Tbx1 and Fgf interactions in mouse models of 22q11DS suggests functional redundancy. *Hum Mol Genet* 15, 3219-28.

Ahlgren, S. C., Thakur, V. and Bronner-Fraser, M. (2002). Sonic hedgehog rescues cranial neural crest from cell death induced by ethanol exposure. *Proc Natl Acad Sci U S A* 99, 10476-81.

Alexander, C., Piloto, S., Le Pabic, P. and Schilling, T. F. (2014). Wnt signaling interacts with bmp and edn1 to regulate dorsal-ventral patterning and growth of the craniofacial skeleton. *PLoS Genet* 10, e1004479.

Alexander, C., Zuniga, E., Blitz, I. L., Wada, N., Le Pabic, P., Javidan, Y., Zhang, T., Cho, K. W., Crump, J. G. and Schilling, T. F. (2011). Combinatorial roles for BMPs and Endothelin 1 in patterning the dorsal-ventral axis of the craniofacial skeleton. *Development* 138, 5135-46.

Ali, S., Champagne, D. L., Alia, A. and Richardson, M. K. (2011). Large-scale analysis of acute ethanol exposure in zebrafish development: a critical time window and resilience. *PLoS One* 6, e20037.

Amacher, S. L., Draper, B. W., Summers, B. R. and Kimmel, C. B. (2002). The zebrafish T-box genes *no tail* and *spadetail* are required for development of trunk and tail mesoderm and medial floor plate. *Development* 129, 3311-23.

Aoto, K., Shikata, Y., Higashiyama, D., Shiota, K. and Motoyama, J. (2008). Fetal ethanol exposure activates protein kinase A and impairs Shh expression in prechordal mesendoderm cells in the pathogenesis of holoprosencephaly. *Birth Defects Res A Clin Mol Teratol* 82, 224-31.

Arenzana, F. J., Carvan, M. J., 3rd, Aijon, J., Sanchez-Gonzalez, R., Arevalo, R. and Porteros, A. (2006). Teratogenic effects of ethanol exposure on zebrafish visual system development. *Neurotoxicol Teratol* 28, 342-8.

Arnhold, T., Elmazar, M. M. and Nau, H. (2002). Prevention of vitamin A teratogenesis by phytol or phytanic acid results from reduced metabolism of retinol to the teratogenic metabolite, all-trans-retinoic acid. *Toxicol Sci* 66, 274-82.

Auer, T. O. and Del Bene, F. (2014). CRISPR/Cas9 and TALEN-mediated knock-in approaches in zebrafish. *Methods* 69, 142-50.

Baker, C. V. and Bronner-Fraser, M. (1997a). The origins of the neural crest. Part I: embryonic induction. *Mech Dev* 69, 3-11.

Baker, C. V. and Bronner-Fraser, M. (1997b). The origins of the neural crest. Part II: an evolutionary perspective. *Mech Dev* 69, 13-29.

Bakkers, J., Kramer, C., Pothof, J., Quaedvlieg, N. E., Spaink, H. P. and Hammerschmidt, M. (2004). Has2 is required upstream of Rac1 to govern dorsal migration of lateral cells during zebrafish gastrulation. *Development* 131, 525-37.

Balczerski, B., Matsutani, M., Castillo, P., Osborne, N., Stainier, D. Y. and Crump, J. G. (2012). Analysis of sphingosine-1-phosphate signaling mutants reveals endodermal requirements for the growth but not dorsoventral patterning of jaw skeletal precursors. *Dev Biol* 362, 230-41.

Balczerski, B., Zakaria, S., Tucker, A. S., Borycki, A. G., Koyama, E., Pacifici, M. and Francis-West, P. (2012). Distinct spatiotemporal roles of hedgehog signalling during chick and mouse cranial base and axial skeleton development. *Dev Biol* 371, 203-14.

Basch, M. L., Bronner-Fraser, M. and Garcia-Castro, M. I. (2006). Specification of the neural crest occurs during gastrulation and requires Pax7. *Nature* 441, 218-22.

Betsholtz, C., Karlsson, L. and Lindahl, P. (2001). Developmental roles of platelet-derived growth factors. *Bioessays* 23, 494-507.

Bilotta, J., Barnett, J. A., Hancock, L. and Saszik, S. (2004). Ethanol exposure alters zebrafish development: a novel model of fetal alcohol syndrome. *Neurotoxicol Teratol* 26, 737-43.

Blader, P. and Strahle, U. (1998). Ethanol impairs migration of the prechordal plate in the zebrafish embryo. *Dev Biol* 201, 185-201.

Boehm, S. L., 2nd, Lundahl, K. R., Caldwell, J. and Gilliam, D. M. (1997). Ethanol teratogenesis in the C57BL/6J, DBA/2J, and A/J inbred mouse strains. *Alcohol* 14, 389-95.

Bohrer, L. R., Chuntova, P., Bade, L. K., Beadnell, T. C., Leon, R. P., Brady, N. J., Ryu, Y., Goldberg, J. E., Schmechel, S. C., Koopmeiners, J. S. et al. (2014). Activation of the FGFR-STAT3 pathway in breast cancer cells induces a hyaluronan-rich microenvironment that licenses tumor formation. *Cancer Res* 74, 374-86.

Brand, M., Heisenberg, C. P., Jiang, Y. J., Beuchle, D., Lun, K., Furutani-Seiki, M., Granato, M., Haffter, P., Hammerschmidt, M., Kane, D. A. et al. (1996). Mutations in zebrafish genes affecting the formation of the boundary between midbrain and hindbrain. *Development* 123, 179-90.

Brennan, D. and Giles, S. (2013). Sonic hedgehog expression is disrupted following in ovo ethanol exposure during early chick eye development. *Reprod Toxicol* 41, 49-56.

Brooks, A. N., Kilgour, E. and Smith, P. D. (2012). Molecular pathways: fibroblast growth factor signaling: a new therapeutic opportunity in cancer. *Clin Cancer Res* 18, 1855-62.

Cai, N., Dai, S. D., Liu, N. N., Liu, L. M., Zhao, N. and Chen, L. (2013). PI3K/AKT/mTOR signaling pathway inhibitors in proliferation of retinal pigment epithelial cells. *Int J Ophthalmol* 5, 675-80.

Calhoun, F. and Warren, K. (2007). Fetal alcohol syndrome: historical perspectives. *Neurosci Biobehav Rev* 31, 168-71.

Camenisch, T. D., Spicer, A. P., Brehm-Gibson, T., Biesterfeldt, J., Augustine, M. L., Calabro, A., Jr., Kubalak, S., Klewer, S. E. and McDonald, J. A. (2000). Disruption of hyaluronan synthase-2 abrogates normal cardiac morphogenesis and hyaluronan-mediated transformation of epithelium to mesenchyme. *J Clin Invest* 106, 349-60.

Carinci, F., Scapoli, L., Palmieri, A., Zollino, I. and Pezzetti, F. (2007). Human genetic factors in nonsyndromic cleft lip and palate: an update. *Int J Pediatr Otorhinolaryngol* 71, 1509-19.

Carracedo, A. and Pandolfi, P. P. (2008). The PTEN-PI3K pathway: of feedbacks and cross-talks. *Oncogene* 27, 5527-41.

Carter, E. P., Fearon, A. E. and Grose, R. P. (2014). Careless talk costs lives: fibroblast growth factor receptor signalling and the consequences of pathway malfunction. *Trends Cell Biol* 25, 221-33.

Carter, E. P., Fearon, A. E. and Grose, R. P. (2014). Careless talk costs lives: fibroblast growth factor receptor signalling and the consequences of pathway malfunction. *Trends Cell Biol* 25, 221-33.

Cartwright, M. M. and Smith, S. M. (1995). Increased cell death and reduced neural crest cell numbers in ethanol-exposed embryos: partial basis for the fetal alcohol syndrome phenotype. *Alcohol Clin Exp Res* 19, 378-86.

Chai, Y., Jiang, X., Ito, Y., Bringas, P., Jr., Han, J., Rowitch, D. H., Soriano, P., McMahon, A. P. and Sucov, H. M. (2000). Fate of the mammalian cranial neural crest during tooth and mandibular morphogenesis. *Development* 127, 1671-9.

Chasnoff, I. J. (1985). Fetal alcohol syndrome in twin pregnancy. *Acta Genet Med Gemellol (Roma)* 34, 229-32.

Chernoff, G. F. (1980). The fetal alcohol syndrome in mice: maternal variables. *Teratology* 22, 71-5.

Chiang, C., Litingtung, Y., Lee, E., Young, K. E., Corden, J. L., Westphal, H. and Beachy, P. A. (1996). Cyclopia and defective axial patterning in mice lacking Sonic hedgehog gene function. *Nature* 383, 407-13.

Choi, H. M., Beck, V. A. and Pierce, N. A. (2014). Multiplexed in situ hybridization using hybridization chain reaction. *Zebrafish* 11, 488-9.

Coffin, A. B., Ou, H., Owens, K. N., Santos, F., Simon, J. A., Rubel, E. W. and Raible, D. W. (2010). Chemical screening for hair cell loss and protection in the zebrafish lateral line. *Zebrafish* 7, 3-11.

Cohen, M. M., Jr. and Sulik, K. K. (1992). Perspectives on holoprosencephaly: Part II. Central nervous system, craniofacial anatomy, syndrome commentary, diagnostic approach, and experimental studies. *J Craniofac Genet Dev Biol* 12, 196-244.

Cooke, J. (1989). *Xenopus* mesoderm induction: evidence for early size control and partial autonomy for pattern development by onset of gastrulation. *Development* 106, 519-29.

Cordero, D., Marcucio, R., Hu, D., Gaffield, W., Tapadia, M. and Helms, J. A. (2004). Temporal perturbations in sonic hedgehog signaling elicit the spectrum of holoprosencephaly phenotypes. *J Clin Invest* 114, 485-94.

Couly, G., Creuzet, S., Bennaceur, S., Vincent, C. and Le Douarin, N. M. (2002). Interactions between Hox-negative cephalic neural crest cells and the foregut endoderm in patterning the facial skeleton in the vertebrate head. *Development* 129, 1061-73.

Couly, G. F., Coltey, P. M. and Le Douarin, N. M. (1992). The developmental fate of the cephalic mesoderm in quail-chick chimeras. *Development* 114, 1-15.

Couly, G. F., Coltey, P. M. and Le Douarin, N. M. (1993). The triple origin of skull in higher vertebrates: a study in quail-chick chimeras. *Development* 117, 409-29.

Creuzet, S., Schuler, B., Couly, G. and Le Douarin, N. M. (2004). Reciprocal relationships between Fgf8 and neural crest cells in facial and forebrain development. *Proc Natl Acad Sci U S A* 101, 4843-7.

Croushore, J. A., Blasiolo, B., Riddle, R. C., Thisse, C., Thisse, B., Canfield, V. A., Robertson, G. P., Cheng, K. C. and Levenson, R. (2005). Ptena and ptenb genes play distinct roles in zebrafish embryogenesis. *Dev Dyn* 234, 911-21.

Crump, J. G., Maves, L., Lawson, N. D., Weinstein, B. M. and Kimmel, C. B. (2004). An essential role for Fgfs in endodermal pouch formation influences later craniofacial skeletal patterning. *Development* 131, 5703-16.

Crump, J. G., Swartz, M. E., Eberhart, J. K. and Kimmel, C. B. (2006). *Moz-dependent Hox expression controls segment-specific fate maps of skeletal precursors in the face.* Development 133, 2661-9.

Crump, J. G., Swartz, M. E. and Kimmel, C. B. (2004). *An integrin-dependent role of pouch endoderm in hyoid cartilage development.* PLoS Biol 2, E244.

Cubbage, C. C. and Mabee, P. M. (1996). *Development of the cranium and paired fins in the zebrafish Danio rerio (Ostariophysi, Cyprinidae).* . Journal of Morphology, 121-160.

Danielian, P. S., Muccino, D., Rowitch, D. H., Michael, S. K. and McMahon, A. P. (1998). *Modification of gene activity in mouse embryos in utero by a tamoxifen-inducible form of Cre recombinase.* Curr Biol 8, 1323-6.

Das, U. G., Cronk, C. E., Martier, S. S., Simpson, P. M. and McCarver, D. G. (2004). *Alcohol dehydrogenase 2*3 affects alterations in offspring facial morphology associated with maternal ethanol intake in pregnancy.* Alcohol Clin Exp Res 28, 1598-606.

David, N. B., Saint-Etienne, L., Tsang, M., Schilling, T. F. and Rosa, F. M. (2002). *Requirement for endoderm and FGF3 in ventral head skeleton formation.* Development 129, 4457-68.

de Beer, G. (1937). The development of the vertebrate skull. Oxford University Press.

de la Monte, S. M., Ganju, N., Banerjee, K., Brown, N. V., Luong, T. and Wands, J. R. (2000). Partial rescue of ethanol-induced neuronal apoptosis by growth factor activation of phosphoinositol-3-kinase. *Alcohol Clin Exp Res* 24, 716-26.

de la Monte, S. M., Ganju, N., Tanaka, S., Banerjee, K., Karl, P. J., Brown, N. V. and Wands, J. R. (1999). Differential effects of ethanol on insulin-signaling through the insulin receptor substrate-1. *Alcohol Clin Exp Res* 23, 770-7.

de la Monte, S. M., Tong, M., Bowling, N. and Moskal, P. (2011). si-RNA inhibition of brain insulin or insulin-like growth factor receptors causes developmental cerebellar abnormalities: relevance to fetal alcohol spectrum disorder. *Mol Brain* 4, 13.

de la Monte, S. M. and Wands, J. R. (2002). Chronic gestational exposure to ethanol impairs insulin-stimulated survival and mitochondrial function in cerebellar neurons. *Cell Mol Life Sci* 59, 882-93.

de la Monte, S. M. and Wands, J. R. (2010). Role of central nervous system insulin resistance in fetal alcohol spectrum disorders. *J Popul Ther Clin Pharmacol* 17, e390-404.

Debelak, K. A. and Smith, S. M. (2000). Avian genetic background modulates the neural crest apoptosis induced by ethanol exposure. *Alcohol Clin Exp Res* 24, 307-14.

Deehan, G. A., Jr., Hauser, S. R., Wilden, J. A., Truitt, W. A. and Rodd, Z. A. (2013). Elucidating the biological basis for the reinforcing actions of alcohol in the mesolimbic dopamine system: the role of active metabolites of alcohol. *Front Behav Neurosci* 7, 104.

Demoulin, J. B. and Essaghir, A. (2014). PDGF receptor signaling networks in normal and cancer cells. *Cytokine Growth Factor Rev* 25, 273-83.

Denoyelle, M., Valles, A. M., Lentz, D., Thiery, J. P. and Boyer, B. (2001). Mesoderm-independent regulation of gastrulation movements by the src tyrosine kinase in *Xenopus* embryo. *Differentiation* 69, 38-48.

Depew, M. J., Lufkin, T. and Rubenstein, J. L. (2002). Specification of jaw subdivisions by *Dlx* genes. *Science* 298, 381-5.

Dessaud, E., McMahon, A. P. and Briscoe, J. (2008). Pattern formation in the vertebrate neural tube: a sonic hedgehog morphogen-regulated transcriptional network. *Development* 135, 2489-503.

Dlugos, C. A. and Rabin, R. A. (2003). Ethanol effects on three strains of zebrafish: model system for genetic investigations. *Pharmacol Biochem Behav* 74, 471-80.

Dlugos, C. A. and Rabin, R. A. (2010). Structural and functional effects of developmental exposure to ethanol on the zebrafish heart. *Alcohol Clin Exp Res* 34, 1013-21.

Dobashi, Y., Watanabe, Y., Miwa, C., Suzuki, S. and Koyama, S. (2011). Mammalian target of rapamycin: a central node of complex signaling cascades. *Int J Clin Exp Pathol* 4, 476-95.

Dong, J., Sulik, K. K. and Chen, S. Y. (2009). The role of NOX enzymes in ethanol-induced oxidative stress and apoptosis in mouse embryos. *Toxicol Lett* 193, 94-100.

Dougherty, M., Kamel, G., Grimaldi, M., Gfrerer, L., Shubinets, V., Ethier, R., Hickey, G., Cornell, R. A. and Liao, E. C. (2013). Distinct requirements for wnt9a and irf6 in extension and integration mechanisms during zebrafish palate morphogenesis. *Development* 140, 76-81.

Dougherty, M., Kamel, G., Shubinets, V., Hickey, G., Grimaldi, M. and Liao, E. C. (2012). Embryonic fate map of first pharyngeal arch structures in the sox10: kaede zebrafish transgenic model. *J Craniofac Surg* 23, 1333-7.

Downing, C., Flink, S., Florez-McClure, M. L., Johnson, T. E., Tabakoff, B. and Kechris, K. J. (2012

). Gene expression changes in C57BL/6J and DBA/2J mice following prenatal alcohol exposure. *Alcohol Clin Exp Res* 36, 1519-29.

Downward, J. (2004). PI 3-kinase, Akt and cell survival. *Semin Cell Dev Biol* 15, 177-82.

Draper, B. W., Morcos, P. A. and Kimmel, C. B. (2001). Inhibition of zebrafish *fgf8* pre-mRNA splicing with morpholino oligos: a quantifiable method for gene knockdown. *Genesis* 30, 154-6.

Dumortier, J. G. and David, N. B. (2015). The TORC2 component, Sin1, controls migration of anterior mesendoderm during zebrafish gastrulation. *PLoS One* 10, e0118474.

Eberhart, J. K., He, X., Swartz, M. E., Yan, Y. L., Song, H., Boling, T. C., Kuerth, A. K., Walker, M. B., Kimmel, C. B. and Postlethwait, J. H. (2008). MicroRNA Mirn140 modulates *Pdgf* signaling during palatogenesis. *Nat Genet* 40, 290-8.

Eberhart, J. K., Swartz, M. E., Crump, J. G. and Kimmel, C. B. (2006). Early Hedgehog signaling from neural to oral epithelium organizes anterior craniofacial development. *Development* 133, 1069-77.

Echevarria, D., Belo, J. A. and Martinez, S. (2005). Modulation of Fgf8 activity during vertebrate brain development. *Brain Res Brain Res Rev* 49, 150-7.

Ehrlich, D., Pirchl, M. and Humpel, C. (2012). Effects of long-term moderate ethanol and cholesterol on cognition, cholinergic neurons, inflammation, and vascular impairment in rats. *Neuroscience* 205, 154-66.

Ellman, M. B., Yan, D., Ahmadinia, K., Chen, D., An, H. S. and Im, H. J. (2013). Fibroblast growth factor control of cartilage homeostasis. *J Cell Biochem* 114, 735-42.

Etheredge, A. J., Christensen, K., Del Junco, D., Murray, J. C. and Mitchell, L. E. (2005). Evaluation of two methods for assessing gene-environment interactions using data from the Danish case-control study of facial clefts. *Birth Defects Res A Clin Mol Teratol* 73, 541-6.

Evans, D. J. and Noden, D. M. (2006). Spatial relations between avian craniofacial neural crest and paraxial mesoderm cells. *Dev Dyn* 235, 1310-25.

Fambrough, D., McClure, K., Kazlauskas, A. and Lander, E. S. (1999). Diverse signaling pathways activated by growth factor receptors induce broadly overlapping, rather than independent, sets of genes. *Cell* 97, 727-41.

Feil, R., Brocard, J., Mascrez, B., LeMeur, M., Metzger, D. and Chambon, P. (1996). Ligand-activated site-specific recombination in mice. *Proc Natl Acad Sci U S A* 93, 10887-90.

Feng, M. J., Yan, S. E. and Yan, Q. S. (2005). Effects of prenatal alcohol exposure on brain-derived neurotrophic factor and its receptor tyrosine kinase B in offspring. *Brain Res* 1042, 125-32.

Fernandes, Y., Rampersad, M. and Gerlai, R. (2015). Impairment of social behaviour persists two years after embryonic alcohol exposure in zebrafish: A model of fetal alcohol spectrum disorders. *Behav Brain Res*.

Fernandes, Y., Rampersad, M. and Gerlai, R. (2015). Embryonic alcohol exposure impairs the dopaminergic system and social behavioral responses in adult zebrafish. *Int J Neuropsychopharmacol* 18.

Finer, L. B. and Henshaw, S. K. (2006). Disparities in rates of unintended pregnancy in the United States, 1994 and 2001. *Perspect Sex Reprod Health* 38, 90-6.

Finnson, K. W., McLean, S., Di Guglielmo, G. M. and Philip, A. (2013). Dynamics of Transforming Growth Factor Beta Signaling in Wound Healing and Scarring. *Adv Wound Care (New Rochelle)* 2, 195-214.

Frisdal, A. and Trainor, P. A. (2014). Development and evolution of the pharyngeal apparatus. *Wiley Interdiscip Rev Dev Biol* 3, 403-18.

Galis, F. and Metz, J. A. (2001). Testing the vulnerability of the phylotypic stage: on modularity and evolutionary conservation. *J Exp Zool* 291, 195-204.

Garcia-Vilas, J. A., Quesada, A. R. and Medina, M. A. (2013). 4-methylumbelliferone inhibits angiogenesis in vitro and in vivo. *J Agric Food Chem* 61, 4063-71.

Gilbert-Barness, E. (2010). Teratogenic causes of malformations. *Ann Clin Lab Sci* 40, 99-114.

Gilliam, D. M. and Irtenkauf, K. T. (1990). Maternal genetic effects on ethanol teratogenesis and dominance of relative embryonic resistance to malformations. *Alcohol Clin Exp Res* 14, 539-45.

Graham, A. (2001). The development and evolution of the pharyngeal arches. *J Anat* 199, 133-41.

Graham, A. and Richardson, J. (2012). Developmental and evolutionary origins of the pharyngeal apparatus. *Evodevo* 3, 24.

Green, M. L., Singh, A. V., Zhang, Y., Nemeth, K. A., Sulik, K. K. and Knudsen, T. B. (2007). Reprogramming of genetic networks during initiation of the Fetal Alcohol Syndrome. *Dev Dyn* 236, 613-31.

Green, R. F. and Stoler, J. M. (2007). Alcohol dehydrogenase 1B genotype and fetal alcohol syndrome: a HuGE minireview. *Am J Obstet Gynecol* 197, 12-25.

Green, S. A., Simoes-Costa, M. and Bronner, M. E. (2015). Evolution of vertebrates as viewed from the crest. *Nature* 520, 474-82.

Greenhalgh, D. G., Sprugel, K. H., Murray, M. J. and Ross, R. (1990). PDGF and FGF stimulate wound healing in the genetically diabetic mouse. *Am J Pathol* 136, 1235-46.

Grevellec, A. and Tucker, A. S. (2010). The pharyngeal pouches and clefts: Development, evolution, structure and derivatives. *Semin Cell Dev Biol* 21, 325-32.

Gross, J. B. and Hanken, J. (2008). Segmentation of the vertebrate skull: neural-crest derivation of adult cartilages in the clawed frog, *Xenopus laevis*. *Integr Comp Biol* 48, 681-96.

Gross, J. B. and Hanken, J. (2008). Review of fate-mapping studies of osteogenic cranial neural crest in vertebrates. *Dev Biol* 317, 389-400.

Guo, R., Zhong, L. and Ren, J. (2009). Overexpression of aldehyde dehydrogenase-2 attenuates chronic alcohol exposure-induced apoptosis, change in Akt and Pim signalling in liver. *Clin Exp Pharmacol Physiol* 36, 463-8.

H.L., K. (1922). A new interpretation of the bones in the palate and upper jaw of fishes: Part 1. *J Anat*, 307-24.

Hall, B. K. (2000). The neural crest as a fourth germ layer and vertebrates as quadroblastic not triploblastic. *Evol Dev* 2, 3-5.

Halpern, M. E., Ho, R. K., Walker, C. and Kimmel, C. B. (1993). Induction of muscle pioneers and floor plate is distinguished by the zebrafish no tail mutation. *Cell* 75, 99-111.

Hamerman, D., Sasse, J. and Klagsbrun, M. (1986). A cartilage-derived growth factor enhances hyaluronate synthesis and diminishes sulfated glycosaminoglycan synthesis in chondrocytes. *J Cell Physiol* 127, 317-22.

Hertzler-Schaefer, K., Mathew, G., Somani, A. K., Tholpady, S., Kadakia, M. P., Chen, Y., Spandau, D. F. and Zhang, X. (2014). Pten loss induces autocrine FGF signaling to promote skin tumorigenesis. *Cell Rep* 6, 818-26.

Herzog, W., Sonntag, C., von der Hardt, S., Roehl, H. H., Varga, Z. M. and Hammerschmidt, M. (2004). Fgf3 signaling from the ventral diencephalon is

required for early specification and subsequent survival of the zebrafish adenohypophysis. *Development* 131, 3681-92.

Hirsinger, E., Stellabotte, F., Devoto, S. H. and Westerfield, M. (2004). Hedgehog signaling is required for commitment but not initial induction of slow muscle precursors. *Dev Biol* 275, 143-57.

Hoch, R. V. and Soriano, P. (2003). Roles of PDGF in animal development. *Development* 130, 4769-84.

Holowacz, T. and Sokol, S. (1999). FGF is required for posterior neural patterning but not for neural induction. *Dev Biol* 205, 296-308.

Hong, M. and Krauss, R. S. (2012). Cdon mutation and fetal ethanol exposure synergize to produce midline signaling defects and holoprosencephaly spectrum disorders in mice. *PLoS Genet* 8, e1002999.

Hong-Brown, L. Q., Brown, C. R., Huber, D. S. and Lang, C. H. (2006). Alcohol and indinavir adversely affect protein synthesis and phosphorylation of MAPK and mTOR signaling pathways in C2C12 myocytes. *Alcohol Clin Exp Res* 30, 1297-307.

Hong-Brown, L. Q., Brown, C. R., Kazi, A. A., Huber, D. S., Pruznak, A. M. and Lang, C. H. (2010). Alcohol and PRAS40 knockdown decrease mTOR activity

and protein synthesis via AMPK signaling and changes in mTORC1 interaction. *J Cell Biochem* 109, 1172-84.

Hong-Brown, L. Q., Brown, C. R., Kazi, A. A., Navaratnarajah, M. and Lang, C. H. (2012). Rag GTPases and AMPK/TSC2/Rheb mediate the differential regulation of mTORC1 signaling in response to alcohol and leucine. *Am J Physiol Cell Physiol* 302, C1557-65.

Hosokawa, R., Urata, M., Han, J., Zehnaly, A., Bringas, P., Jr., Nonaka, K. and Chai, Y. (2007). TGF-beta mediated Msx2 expression controls occipital somites-derived caudal region of skull development. *Dev Biol* 310, 140-53.

Hoyme, H. E., May, P. A., Kalberg, W. O., Kodituwakku, P., Gossage, J. P., Trujillo, P. M., Buckley, D. G., Miller, J. H., Aragon, A. S., Khaole, N. et al. (2005). A practical clinical approach to diagnosis of fetal alcohol spectrum disorders: clarification of the 1996 institute of medicine criteria. *Pediatrics* 115, 39-47.

Hsu, P. P., Kang, S. A., Rameseder, J., Zhang, Y., Ottina, K. A., Lim, D., Peterson, T. R., Choi, Y., Gray, N. S., Yaffe, M. B. et al. (2011). The mTOR-regulated phosphoproteome reveals a mechanism of mTORC1-mediated inhibition of growth factor signaling. *Science* 332, 1317-22.

Hsuan, J. J. and Tan, S. H. (1997). Growth factor-dependent phosphoinositide signalling. *Int J Biochem Cell Biol* 29, 415-35.

Hu, D. and Marcucio, R. S. (2009). A SHH-responsive signaling center in the forebrain regulates craniofacial morphogenesis via the facial ectoderm. *Development* 136, 107-16.

Hunt, P. S. (2012). Supplemental choline during the periweaning period protects against trace conditioning impairments attributable to post-training ethanol exposure in adolescent rats. *Behav Neurosci* 126, 593-8.

Itoh, N. (2007). The Fgf families in humans, mice, and zebrafish: their evolutionary processes and roles in development, metabolism, and disease. *Biol Pharm Bull* 30, 1819-25.

Itoh, N. (2007). The Fgf families in humans, mice, and zebrafish: their evolutionary processes and roles in development, metabolism, and disease. *Biol Pharm Bull* 30, 1819-25.

Jacobson, S. W., Carr, L. G., Croxford, J., Sokol, R. J., Li, T. K. and Jacobson, J. L. (2006). Protective effects of the alcohol dehydrogenase-ADH1B allele in children exposed to alcohol during pregnancy. *J Pediatr* 148, 30-7.

Jegou, S., El Ghazi, F., de Lendeu, P. K., Marret, S., Laudenbach, V., Uguen, A., Marcorelles, P., Roy, V., Laquerriere, A. and Gonzalez, B. J. (2013). Prenatal alcohol exposure affects vasculature development in the neonatal brain. *Ann Neurol* 72, 952-60.

Jiang, X., Iseki, S., Maxson, R. E., Sucov, H. M. and Morriss-Kay, G. M. (2002). Tissue origins and interactions in the mammalian skull vault. *Dev Biol* 241, 106-16.

Johnson, C. Y. and Rasmussen, S. A. (2010). Non-genetic risk factors for holoprosencephaly. *Am J Med Genet C Semin Med Genet* 154C, 73-85.

Johnston, M. C. and Bronsky, P. T. (1995). Prenatal craniofacial development: new insights on normal and abnormal mechanisms. *Crit Rev Oral Biol Med* 6, 368-422.

Jones, K. L. (2011). The effects of alcohol on fetal development. *Birth Defects Res C Embryo Today* 93, 3-11.

Jones, K. L., Robinson, L. K., Bakhireva, L. N., Marintcheva, G., Storojev, V., Strahova, A., Sergeevskaya, S., Budantseva, S., Mattson, S. N., Riley, E. P. et al. (2006). Accuracy of the diagnosis of physical features of fetal alcohol syndrome by pediatricians after specialized training. *Pediatrics* 118, e1734-8.

Jones, K. L. and Smith, D. W. (1973). Recognition of the fetal alcohol syndrome in early infancy. *Lancet* 302, 999-1001.

Jones, K. L., Smith, D. W., Ulleland, C. N. and Streissguth, P. (1973). Pattern of malformation in offspring of chronic alcoholic mothers. *Lancet* 1, 1267-71.

Jowett, T. and Yan, Y. L. (1996). Double fluorescent in situ hybridization to zebrafish embryos. *Trends Genet* 12, 387-9.

Joya, X., Garcia-Algar, O., Vall, O. and Pujades, C. (2014). Transient exposure to ethanol during zebrafish embryogenesis results in defects in neuronal differentiation: an alternative model system to study FASD. *PLoS One* 9, e112851.

Kague, E., Gallagher, M., Burke, S., Parsons, M., Franz-Odenaal, T. and Fisher, S. (2012). Skeletogenic fate of zebrafish cranial and trunk neural crest. *PLoS One* 7, e47394.

Kaslin, J., Ganz, J., Geffarth, M., Grandel, H., Hans, S. and Brand, M. (2009). Stem cells in the adult zebrafish cerebellum: initiation and maintenance of a novel stem cell niche. *J Neurosci* 29, 6142-53.

Kawakami, K., Takeda, H., Kawakami, N., Kobayashi, M., Matsuda, N. and Mishina, M. (2004). A transposon-mediated gene trap approach identifies developmentally regulated genes in zebrafish. *Dev Cell* 7, 133-44.

Kikuchi, K., Holdway, J. E., Werdich, A. A., Anderson, R. M., Fang, Y., Egnaczyk, G. F., Evans, T., Macrae, C. A., Stainier, D. Y. and Poss, K. D. (2010). Primary contribution to zebrafish heart regeneration by *gata4*(+) cardiomyocytes. *Nature* 464, 601-5.

Kim, S. M., Park, J. H., Kim, K. D., Nam, D., Shim, B. S., Kim, S. H., Ahn, K. S. and Choi, S. H. (2013). Brassinin Induces Apoptosis in PC-3 Human Prostate Cancer Cells through the Suppression of PI3K/Akt/mTOR/S6K1 Signaling Cascades. *Phytother Res*.

Kimball, S. R. and Jefferson, L. S. (2006). Signaling pathways and molecular mechanisms through which branched-chain amino acids mediate translational control of protein synthesis. *J Nutr* 136, 227S-31S.

Kimmel, C. B., Miller, C. T. and Keynes, R. J. (2001). Neural crest patterning and the evolution of the jaw. *J Anat* 199, 105-20.

Kimmel, C. B., Miller, C. T., Kruze, G., Ullmann, B., BreMiller, R. A., Larison, K. D. and Snyder, H. C. (1998). The shaping of pharyngeal cartilages during early development of the zebrafish. *Dev Biol* 203, 245-63.

Kimmel, C. B., Miller, C. T., Kruze, G., Ullmann, B., BreMiller, R. A., Larison, K. D. and Snyder, H. C. (1998). The shaping of pharyngeal cartilages during early development of the zebrafish. *Dev Biol* 203, 245-63.

Kimmel, C. B., Miller, C. T. and Moens, C. B. (2001). Specification and morphogenesis of the zebrafish larval head skeleton. *Dev Biol* 233, 239-57.

Kimmel, C. B., Warga, R. M. and Schilling, T. F. (1990). Origin and organization of the zebrafish fate map. *Development* 108, 581-94.

Klinghoffer, R. A., Hamilton, T. G., Hoch, R. and Soriano, P. (2002). An allelic series at the PDGFalphaR locus indicates unequal contributions of distinct signaling pathways during development. *Dev Cell* 2, 103-13.

Klinghoffer, R. A., Mueting-Nelsen, P. F., Faerman, A., Shani, M. and Soriano, P. (2001). The two PDGF receptors maintain conserved signaling in vivo despite divergent embryological functions. *Mol Cell* 7, 343-54.

Klinghoffer, R. A., Mueting-Nelsen, P. F., Faerman, A., Shani, M. and Soriano, P. (2001). The two PDGF receptors maintain conserved signaling in vivo despite divergent embryological functions. *Mol Cell* 7, 343-54.

Knight, R. D. and Schilling, T. F. (2006). Cranial neural crest and development of the head skeleton. *Adv Exp Med Biol* 589, 120-33.

Kobayashi, T. and Kronenberg, H. M. (2014). Overview of skeletal development. *Methods Mol Biol* 1130, 3-12.

Kok, F. O., Shin, M., Ni, C. W., Gupta, A., Grosse, A. S., van Impel, A., Kirchmaier, B. C., Peterson-Maduro, J., Kourkoulis, G., Male, I. et al. (2014). Reverse genetic screening reveals poor correlation between morpholino-induced and mutant phenotypes in zebrafish. *Dev Cell* 32, 97-108.

Kontges, G. and Lumsden, A. (1996). Rhombencephalic neural crest segmentation is preserved throughout craniofacial ontogeny. *Development* 122, 3229-42.

Kontges, G. and Lumsden, A. (1996). Rhombencephalic neural crest segmentation is preserved throughout craniofacial ontogeny. *Development* 122, 3229-42.

Kunisada, T., Tezulka, K., Aoki, H. and Motohashi, T. (2014). The stemness of neural crest cells and their derivatives. *Birth Defects Res C Embryo Today* 102, 251-62.

Lamb, T. M. and Harland, R. M. (1995). Fibroblast growth factor is a direct neural inducer, which combined with noggin generates anterior-posterior neural pattern. *Development* 121, 3627-36.

Landrigan, P. J., De Garbino, J. P. and Newman, B. (2006). Framing the future in light of the past: living in a chemical world. *Ann N Y Acad Sci* 1076, 657-9.

Lange, J. E. and Voas, R. B. (2000). Defining binge drinking quantities through resulting BACs. *Annu Proc Assoc Adv Automot Med* 44, 389-404.

Langevin, F., Crossan, G. P., Rosado, I. V., Arends, M. J. and Patel, K. J. (2011). *Fancd2* counteracts the toxic effects of naturally produced aldehydes in mice. *Nature* 475, 53-8.

Le Pabic, P., Ng, C. and Schilling, T. F. (2014). Fat-Dachsous signaling coordinates cartilage differentiation and polarity during craniofacial development. *PLoS Genet* 10, e1004726.

Leger, S. and Brand, M. (2002). Fgf8 and Fgf3 are required for zebrafish ear placode induction, maintenance and inner ear patterning. *Mech Dev* 119, 91-108.

LeLievre, C. S. (1978). Participation of neural crest-derived cells in the genes of the skull in birds. *Journal of Embryology and Experimental Morphology*, 17-37.

Lemoine, P., Harousseau, H., Borteyru, J. P. and Menuet, J. C. (1968). Les enfants des parents alcooliques: anomalies observees a propos de 127 cas (The children of alcoholic parents: anomalies observed in 127 cases). *Quest Medical*, 476-482.

Lettice, L. A., Purdie, L. A., Carlson, G. J., Kilanowski, F., Dorin, J. and Hill, R. E. (1999). The mouse bagpipe gene controls development of axial skeleton, skull, and spleen. *Proc Natl Acad Sci U S A* 96, 9695-700.

Li, Y. X., Yang, H. T., Zdanowicz, M., Sicklick, J. K., Qi, Y., Camp, T. J. and Diehl, A. M. (2007). Fetal alcohol exposure impairs Hedgehog cholesterol modification and signaling. *Lab Invest* 87, 231-40.

Liu, D., Chu, H., Maves, L., Yan, Y. L., Morcos, P. A., Postlethwait, J. H. and Westerfield, M. (2003). Fgf3 and Fgf8 dependent and independent transcription factors are required for otic placode specification. *Development* 130, 2213-24.

Liu, L., Korzh, V., Balasubramanian, N. V., Ekker, M. and Ge, R. (2002). Platelet-derived growth factor A (pdgf-a) expression during zebrafish embryonic development. *Dev Genes Evol* 212, 298-301.

Lockwood, B., Bjerke, S., Kobayashi, K. and Guo, S. (2004). Acute effects of alcohol on larval zebrafish: a genetic system for large-scale screening. *Pharmacol Biochem Behav* 77, 647-54.

Loucks, E. and Carvan, M. J., 3rd. (2004). Strain-dependent effects of developmental ethanol exposure in zebrafish. *Neurotoxicol Teratol* 26, 745-55.

Loucks, E. J. and Ahlgren, S. C. (2009). Deciphering the role of Shh signaling in axial defects produced by ethanol exposure. *Birth Defects Res A Clin Mol Teratol* 85, 556-67.

Mann, R. K. and Beachy, P. A. (2000). Cholesterol modification of proteins. *Biochim Biophys Acta* 1529, 188-202.

Manning, B. D. and Cantley, L. C. (2007). AKT/PKB signaling: navigating downstream. *Cell* 129, 1261-74.

Mao, H., Diehl, A. M. and Li, Y. X. (2009). Sonic hedgehog ligand partners with caveolin-1 for intracellular transport. *Lab Invest* 89, 290-300.

Marcucio, R. S., Cordero, D. R., Hu, D. and Helms, J. A. (2005). Molecular interactions coordinating the development of the forebrain and face. *Dev Biol* 284, 48-61.

Marcucio, R. S., Young, N. M., Hu, D. and Hallgrimsson, B. (2011). Mechanisms that underlie co-variation of the brain and face. *Genesis* 49, 177-89.

Marrs, J. A., Clendenon, S. G., Ratcliffe, D. R., Fielding, S. M., Liu, Q. and Bosron, W. F. (2010). Zebrafish fetal alcohol syndrome model: effects of ethanol are rescued by retinoic acid supplement. *Alcohol* 44, 707-15.

Matsumoto, K., Li, Y., Jakuba, C., Sugiyama, Y., Sayo, T., Okuno, M., Dealy, C. N., Toole, B. P., Takeda, J., Yamaguchi, Y. et al. (2009). Conditional inactivation of Has2 reveals a crucial role for hyaluronan in skeletal growth, patterning, chondrocyte maturation and joint formation in the developing limb. *Development* 136, 2825-35.

Mattson, S. N., Foroud, T., Sowell, E. R., Jones, K. L., Coles, C. D., Fagerlund, A., Autti-Ramo, I., May, P. A., Adnams, C. M., Konovalova, V. et al. (2010). Collaborative initiative on fetal alcohol spectrum disorders: methodology of clinical projects. *Alcohol* 44, 635-41.

Maves, L., Jackman, W. and Kimmel, C. B. (2002). FGF3 and FGF8 mediate a rhombomere 4 signaling activity in the zebrafish hindbrain. *Development* 129, 3825-37.

May, P. A., Blankenship, J., Marais, A. S., Gossage, J. P., Kalberg, W. O., Barnard, R., De Vries, M., Robinson, L. K., Adnams, C. M., Buckley, D. et al. (2013). Approaching the prevalence of the full spectrum of fetal alcohol spectrum disorders in a South African population-based study. *Alcohol Clin Exp Res* 37, 818-30.

May, P. A., Gossage, J. P., Brooke, L. E., Snell, C. L., Marais, A. S., Hendricks, L. S., Croxford, J. A. and Viljoen, D. L. (2005). Maternal risk factors for fetal alcohol syndrome in the Western cape province of South Africa: a population-based study. *Am J Public Health* 95, 1190-9.

May, P. A., Gossage, J. P., Marais, A. S., Adnams, C. M., Hoyme, H. E., Jones, K. L., Robinson, L. K., Khaole, N. C., Snell, C., Kalberg, W. O. et al. (2007). The epidemiology of fetal alcohol syndrome and partial FAS in a South African community. *Drug Alcohol Depend* 88, 259-71.

Mayor, R. and Theveneau, E. (2013). The neural crest. *Development* 140, 2247-51.

McBratney-Owen, B., Iseki, S., Bamforth, S. D., Olsen, B. R. and Morriss-Kay, G. M. (2008). Development and tissue origins of the mammalian cranial base. *Dev Biol* 322, 121-32.

McCarthy, N., Wetherill, L., Lovely, C. B., Swartz, M. E., Foroud, T. M. and Eberhart, J. K. (2013). *Pdgfra* protects against ethanol-induced craniofacial defects in a zebrafish model of FASD. *Development* 140, 3254-65.

McCarthy, N. and Eberhart, J. K. (2014). Gene-ethanol interactions underlying fetal alcohol spectrum disorders. *Cell Mol Life Sci* 71, 2699-706.

McCarver, D. G., Thomasson, H. R., Martier, S. S., Sokol, R. J. and Li, T. (1997). Alcohol dehydrogenase-2*3 allele protects against alcohol-related birth defects among African Americans. *J Pharmacol Exp Ther* 283, 1095-101.

McClure, K. D., French, R. L. and Heberlein, U. (2011). A *Drosophila* model for fetal alcohol syndrome disorders: role for the insulin pathway. *Dis Model Mech* 4, 335-46.

McGough, N. N., Thomas, J. D., Dominguez, H. D. and Riley, E. P. (2009). Insulin-like growth factor-I mitigates motor coordination deficits associated with neonatal alcohol exposure in rats. *Neurotoxicol Teratol* 31, 40-8.

McKinnon, R. D., Waldron, S. and Kiel, M. E. (2005). PDGF alpha-receptor signal strength controls an RTK rheostat that integrates phosphoinositol 3'-kinase and

phospholipase Cgamma pathways during oligodendrocyte maturation. *J Neurosci* 25, 3499-508.

Mirchandani, K. D. and D'Andrea, A. D. (2006). The Fanconi anemia/BRCA pathway: a coordinator of cross-link repair. *Exp Cell Res* 312, 2647-53.

Mitchell, L. E., Murray, J. C., O'Brien, S. and Christensen, K. (2001). Evaluation of two putative susceptibility loci for oral clefts in the Danish population. *Am J Epidemiol* 153, 1007-15.

Moffatt, P., Lee, E. R., St-Jacques, B., Matsumoto, K., Yamaguchi, Y. and Roughley, P. J. (2011). Hyaluronan production by means of Has2 gene expression in chondrocytes is essential for long bone development. *Dev Dyn* 240, 404-12.

Mongera, A., Singh, A. P., Levesque, M. P., Chen, Y. Y., Konstantinidis, P. and Nusslein-Volhard, C. (2013). Genetic lineage labeling in zebrafish uncovers novel neural crest contributions to the head, including gill pillar cells. *Development* 140, 916-25.

Mongera, A., Singh, A. P., Levesque, M. P., Chen, Y. Y., Konstantinidis, P. and Nusslein-Volhard, C. (2013). Genetic lineage labeling in zebrafish uncovers novel neural crest contributions to the head, including gill pillar cells. *Development* 140, 916-25.

Monsoro-Burq, A. H., Fletcher, R. B. and Harland, R. M. (2003). Neural crest induction by paraxial mesoderm in *Xenopus* embryos requires FGF signals. *Development* 130, 3111-24.

Moore, E. M., Migliorini, R., Infante, M. A. and Riley, E. P. (2014). Fetal Alcohol Spectrum Disorders: Recent Neuroimaging Findings. *Curr Dev Disord Rep* 1, 161-172.

Moore, E. S., Ward, R. E., Wetherill, L. F., Rogers, J. L., Autti-Ramo, I., Fagerlund, A., Jacobson, S. W., Robinson, L. K., Hoyme, H. E., Mattson, S. N. et al. (2007). Unique facial features distinguish fetal alcohol syndrome patients and controls in diverse ethnic populations. *Alcohol Clin Exp Res* 31, 1707-13.

Mosimann, C., Kaufman, C. K., Li, P., Pugach, E. K., Tamplin, O. J. and Zon, L. I. (2011). Ubiquitous transgene expression and Cre-based recombination driven by the ubiquitin promoter in zebrafish. *Development* 138, 169-77.

Munaim, S. I., Klagsbrun, M. and Toole, B. P. (1991). Hyaluronan-dependent pericellular coats of chick embryo limb mesodermal cells: induction by basic fibroblast growth factor. *Dev Biol* 143, 297-302.

Nagel, M., Tahinci, E., Symes, K. and Winklbauer, R. (2004). Guidance of mesoderm cell migration in the *Xenopus* gastrula requires PDGF signaling. *Development* 131, 2727-36.

Necas, J., Bartosikova, L., Brauner, P. and Kolar, J. (2008). Hyaluronic acid (hyaluronan): a review. *Veterinari Medicina* 53.

Nie, X., Luukko, K. and Kettunen, P. (2006). FGF signalling in craniofacial development and developmental disorders. *Oral Dis* 12, 102-11.

Nie, X., Luukko, K. and Kettunen, P. (2006). FGF signalling in craniofacial development and developmental disorders. *Oral Dis* 12, 102-11.

Noden, D. M. (1978). The control of avian cephalic neural crest cytodifferentiation. I. Skeletal and connective tissues. *Dev Biol* 67, 296-312.

Noden, D. M. (1983). The role of the neural crest in patterning of avian cranial skeletal, connective, and muscle tissues. *Dev Biol* 96, 144-65.

Noden, D. M. and Trainor, P. A. (2005). Relations and interactions between cranial mesoderm and neural crest populations. *J Anat* 207, 575-601.

Northcutt, R. G. and Gans, C. (1983). The genesis of neural crest and epidermal placodes: a reinterpretation of vertebrate origins. *Q Rev Biol* 58, 1-28.

Ornitz, D. M. and Itoh, N. (2001). Fibroblast growth factors. *Genome Biol* 2, REVIEWS3005.

Ota, S., Tonou-Fujimori, N., Nakayama, Y., Ito, Y., Kawamura, A. and Yamasu, K. (2010). FGF receptor gene expression and its regulation by FGF signaling during early zebrafish development. *Genesis* 48, 707-16.

Pan, A., Chang, L., Nguyen, A. and James, A. W. (2013). A review of hedgehog signaling in cranial bone development. *Front Physiol* 4, 61.

Payne, E. M., Virgilio, M., Narla, A., Sun, H., Levine, M., Paw, B. H., Berliner, N., Look, A. T., Ebert, B. L. and Khanna-Gupta, A. (2012). L-Leucine improves the anemia and developmental defects associated with Diamond-Blackfan anemia and del(5q) MDS by activating the mTOR pathway. *Blood* 120, 2214-24.

Penn, J. W., Grobbelaar, A. O. and Rolfe, K. J. (2012). The role of the TGF-beta family in wound healing, burns and scarring: a review. *Int J Burns Trauma* 2, 18-28.

Pera, E. M., Acosta, H., Gougnard, N., Climent, M. and Arregi, I. (2014). Active signals, gradient formation and regional specificity in neural induction. *Exp Cell Res* 321, 25-31.

Perkins, A., Lehmann, C., Lawrence, R. C. and Kelly, S. J. (2013

). Alcohol exposure during development: Impact on the epigenome. *Int J Dev Neurosci* 31, 391-7.

Piotrowski, T. and Nusslein-Volhard, C. (2000). The endoderm plays an important role in patterning the segmented pharyngeal region in zebrafish (*Danio rerio*). *Dev Biol* 225, 339-56.

Polley, A. and Vemparala, S. (2012). Partitioning of ethanol in multi-component membranes: effects on membrane structure. *Chem Phys Lipids* 166, 1-11.

Porter, J. A., Young, K. E. and Beachy, P. A. (1996). Cholesterol modification of hedgehog signaling proteins in animal development. *Science* 274, 255-9.

Price, A. L., Patterson, N. J., Plenge, R. M., Weinblatt, M. E., Shadick, N. A. and Reich, D. (2006). Principal components analysis corrects for stratification in genome-wide association studies. *Nat Genet* 38, 904-9.

Ramachandran, V., Perez, A., Chen, J., Senthil, D., Schenker, S. and Henderson, G. I. (2001). In utero ethanol exposure causes mitochondrial dysfunction, which can result in apoptotic cell death in fetal brain: a potential role for 4-hydroxynonenal. *Alcohol Clin Exp Res* 25, 862-71.

Ramachandran, V., Watts, L. T., Maffi, S. K., Chen, J., Schenker, S. and Henderson, G. (2003). Ethanol-induced oxidative stress precedes mitochondrially mediated apoptotic death of cultured fetal cortical neurons. *J Neurosci Res* 74, 577-88.

Rattanasopha, S., Tongkobpetch, S., Srichomthong, C., Siriwan, P., Suphapeetiporn, K. and Shotelersuk, V. (2012). PDGFRa mutations in humans with isolated cleft palate. *Eur J Hum Genet* 20, 1058-62.

Reifers, F., Bohli, H., Walsh, E. C., Crossley, P. H., Stainier, D. Y. and Brand, M. (1998). *Fgf8* is mutated in zebrafish acerebellar (*ace*) mutants and is required for maintenance of midbrain-hindbrain boundary development and somitogenesis. *Development* 125, 2381-95.

Ribisi, S., Jr., Mariani, F. V., Amar, E., Lamb, T. M., Frank, D. and Harland, R. M. (2000). Ras-mediated FGF signaling is required for the formation of posterior but not anterior neural tissue in *Xenopus laevis*. *Dev Biol* 227, 183-96.

Rice, D. P., Aberg, T., Chan, Y., Tang, Z., Kettunen, P. J., Pakarinen, L., Maxson, R. E. and Thesleff, I. (2000). Integration of FGF and TWIST in calvarial bone and suture development. *Development* 127, 1845-55.

Rice, D. P., Aberg, T., Chan, Y., Tang, Z., Kettunen, P. J., Pakarinen, L., Maxson, R. E. and Thesleff, I. (2000). Integration of FGF and TWIST in calvarial bone and suture development. *Development* 127, 1845-55.

Richarte, A. M., Mead, H. B. and Tallquist, M. D. (2007). Cooperation between the PDGF receptors in cardiac neural crest cell migration. *Dev Biol* 306, 785-96.

Richtsmeier, J. T. and Flaherty, K. (2013). Hand in glove: brain and skull in development and dysmorphogenesis. *Acta Neuropathol* 125, 469-89.

Rijli, F. M., Mark, M., Lakkaraju, S., Dierich, A., Dolle, P. and Chambon, P. (1993). A homeotic transformation is generated in the rostral branchial region of the head by disruption of *Hoxa-2*, which acts as a selector gene. *Cell* 75, 1333-49.

Roessler, E. and Muenke, M. (2010). The molecular genetics of holoprosencephaly. *Am J Med Genet C Semin Med Genet* 154C, 52-61.

Rohde, L. A. and Heisenberg, C. P. (2007). Zebrafish gastrulation: cell movements, signals, and mechanisms. *Int Rev Cytol* 261, 159-92.

Romitti, P. A., Lidral, A. C., Munger, R. G., Daack-Hirsch, S., Burns, T. L. and Murray, J. C. (1999). Candidate genes for nonsyndromic cleft lip and palate and maternal cigarette smoking and alcohol consumption: evaluation of genotype-environment interactions from a population-based case-control study of orofacial clefts. *Teratology* 59, 39-50.

Ross, R. G., Hunter, S. K., McCarthy, L., Beuler, J., Hutchison, A. K., Wagner, B. D., Leonard, S., Stevens, K. E. and Freedman, R. (2013). Perinatal choline effects on neonatal pathophysiology related to later schizophrenia risk. *Am J Psychiatry* 170, 290-8.

Ruiz i Altaba, A., Palma, V. and Dahmane, N. (2002). Hedgehog-Gli signalling and the growth of the brain. *Nat Rev Neurosci* 3, 24-33.

Saavalainen, K., Pasonen-Seppanen, S., Dunlop, T. W., Tammi, R., Tammi, M. I. and Carlberg, C. (2005). The human hyaluronan synthase 2 gene is a primary retinoic acid and epidermal growth factor responding gene. *J Biol Chem* 280, 14636-44.

Sai, X. and Ladher, R. K. (2015). Early steps in inner ear development: induction and morphogenesis of the otic placode. *Front Pharmacol* 6, 19.

Sampson, P. D., Streissguth, A. P., Bookstein, F. L., Little, R. E., Clarren, S. K., Dehaene, P., Hanson, J. W. and Graham, J. M., Jr. (1997). Incidence of fetal alcohol syndrome and prevalence of alcohol-related neurodevelopmental disorder. *Teratology* 56, 317-26.

Sanna, P. P., Simpson, C., Lutjens, R. and Koob, G. (2002). ERK regulation in chronic ethanol exposure and withdrawal. *Brain Res* 948, 186-91.

Sasaki, Y., Hayashi, N., Ito, T., Fusamoto, H., Kamada, T. and Wands, J. R. (1994). Influence of ethanol on insulin receptor substrate-1-mediated signal transduction during rat liver regeneration. *Alcohol Alcohol Suppl* 29, 99-106.

Satoh, N., Tagawa, K. and Takahashi, H. (2012). How was the notochord born? *Evol Dev* 14, 56-75.

Sauka-Spengler, T. and Bronner, M. (2010). Snapshot: neural crest. *Cell* 143, 486-486 e1.

Sauka-Spengler, T. and Bronner-Fraser, M. (2008). Evolution of the neural crest viewed from a gene regulatory perspective. *Genesis* 46, 673-82.

Schatteman, G. C., Morrison-Graham, K., van Koppen, A., Weston, J. A. and Bowen-Pope, D. F. (1992). Regulation and role of PDGF receptor alpha-subunit expression during embryogenesis. *Development* 115, 123-31.

Schilling, T. F. and Kimmel, C. B. (1994). Segment and cell type lineage restrictions during pharyngeal arch development in the zebrafish embryo. *Development* 120, 483-94.

Schilling, T. F. and Kimmel, C. B. (1997). Musculoskeletal patterning in the pharyngeal segments of the zebrafish embryo. *Development* 124, 2945-60.

Schilling, T. F., Prince, V. and Ingham, P. W. (2001). Plasticity in zebrafish hox expression in the hindbrain and cranial neural crest. *Dev Biol* 231, 201-16.

Schmidt, K. and Starck, J. M. (2010). Developmental plasticity, modularity, and heterochrony during the phylotypic stage of the zebra fish, *Danio rerio*. *J Exp Zool B Mol Dev Evol* 314, 166-78.

Schneider, C. A., Rasband, W. S. and Eliceiri, K. W. (2012). NIH Image to ImageJ: 25 years of image analysis. *Nat Methods* 9, 671-5.

Schulte-Merker, S., van Eeden, F. J., Halpern, M. E., Kimmel, C. B. and Nusslein-Volhard, C. (1994). no tail (ntl) is the zebrafish homologue of the mouse T (Brachyury) gene. *Development* 120, 1009-15.

Sefton, E. M., Piekarski, N. and Hanken, J. (2015). Dual embryonic origin and patterning of the pharyngeal skeleton in the axolotl (*Ambystoma mexicanum*). *Evol Dev* 17, 175-84.

Seufert, D. W. and Hall, B. K. (1990). Tissue interactions involving cranial neural crest in cartilage formation in *Xenopus laevis* (Daudin). *Cell Differ Dev* 32, 153-65.

Shah, R. M., Donaldson, E. M. and Scudder, G. G. (1990). Toward the origin of the secondary palate. A possible homologue in the embryo of fish, *Onchorhynchus kisutch*, with description of changes in the basement membrane area. *Am J Anat* 189, 329-38.

Sheehan-Rooney, K., Swartz, M. E., Lovely, C. B., Dixon, M. J. and Eberhart, J. K. (2013). Bmp and Shh signaling mediate the expression of *satb2* in the pharyngeal arches. *PLoS One* 8, e59533.

Shin, J., Park, H. C., Topczewska, J. M., Mawdsley, D. J. and Appel, B. (2003). Neural cell fate analysis in zebrafish using olig2 BAC transgenics. *Methods Cell Sci* 25, 7-14.

Siegenthaler, J. A. and Miller, M. W. (2005). Ethanol disrupts cell cycle regulation in developing rat cortex interaction with transforming growth factor beta1. *J Neurochem* 95, 902-12.

Sivak, J. M., Petersen, L. F. and Amaya, E. (2005). FGF signal interpretation is directed by Sprouty and Spred proteins during mesoderm formation. *Dev Cell* 8, 689-701.

Smith, C. L., Baek, S. T., Sung, C. Y. and Tallquist, M. D. (2011). Epicardial-derived cell epithelial-to-mesenchymal transition and fate specification require PDGF receptor signaling. *Circ Res* 108, e15-26.

Soares, H. P., Ni, Y., Kisfalvi, K., Sinnett-Smith, J. and Rozengurt, E. (2013). Different patterns of Akt and ERK feedback activation in response to rapamycin, active-site mTOR inhibitors and metformin in pancreatic cancer cells. *PLoS One* 8, e57289.

Solomon, K. S. and Fritz, A. (2002). Concerted action of two dlx paralogs in sensory placode formation. *Development* 129, 3127-36.

Solomon, K. S., Kudoh, T., Dawid, I. B. and Fritz, A. (2003). Zebrafish *foxi1* mediates otic placode formation and jaw development. *Development* 130, 929-40.

Soriano, P. (1994). Abnormal kidney development and hematological disorders in PDGF beta-receptor mutant mice. *Genes Dev* 8, 1888-96.

Soriano, P. (1997). The PDGF alpha receptor is required for neural crest cell development and for normal patterning of the somites. *Development* 124, 2691-700.

Stafford, D., White, R. J., Kinkel, M. D., Linville, A., Schilling, T. F. and Prince, V. E. (2006). Retinoids signal directly to zebrafish endoderm to specify insulin-expressing beta-cells. *Development* 133, 949-56.

Stanier, P. and Moore, G. E. (2004). Genetics of cleft lip and palate: syndromic genes contribute to the incidence of non-syndromic clefts. *Hum Mol Genet* 13 Spec No 1, R73-81.

Staudt, N., Muller-Sienerth, N., Fane-Dremucheva, A., Yusaf, S. P., Millrine, D. and Wright, G. J. (2015). A panel of recombinant monoclonal antibodies against zebrafish neural receptors and secreted proteins suitable for wholemount immunostaining. *Biochem Biophys Res Commun* 456, 527-33.

Stockard, C. (1910). The influence of alcohol and other anaesthetics on embryonic development. *American Journal of Anatomy*, 369-392.

Stone, D. M., Hynes, M., Armanini, M., Swanson, T. A., Gu, Q., Johnson, R. L., Scott, M. P., Pennica, D., Goddard, A., Phillips, H. et al. (1996). The tumour-suppressor gene patched encodes a candidate receptor for Sonic hedgehog. *Nature* 384, 129-34.

Streissguth, A. P. and Dehaene, P. (1993). Fetal alcohol syndrome in twins of alcoholic mothers: concordance of diagnosis and IQ. *Am J Med Genet* 47, 857-61.

Sulik, K. K. (2005). Genesis of alcohol-induced craniofacial dysmorphism. *Exp Biol Med (Maywood)* 230, 366-75.

Sulik, K. K., Johnston, M. C., Daft, P. A., Russell, W. E. and Dehart, D. B. (1986). Fetal alcohol syndrome and DiGeorge anomaly: critical ethanol exposure periods for craniofacial malformations as illustrated in an animal model. *Am J Med Genet Suppl* 2, 97-112.

Swartz, M. E., Sheehan-Rooney, K., Dixon, M. J. and Eberhart, J. K. (2011). Examination of a palatogenic gene program in zebrafish. *Dev Dyn* 240, 2204-20.

Swayze, V. W., 2nd, Johnson, V. P., Hanson, J. W., Piven, J., Sato, Y., Giedd, J. N., Mosnik, D. and Andreasen, N. C. (1997). Magnetic resonance imaging of brain anomalies in fetal alcohol syndrome. *Pediatrics* 99, 232-40.

Takechi, M., Adachi, N., Hirai, T., Kuratani, S. and Kuraku, S. (2013). The Dlx genes as clues to vertebrate genomics and craniofacial evolution. *Semin Cell Dev Biol* 24, 110-8.

Talbot, J. C., Johnson, S. L. and Kimmel, C. B. (2010). *hand2* and Dlx genes specify dorsal, intermediate and ventral domains within zebrafish pharyngeal arches. *Development* 137, 2507-17.

Tallquist, M. and Kazlauskas, A. (2004). PDGF signaling in cells and mice. *Cytokine Growth Factor Rev* 15, 205-13.

Tallquist, M. D., French, W. J. and Soriano, P. (2003). Additive effects of PDGF receptor beta signaling pathways in vascular smooth muscle cell development. *PLoS Biol* 1, E52.

Tallquist, M. D. and Soriano, P. (2003). Cell autonomous requirement for PDGFRalpha in populations of cranial and cardiac neural crest cells. *Development* 130, 507-18.

Tallquist, M. D. and Soriano, P. (2003). Cell autonomous requirement for PDGFRalpha in populations of cranial and cardiac neural crest cells. *Development* 130, 507-18.

Theveneau, E. and Mayor, R. (2012). Neural crest delamination and migration: from epithelium-to-mesenchyme transition to collective cell migration. *Dev Biol* 366, 34-54.

Thisse, B. and Thisse, C. (2005). Functions and regulations of fibroblast growth factor signaling during embryonic development. *Dev Biol* 287, 390-402.

Thisse, B. and Thisse, C. (2005). Functions and regulations of fibroblast growth factor signaling during embryonic development. *Dev Biol* 287, 390-402.

Thomas, J. D., Melcer, T., Weinert, S. and Riley, E. P. (1998). Neonatal alcohol exposure produces hyperactivity in high-alcohol-sensitive but not in low-alcohol-sensitive rats. *Alcohol* 16, 237-42.

Tokumaru, A. M., Barkovich, A. J., Ciricillo, S. F. and Edwards, M. S. (1996). Skull base and calvarial deformities: association with intracranial changes in craniofacial syndromes. *AJNR Am J Neuroradiol* 17, 619-30.

Tokumaru, A. M., Barkovich, A. J., Ciricillo, S. F. and Edwards, M. S. (1996). Skull base and calvarial deformities: association with intracranial changes in craniofacial syndromes. *AJNR Am J Neuroradiol* 17, 619-30.

Trainor, P. and Krumlauf, R. (2000). Plasticity in mouse neural crest cells reveals a new patterning role for cranial mesoderm. *Nat Cell Biol* 2, 96-102.

Trainor, P. A. (2003). Making headway: the roles of Hox genes and neural crest cells in craniofacial development. *ScientificWorldJournal* 3, 240-64.

Trainor, P. A. (2010). Craniofacial birth defects: The role of neural crest cells in the etiology and pathogenesis of Treacher Collins syndrome and the potential for prevention. *Am J Med Genet A* 152A, 2984-94.

Urness, L. D., Paxton, C. N., Wang, X., Schoenwolf, G. C. and Mansour, S. L. (2010). FGF signaling regulates otic placode induction and refinement by controlling both ectodermal target genes and hindbrain *Wnt8a*. *Dev Biol* 340, 595-604.

van der Geer, P., Hunter, T. and Lindberg, R. A. (1994). Receptor protein-tyrosine kinases and their signal transduction pathways. *Annu Rev Cell Biol* 10, 251-337.

Van Stry, M., Kazlauskas, A., Schreiber, S. L. and Symes, K. (2005). Distinct effectors of platelet-derived growth factor receptor- α signaling are required for cell survival during embryogenesis. *Proc Natl Acad Sci U S A* 102, 8233-8.

Van Stry, M., McLaughlin, K. A., Ataliotis, P. and Symes, K. (2004). The mitochondrial-apoptotic pathway is triggered in *Xenopus* mesoderm cells deprived of PDGF receptor signaling during gastrulation. *Dev Biol* 268, 232-42.

Varga, Z. M., Amores, A., Lewis, K. E., Yan, Y. L., Postlethwait, J. H., Eisen, J. S. and Westerfield, M. (2001). Zebrafish smoothed functions in ventral neural tube specification and axon tract formation. *Development* 128, 3497-509.

Vary, T. C., Deiter, G. and Lantry, R. (2008). Chronic alcohol feeding impairs mTOR(Ser 2448) phosphorylation in rat hearts. *Alcohol Clin Exp Res* 32, 43-51.

Vasudevan, H. N. and Soriano, P. (2014). SRF regulates craniofacial development through selective recruitment of MRTF cofactors by PDGF signaling. *Dev Cell* 31, 332-44.

Viljoen, D. L., Carr, L. G., Foroud, T. M., Brooke, L., Ramsay, M. and Li, T. K. (2001). Alcohol dehydrogenase-2*2 allele is associated with decreased prevalence of fetal alcohol syndrome in the mixed-ancestry population of the Western Cape Province, South Africa. *Alcohol Clin Exp Res* 25, 1719-22.

Wada, N., Javidan, Y., Nelson, S., Carney, T. J., Kelsh, R. N. and Schilling, T. F. (2005). Hedgehog signaling is required for cranial neural crest morphogenesis and chondrogenesis at the midline in the zebrafish skull. *Development* 132, 3977-88.

Wada, N., Nohno, T. and Kuratani, S. (2011). Dual origins of the prechordal cranium in the chicken embryo. *Dev Biol* 356, 529-40.

Walker, M. B. and Kimmel, C. B. (2007). A two-color acid-free cartilage and bone stain for zebrafish larvae. *Biotech Histochem* 82, 23-8.

Warren, K. R. and Li, T. K. (2005). Genetic polymorphisms: impact on the risk of fetal alcohol spectrum disorders. *Birth Defects Res A Clin Mol Teratol* 73, 195-203.

Weigel, P. H., Hascall, V. C. and Tammi, M. (1997). Hyaluronan synthases. *J Biol Chem* 272, 13997-4000.

Wentzel, P. and Eriksson, U. J. (2006). Ethanol-induced fetal dysmorphogenesis in the mouse is diminished by high antioxidative capacity of the mother. *Toxicol Sci* 92, 416-22.

Westerfield, M. (1993). *The Zebrafish Book: A guide for the laboratory use of zebrafish (Brachydanio rerio)*.

Wiens, K. M., Lee, H. L., Shimada, H., Metcalf, A. E., Chao, M. Y. and Lien, C. L. (2010). Platelet-derived growth factor receptor beta is critical for zebrafish intersegmental vessel formation. *PLoS One* 5, e11324.

Wilkie, A. O. and Morriss-Kay, G. M. (2001). Genetics of craniofacial development and malformation. *Nat Rev Genet* 2, 458-68.

Wilson, J. and Tucker, A. S. (2004). Fgf and Bmp signals repress the expression of Bapx1 in the mandibular mesenchyme and control the position of the developing jaw joint. *Dev Biol* 266, 138-50.

Wilson, S. I., Graziano, E., Harland, R., Jessell, T. M. and Edlund, T. (2000). An early requirement for FGF signalling in the acquisition of neural cell fate in the chick embryo. *Curr Biol* 10, 421-9.

Wolpert, L. (1992). Gastrulation and the evolution of development. *Dev Suppl*, 7-13.

Woo, K. and Fraser, S. E. (1995). Order and coherence in the fate map of the zebrafish nervous system. *Development* 121, 2595-609.

Wu, E., Palmer, N., Tian, Z., Moseman, A. P., Galdzicki, M., Wang, X., Berger, B., Zhang, H. and Kohane, I. S. (2008). Comprehensive dissection of PDGF-PDGFR signaling pathways in PDGFR genetically defined cells. *PLoS One* 3, e3794.

Wu, T., Schwender, H., Ruczinski, I., Murray, J. C., Marazita, M. L., Munger, R. G., Hetmanski, J. B., Parker, M. M., Wang, P., Murray, T. et al. (2014). Evidence of gene-environment interaction for two genes on chromosome 4 and

environmental tobacco smoke in controlling the risk of nonsyndromic cleft palate. PLoS One 9, e88088.

Xiong, W., Cheng, B. H., Jia, S. B. and Tang, L. S. (2010). Involvement of the PI3K/Akt signaling pathway in platelet-derived growth factor-induced migration of human lens epithelial cells. Curr Eye Res 35, 389-401.

Xu, J., Yeon, J. E., Chang, H., Tison, G., Chen, G. J., Wands, J. and de la Monte, S. (2003). Ethanol impairs insulin-stimulated neuronal survival in the developing brain: role of PTEN phosphatase. J Biol Chem 278, 26929-37.

Yan, Y. L., Hatta, K., Riggleman, B. and Postlethwait, J. H. (1995). Expression of a type II collagen gene in the zebrafish embryonic axis. Dev Dyn 203, 363-76.

Yoshida, M., Itano, N., Yamada, Y. and Kimata, K. (2000). In vitro synthesis of hyaluronan by a single protein derived from mouse HAS1 gene and characterization of amino acid residues essential for the activity. J Biol Chem 275, 497-506.

Yoshida, T., Vivatbutsiri, P., Morriss-Kay, G., Saga, Y. and Iseki, S. (2008). Cell lineage in mammalian craniofacial mesenchyme. Mech Dev 125, 797-808.

Young, J. K., Giesbrecht, H. E., Eskin, M. N., Aliani, M. and Suh, M. (2014). Nutrition implications for fetal alcohol spectrum disorder. Adv Nutr 5, 675-92.

Yu, J. K. (2010). The evolutionary origin of the vertebrate neural crest and its developmental gene regulatory network--insights from amphioxus. *Zoology (Jena)* 113, 1-9.

Zhang, C., Ojiaku, P. and Cole, G. J. (2012). Forebrain and hindbrain development in zebrafish is sensitive to ethanol exposure involving agrin, Fgf, and sonic hedgehog function. *Birth Defects Res A Clin Mol Teratol* 97, 8-27.

Zhang, C., Turton, Q. M., Mackinnon, S., Sulik, K. K. and Cole, G. J. (2011). Agrin function associated with ocular development is a target of ethanol exposure in embryonic zebrafish. *Birth Defects Res A Clin Mol Teratol* 91, 129-41.

Zhou, H. and Huang, S. (2010). The complexes of mammalian target of rapamycin. *Curr Protein Pept Sci* 11, 409-24.

Zhu, Q., Zhao, X., Zheng, K., Li, H., Huang, H., Zhang, Z., Mastracci, T., Wegner, M., Chen, Y., Sussel, L. et al. (2014). Genetic evidence that Nkx2.2 and Pdgfra are major determinants of the timing of oligodendrocyte differentiation in the developing CNS. *Development* 141, 548-55.

Vita

Neil McCarthy was born October 19, 1985 in Aberdeen, Scotland. After graduating from the Woodlands High School in the Woodlands, Texas, he moved to Batesville, Arkansas to attend Lyon College. He graduated with a B.S. in Biology in 2008, and began his graduate studies at the University of Texas at Austin that same year. After receiving his PhD, he plans to work as a postdoc in the lab of Ramesh Shivdasani at Harvard in Boston, Massachusetts.